Ion Conducting Polyelectrolytes in Conductive Network Composites and Humidity Sensing Applications for Ionic Polymer-Metal Composite Actuators

Anna P. Skinner

Thesis submitted to the faculty of the Virginia Polytechnic Institute and State University in partial fulfillment of the requirements for the degree of

Master of Science
In
Materials Science and Engineering

James R. Heflin, Committee Chair
Timothy E. Long
Abby R. Whittington

May 3rd, 2016
Blacksburg, VA

Keywords: Ionic self-assembled multilayers, Ionic polymer-metal composite, actuator, humidity sensor

Ion Conducting Polyelectrolytes in Conductive Network Composites and Humidity Sensing Applications for Ionic Polymer-Metal Composite Actuators

Anna P. Skinner

ABSTRACT

Ionic polymer-metal composites (IPMCs) are widely studied for their potential as electromechanical sensors and actuators. Bending of the IMPC depends on internal ion motion under an electric potential, and the addition of an ionic liquid and ionic self-assembled multilayer (ISAM) conductive network composite (CNC) strongly enhances bending and improves lifetime.

Ion conducting polyelectrolytes poly(2-acrylamido-2-methyl-1-propanesulfonic acid) (PAMPS) and Nafion® were incorporated into an ISAM CNC film with poly(allylamine hydrochloride) (PAH) and anionic gold nanoparticles actuators to further improve bending. CNC films were optimized for bending through pH adjustments in PAH and adding NaCl to the PAMPS and Nafion® solutions. PAMPS-containing actuators showed larger and faster bending than those containing Nafion® in the CNC.

The IPMC actuator was also evaluated for its potential as a humidity sensor based on its relative humidity (RH) dependent steady-state current. The detection range is at least 10-80%RH, with 5%RH increment differentiation and likely better resolution. Effects of CNC presence and thickness were studied, in conjunction with ionic liquid at a range of RH values. A thin CNC (pH 4.0 PAH) produced the greatest current differentiation between RH values. The current's response speed to a large RH decrease was approximately 4 times faster than that of a fast commercial digital hygrometer. Additionally, the presence of a CNC and ionic liquid improved the current response time. These results indicate that an IPMC based humidity sensor using a CNC and ionic liquid is very promising and merits further study.

Ion Conducting Polyelectrolytes in Conductive Network Composites and Humidity Sensing Applications for Ionic Polymer-Metal Composite Actuators

Anna P. Skinner

PUBLIC ABSTRACT

Ionic polymer-metal composites (IPMCs) are composite thin films composed of metal and conducting polymer, and have a number of applications as sensors, artificial muscles, and even robotics. They are widely studied for their potential as electromechanical sensors and actuators, since they display a mechanical bending response to an electric stimulus. The electromechanical relationship can also be used in the reverse direction, with a mechanical stimulus causing an electric response. These devices typically have a central ionic electroactive polymer layer, which displays large bending motion under an applied electric field. This response depends on internal ion motion under an electric potential, and the addition of an ionic liquid (a liquid salt) as an ion source strongly enhances bending and improves lifetime. A conductive network composite (CNC), is an optional component of an IPMC, which is a porous composite structure typically containing conductive nanoparticles. The CNC also enhances bending, especially when deposited as a thin ionic self-assembled multilayer (ISAM) film. The ISAM film growth process builds nanoscale film layers from oppositely charged materials one layer at a time.

In this work, the ion conducting charged polymers poly(2-acrylamido-2-methyl-1-propanesulfonic acid) (PAMPS) and Nafion® were incorporated into an ISAM CNC film with poly(allylamine hydrochloride) (PAH) and negatively charged gold nanoparticles (AuNPs). The conducting polymers were introduced with a goal of improving actuator bending curvature and speed. CNC films were optimized for bending through tailoring the individual layers by pH adjustments and adding salt to the polymer solutions. Devices containing PAMPS showed superior actuation performance compared to those containing Nafion®, but both enhanced bending speed and curvature over actuators with CNCs with only PAH and AuNPs.

Lastly, evaluation of the IPMC actuator for its potential as a humidity sensor based on its relative humidity (RH) dependent steady state current was conducted, after early success in a prior study. The IPMC actuator device was investigated with the intent of determining if a commercial-quality relative humidity sensing device could be fabricated out of an IPMC

actuator, and to identify the optimal CNC and device parameters. The relative humidity sensing range, detection speed, and effects of CNC presence and thickness were studied, in conjunction with ionic liquid at a range of RH values. It was found that the current scales over a large humidity range with promising resolution. Additionally, the presence of a CNC and ionic liquid allowed for faster humidity detection. The current's response speed to a large RH decrease was approximately 4 times faster than that of a fast digital hygrometer. The most successful device included a thin CNC and ionic liquid, based on the advantages in speed and dynamic current range gained through these additions. All of the results presented show great promise for a relative humidity sensing device, and indicate that the IPMC actuator humidity sensor merits additional study to further refine the current measurements at varying RH in these devices.

Acknowledgements

Firstly, I would like to thank my advisor, Dr. Randy Heflin for his guidance, time, insight, and comments throughout my graduate student career, as well as the opportunity to be a part of his research group. Thank you also to my committee members Dr. Tim Long and Dr. Abby Whittington for their time, as well as their advice, helpful comments and questions.

Also, thanks to the members of my research group, both former and present. You helped with my many questions about equipment and materials, and I appreciate our conversations and friendship over the years. Dr. Dong Wang especially taught me much about procedures and experimentation, as well as answered my many questions. Thanks to Jonathan Metzman, Kelly Mccutcheon, Jeong-Ah Lee, Yanlong Li, and Moataz Khalifa for their advice, support, and many kindnesses.

The Virginia Tech Physics Department provided essential financial support to me throughout my graduate career. Special thanks to Dr. John Simonetti and Alma Robinson for their encouragement, confidence, and trust.

Lastly, many thanks to my parents, without whose love, support, and guidance I would never have made it this far. Thanks also to Chip Jackson and Sydney Skinner for their support. Both listened to my research concerns without complaint and their friendship is deeply appreciated.

Thank you all for your support, encouragement, and help in conducting and completing this research project.

-Anna

Table of Contents:

List of Figures:

List of Tables:

List of Acronyms

AuNPs	gold nanoparticles
BMMI-Cl	1-butyl-2,3-dimethylimidazolium chloride
CNC	conductive network composite
DAP	direct assembly process
DSC	differential scanning calorimetry
EMI-Tf	1-ethyl-3-methylimidazolium trifluoromethanesulfonate
IEAP	ionic electroactive polymer
IEC	ion exchange capacity
IPCNC	ionic polymer conductive network composite (IPMC with a CNC)
IPMC	ionic polymer-metal composite
IPT	ionic polymer transducer
ISAM	ionic self-assembled multilayers
LbL	Layer-by-layer (electrostatic)
LPEI	linear poly(ethyleneimine)
PAH	poly(allylamine hydrochloride)
PAMPS	poly(2-acrylamido-2-methyl-1-propanesulfonic acid)
PE	polyelectrolyte
PEM	polyelectrolyte multilayer
polyAMPS	see PAMPS
PTFE	polytetrafluoroethylene
PVA	poly(vinyl alcohol)
QCM	quartz crystal microbalance
RH (%RH)	relative humidity
RO	reverse osmosis
SEM	scanning electron microscopy
TFE	fluorotetraethylene
TGA	thermogravimetric analysis
TiC-CDC	titanium carbide-derived carbon
WAXD	wide angle x-ray diffraction
XPS	x-ray photoelectron spectroscopy

Chapter 1: Introduction and Literature Review

1.1 Introduction

Polymer-based actuators have been heavily studied for their wide applicability in devices such as electromechanical sensors, artificial muscles and organs, biomedical and energy harvesting devices, and robotics.[1-17] Ionic polymer-metal composite (IPMC) actuators fall into this category, and have been used in all of these applications. While the results are very promising and successful already, further study has the potential to improve those devices, as well as allow for better understanding of their mechanisms. This thesis presents further development of an IPMC actuator with ionic self-assembled multilayer (ISAM) conductive network composite electrodes. In prior work from our group, the ISAM composite electrodes were fabricated with a polycation, poly(allylamine hydrochloride) (PAH) and anionic gold nanoparticles (AuNPs).

The bulk of this thesis involves the incorporation of additional polyanionic ion conducting polymers into the ISAM composite electrode, with the goal of improving bending curvature and actuation speed. By interspacing bilayers of PAH and AuNPs on IPMC actuators with Nafion® or poly(2-acrylamido-2-methyl-1-propanesulfonic acid) (PAMPS or polyAMPS), both conducting polymers with hydrophilic sulfonic acid side groups, actuator bending and speed was enhanced. Additional work focuses the further development of humidity sensing using the IPMC actuator with ISAM composite electrode. Under an applied voltage the IPMC actuator shows a relative humidity dependent electrolysis current, which can be measured to determine relative humidity.

The following will examine the advantages of IPMC actuators with a conductive network composite (CNC) compared to other actuators and summarize the structure, fabrication methods, and materials used in fabricating IPMC actuators utilizing electrostatic self-assembly in building the conductor network composite structure. Additionally, characterization techniques, issues, and areas where progress is desired will be discussed. Ionic self-assembled multilayer films, or electrostatic layer-by-layer films will also be discussed, as well as ways to tailor the resulting film morphology using this technique.

1.2 Background on IPMC actuators

1.2.1 IPMC actuators and applications

Ionic electroactive polymer actuators (IEAPs), sometimes called ionic polymer transducers (IPTs) or ionic polymer metal composite actuators (IPMCs), are typically a 3 layer structure fashioned from an ionomer membrane, often Nafion, with two conductive electrodes on either side of the ionomer. The electrodes are frequently made of a thin layer of gold, platinum, or other metal.[1, 3, 8, 9, 11, 12, 17-21] Electroactive polymer based actuators exhibit large bending when a low voltage is applied across them.[1, 3, 8, 11, 12, 15, 18, 20, 22-27] IEAP devices are particularly attractive in this regard when compared to ceramic and metallic devices such as electroactive ceramics and shape memory alloys, or even other types of electroactive polymers such as dielectric electroactive polymers. The key advantages include the low weight, low operating voltage (2-4 V, voltages batteries can supply), high produced strain (on the order of 5%), large bending deformation, stability, low cost, facile fabrication, high ionic conductivity, and reliability of IEAPs.[1-3, 7-9, 11, 12, 15, 18, 21, 22, 24, 26-28] A wide variety of potential applications of these actuators have been described in the literature including electromechanical sensors and actuators[1-4], underwater propulsion (such as seen in an autonomous jellyfish vehicle)[22], biomimetic devices[7, 9, 15], robotics[15], artificial muscles[8, 17, 29], artificial organs[20], biomedical devices, energy harvesting devices[7, 9], and electroactive coatings.[6]

1.2.2 Use of ionic liquids in IPMC actuators

As will be discussed further in the next section, actuator bending stems from mobile ions in the ionomer and CNC layers. This works in ambient environmental conditions by using water vapor adsorbed from the air, or by soaking the device in water.[30] Unfortunately, using water as the ion source comes with some restrictions. Over time the internal water from soaking evaporates, which reduces actuation.[1, 19, 31, 32] In general, the greater the ion concentration in the device, the larger the bending, as larger volume imbalances are created with greater ion concentration, as discussed in section 1.2.3. Low pressure environment applications of a water-containing actuator are significantly reduced because of the evaporation.[21] Also, applied voltage is limited to less than the water electrolysis voltage (~1.3-1.5 V).[32]

These problems can be solved by providing another ion source that is more stable within the membrane. Ionic liquids are a popular approach to solve this problem. Ionic liquids are salts that are liquid at temperatures below 100 °C, though the exact definition with respect to

temperature varies. They have become popular for their applications in many types of devices including energy storage and conversion devices, actuators, batteries, fuel cells, supercapacitors.[33] They also have very low vapor pressure, which widens the environments for IPMC applications.[21, 27, 32, 34] They stay within the membrane for extended periods of time with minimal evaporation, thereby significantly extending the lifetime.[19, 35] With ionic liquids being used as the ion source, it has been shown that these bending actuators last for thousands of bending cycles.[30, 31] They are also stable at greater voltages than that of water, allowing for greater actuation simply by increased electric potential.[19, 32, 35]

1.2.3 Bending mechanism for IPMC actuators

In ionic electroactive polymers, bending deformation is caused by mobile ions in the ionomer, and the conductive network composite when it is present, which cause a volume imbalance at the opposite sides of the actuator. If there is only one mobile ion type present, it will move toward the oppositely charged electrode. This leads to swelling at that electrode, and deswelling at the other electrode, resulting in electrode curvature. The outer edge of the curved surface is the side with the ion accumulation. The mobile ion source is usually either water, which is present inside the polymer membrane when the IEAP is in air, or an ionic liquid. As ionic liquids have largely replaced water as the primary ion source, further discussion revolves around ionic liquid ions as the bending mechanism. The IPMC actuators discussed in this thesis show bidirectional bending behavior. When an electric field is applied, the mobile cations and anions inside the membrane migrate toward the oppositely charged electrodes. However, ion motion does not occur at the same speed for both ion types. Typically, single atom cations are smaller than single atom anions, though in polyatomic ions such as those in ionic liquids, this may not be the case. In the majority of the actuators we study, bending occurs first when positive ions reach the edge of the membrane. This movement causes volume depletion in the rest of the membrane, so bending occurs. The negative ions eventually make their way to the opposite side of the membrane, and since they are larger, they cause an even larger volume difference, and the actuator bends in the opposite direction. As the ions are typically different sizes, a volume imbalance is created, causing bending.[1, 4, 8, 15, 19-21, 24-26, 36, 37]

Hong *et al*.[37] showed the Van der Waals radii of various ionic liquid ions. For EMI-Tf (1-ethyl-3-methylimidazolium trifluoromethanesulfonate), the ionic liquid used in these studies, the cation is actually about 20 pm larger than the anion. However, this small difference doesn't

change the end result in this case. The EMI^+ ion has a faster drift velocity, causing the fast cationic bending, and when combined with the fact that the Tf^- ion forms clusters, the result is slower but stronger anionic bending.[37, 38] As a result of this mechanism, depending on relative ion sizes from the ionic liquid, bending direction and speed may be reversed.

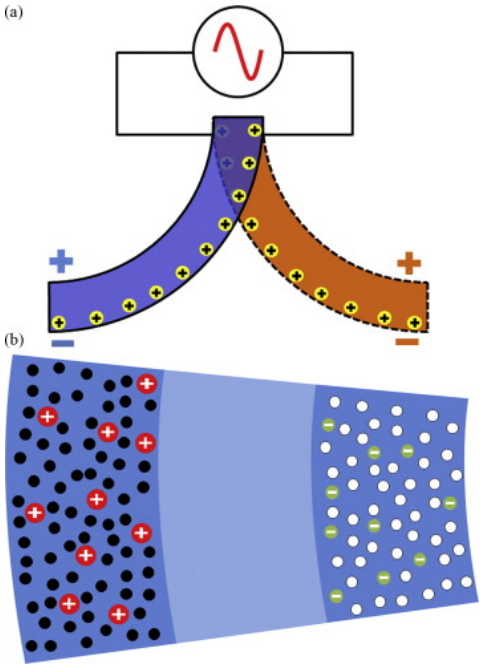

Figure 1.1: (a) Diagram of the bending IPMC actuator under an alternating electric field, showing the cation position with respect to the electrode. (b) The bending of the CNC with positive and negative ions near the oppositely charged electrodes. Reprinted from Sensors and Actuators A: Physical, Volume 157, Issue 2, Sheng Liu, Reza Montazami, Yang Liu, Vaibhav Jain, Minren Lin, Xin Zhou, James R. Heflin, Q.M. Zhang, Influence of the conductor network composites on the electromechanical performance of ionic polymer conductor network composite actuators, Pages 267-275, Copyright 2009, with permission from Elsevier.[25]

The ionic liquid ion depths within the ionomer layer in electromechanical actuators were studied directly by Liu *et al*.[33, 37] using ToF- SIMS (Time-of-Flight Secondary Ion Mass Spectrometry). Their study confirmed the theory that IL cations and anions accumulate near the oppositely charged electrode under constant applied voltage, and attempt to neutralize the electric field, and the resulting volume difference is responsible for bending actuation. The device they studied was an Aquivion ionomer membrane with 1-butyl-2,3-dimethylimidazolium chloride (BMMI-Cl) ionic liquid, which has a large difference in cation and anion relative size, larger than EMI-Tf, though it has a much higher melting point (99° C). In order to look at the ion profile, they applied a voltage at temperature higher than the melting point, then rapidly froze

it at -40 °C in order to prevent the IL ions from moving. They also stated their Aquivion/BMMI-Cl system had a critical ionic liquid wt % uptake of about 40 wt % to produce large bending under actuation, which they found in an earlier study.[33]

Liu *et al's.*[33] results showed both ion types are present at both electrodes, though there are a higher concentration of them at the oppositely charged electrode. The ion concentration on both sides was unevenly distributed, likely because of the Cl^- anions were so much smaller than the cations. Based on the timing, they concluded that diffusion layers of ions cause the actuation. Both sides of the actuator undergo strain from ion accumulation, but the larger ion wins the battle and forces bending. This system shows no back relaxation, unlike EMI-Tf/Aquivion, which has larger anions, causing the back-relaxation.[33]

More recently, Hong *et al*.[37] conducted studies on which ions in IPMC actuators contribute to bending during actuation. The Nafion's counterions were exchanged with cations of varying sizes, and different ionic liquids were used. Both counterions of the Nafion and the ionic liquid's dopant ions moved under an applied electric field, and both contribute to bending. However their relative sizes determine bending direction and curvature. Typically Nafion has H^+ as the counterion, which is too small to cause noticeable bending. After ion exchange occurred with the much larger EMI^+ polyion, the entire bending curve was shifted toward cationic strain.[37]

1.2.4 History of Conductive Network Composites in IPMC actuators: Direct Assembly Process, ISAM films, and Impregnation-reduction

There is some variation in the possible structures of IPMC actuators, as well as methods to form the electrodes. One subset of IPMC actuators includes a conductive network composite (CNC) structure between the ionomer layer and the thin metal electrodes. This transforms the actuator from a three layer structure into a five layer structure. One simple method of building a CNC on the ionomer is to use electrostatic self-assembled multilayer techniques. Actuators making use of a CNC are sometimes called ionic polymer conductor network composite (IPCNC) actuators.[7, 9, 15, 20, 21, 24-26, 35, 36]

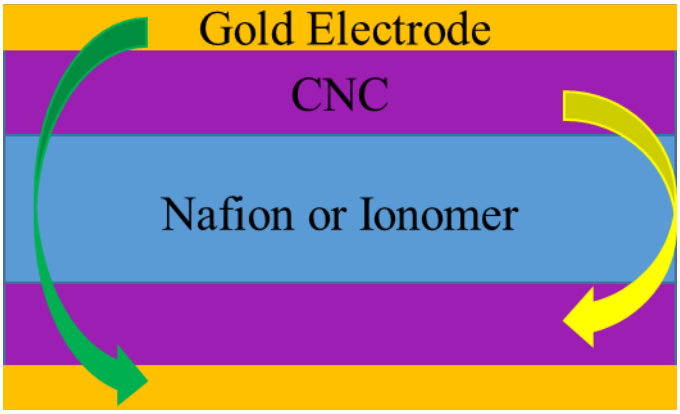

Figure 1.2: Setup of an IPMC actuator including CNC composite electrode layers. Not to scale.

There are a number of advantages to adding more layers of CNC on the ionomer surface, including some specific benefits gained by using electrostatic self-assembly to build the CNC. The CNC, which is sometimes called a porous composite electrode, functions as a reservoir for the ions from the electrolyte. With more layers, the uptake of ionic liquid or water from the environment is significantly increased. As a result, a greater number of ions are mobile during actuation, which increases the bending and strain performance.[15, 24, 25, 36] One method of building a CNC is the electrostatic layer-by-layer (LbL) self-assembly or ionic self-assembled multilayer (ISAM) method, first applied to IEAP actuators by S. Liu *et al.* in 2009.[24] In this method, CNCs are fabricated by placing the Nafion or other ionomer film into two aqueous solutions in an alternating manner. The cationic layers are commonly poly(allylamine hydrochloride) (PAH), while the anionic layers are usually 2 nm gold nanoparticles.[24] Another technique to build a CNC is called a direct assembly process (DAP), which was originally performed by Akle *et al*.[2] DAP on dry membranes involves dissolving the ionomer, mixing in a conductive powder, then painting and hot pressing layers of the mixture on a polymer or a strip of Furon. Metal electrodes are then added to the surfaces. Solvated actuators are made by soaking the ionomer in a solvent or ionic liquid, then painting the solvated membrane with the electrode mixture, followed by hot pressing gold electrodes on the outer edges.[2]

Prior to the DAP, a widely used method was the impregnation-reduction process which involves electroless chemical plating on ion selective ionomers. First the ionomer is soaked in a metal salt solution to add a metal that is reduced in the second step with sodium or lithium borohydride. Then the polymer is electroplated with a thin gold electrode. This technique yields

good polymer-metal interfacial area but the high density of metal particles limits the amount of electrolyte that can be stored and thereby reduces the actuator function.[2, 15, 39] A variation of this technique was performed by the same group in which metal or graphite particles are incorporated into the ionomer by physical loading. Metal powders are hot pressed on the ionomer surface, and then the impregnation-reduction method is used.[2, 23]

1.2.5 Improvements in CNCs in IPMC actuators:

Our group and collaborators have shown that IPCNC actuators composed of self-assembled CNC layers have increased strain and faster response time compared to other IPCNC actuators with CNC layers fabricated via other techniques.[20] In fact, S. Liu *et al.*[24] displayed that actuators with a gold nanoparticle and PAH CNC fabricated via the layer-by-layer self-assembly method, showed a 0.18 s response time, compared to a 1.03 s response time for a DAP fabricated CNC made of a RuO_2 and Nafion nanocomposite. Additionally the strain produced by the gold nanoparticle/PAH actuator was more than twice the strain produced by the RuO_2/Nafion nanocomposite actuator under the same conditions.[2, 24]

One desirable characteristic of the CNC includes a porous structure, which can be thought of as a high surface area electrode. The large surface area allows ions to move more freely, and results in enhanced bending and strain when a large number of mobile ions collect at the electrodes. The DAP method was an improvement of the porosity and surface area of the CNC, due to the nanosized metal particles. It also provides a simpler fabrication method and results in actuators that that have a higher performance than IPCNC actuators fabricated through other methods. However, IPCNC actuators fabricated through the layer-by-layer self-assembly method have shown even greater bending performance and strain production. The self-assembled structure is porous, as is the DAP structure, but the self-assembled structure is thinner compared to the DAP structure. This contributes to the increased performance of the LbL self-assembled IPCNC actuator.[15, 25] Other benefits of the LbL self-assembly method for building CNCs include that it is self-limiting; once the charge of the layer is neutralized, the next layer will not continue to deposit on the surface. In addition, it is a simple, inexpensive, well-controlled, and replicable process for producing nanoscale thin films.[40, 41]

In IPCNC actuators, some of the major goals for improving actuator performance are to increase the actuation speed, bending strain, efficiency, and lifetime for a working actuator.[25] Effort is also focused on fabricating soft and light actuators that function at a low operating

voltage, but these tasks are largely being accomplished by work on IPCNCs, as the ionomers used in these actuators fit both of these requirements. Ion motion through the CNC depends on the structure of small channels inside and the interaction between the mobile ions and the CNC molecules.[15] A major area where improvement is still desired is in understanding the ion transport process through the ionomer membrane and the CNC. Understanding ion transport will allow for better optimization of actuator performance. Despite the progress in IPCNC actuator performance, an IPCNC actuator with high strain and fast ion transport is still needed.

The ISAM CNC has been studied to gain understanding of its structure and effects on the actuator performance. These CNCs were composed of gold nanoparticles and PAH, which are the most commonly used CNC materials for self-assembly fabrication. The concentration of gold nanoparticles in the CNC was varied in order to provide information on how concentration of gold nanoparticles during the fabrication process affected the actuator performance. It was found that higher concentrations of gold nanoparticles resulted in actuators that bent more quickly and produced a larger strain.[36]

Performance comparisons between the self-assembly fabrication method to other methods such as the DAP have been made. S. Liu *et al.*[42] showed that self-assembled IPCNC actuators had better actuation performance and speed when compared to the direct assembled IPCNCs. This is a result of the thinner CNC layers generated by electrostatic self-assembly, which deposits nanoscale thin films with each monolayer. There is a tradeoff between thicker CNCs, which are capable of providing more strain to the actuation, and thinner CNCs, which provide faster bending.[25]

Montazami *et al.*[15] focused on understanding how the number of layers in the self-assembled CNC affected actuator performance. Each additional bilayer added 2 nm to the actuator thickness. Thicker CNCs allowed for larger actuation. Maximum bending curvature increased linearly with increasing thickness of the CNC since a thicker CNC stores more ions. This allows for a greater volume imbalance in the membrane, causing more bending. The net intrinsic strain was independent of CNC thickness, implying that the whole CNC provides an equal contribution to actuation for the studied range of 10 to 40 bilayers. Actuation time for the anionic motion was also independent of the number of CNC layers, thus Montazami *et al*.[15] concluded that the anion transport through the Nafion ionomer is the limiting factor.[15]

Modeling has also been an important area of research in order to better understand IPCNC systems. Equivalent circuit modeling is used to determine the complex frequency-dependent impedance of the actuator system, which provides understanding of ion movement.[26] Nonlinear dynamic modeling has been used in an attempt to predict IPMC and IPCNC actuator behavior.[20] Further, other modeling studies to understand charge conduction and bending have been completed.[3, 4, 18]

Ion transport through both self-assembled and direct assembled IPCNC actuators were studied by Y. Liu *et al.*[13] These results showed that cation motion was faster than anion motion, as predicted from diffusion data from NMR measurements, and that anions produce more strain during bending. This was attributed to either the anions aggregating inside the CNC or the anions interacting more strongly with the CNC.[35]

Other research focused on applying self-assembled CNCs to newly fabricated ionomers instead of the commonly used, commercially available Nafion. CNCs composed of gold nanoparticles and PAH were applied to two imidazolium ABA triblock copolymers and an imidazolium sulfonate-containing pentablock copolymer. Both copolymers displayed promising results in ionic conductivity, ion concentration, bending curvature, and static dielectric constant.[7, 9, 27] Another new ABA triblock copolymer was fabricated using RAFT synthesis, and was shown to be electroactive and could provide a method for tuning and better understanding the structure and morphology of IPCNC actuators.[21]

1.2.6 Characterization techniques for IPMC actuators

A number of characterization techniques that evaluate electrical, mechanical, and structural properties are used to determine actuator performance - ionic conductivity, and strain produced, among other actuator characteristics. A number of groups studied the ion exchange capacity (IEC), of the ionomer membrane, which can be calculated, as well as the in the CNC. The IEC is an important characteristic for determining actuator functionality. Ionic conductivity is another important measurement obtained by using impedance spectroscopy. For both IEC and ionic conductivity measurements, higher values are desired traits for improving actuator performance.[7, 9, 12, 21, 27, 29, 40, 43] Bending has been measured by non-contact laser vibrometers that measure distance moved during bending, as well as actuation speed, and stiffness, which is another important property that is characterized. Strain is an important property that can be calculated using the free deflection frequency response obtained from these measurements.[1, 2, 4]

Other techniques to measure actuator bending use CCD cameras to record the bending process, where it is later analyzed through image processing.[24, 36, 37]

Mechanical material properties are important to electromechanical actuator performance determination in addition to electrical and conductivity properties. Load cells have been used to measure stress in IEAP actuator samples, and elastic modulus is another material property important in choosing better actuators.[15, 23-25] Other techniques that have been used in evaluating the structure of such devices are x-ray photoelectron spectroscopy (XPS) and scanning electron microscopy (SEM). XPS was used to study the metal content in a variation of the IEAP actuators with platinum nanocluster/polymer composites on self-assembled actuators.[44] SEM is another tool for obtaining structural information of the CNC on IPCNC actuators.[3, 15, 25] Lastly, as these IPMC actuators depend on water or ionic liquid ions for the actuation mechanism, humidity is an important factor in bending performance, and as such, measurements are taken at different percent relative humidity in the surrounding environment.[40, 43]

1.3 Self-assembly

Ionic self-assembled multilayers (ISAM), also called electrostatic layer-by-layer deposition is a bottom-up film growth process that relies on sequential adsorption of oppositely charged species. A charged substrate is used to start the process, followed by deposition of a material with opposite charge than the substrate. This occurs simply by submerging the substrate in a solution containing the polyelectrolyte, and a layer of material deposits in usually just a few minutes. This overcompensates for the surface charge, allowing for another layer of material with the same charge as the substrate to be deposited in the same way. Growth is self-limiting in that once the surface charge has been neutralized, further deposition cannot occur. In this manner, a multilayer film can be formed by repetitive depositions between oppositely charged substances, for many layers.[40, 41, 43] LbL films are commonly fabricated by immersion in solution, but other techniques like spraying have been used as well.[45]

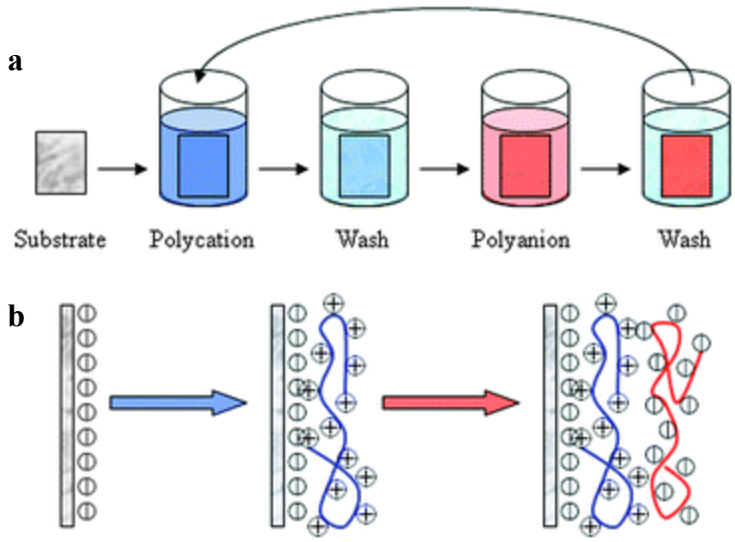

Figure 1.3: The top image sequence shows the LbL film growth process. The substrate is dipped in the polycation solution, followed by rinsing, dipping in the anion solution, then another rinsing step. The bottom image sequence shows the film growth after the polycation deposition step, and then the polyanion deposition step. Reproduced from Y. Xiang, S. Lu and S. P. Jiang, Chemical Society Reviews 41 (21), 7291-7321 (2012). with permission of The Royal Society of Chemistry.[46]

Layer-by-layer (LbL) films have been used in numerous applications and devices, just a few of which include reducing methanol crossover in direct methanol fuel cells[47-50], biosensors[51, 52], electrochromic devices[53-55], and humidity sensors.[56, 57] The technique has been widely used since its initial rediscovery by Decher and Hong[41, 58] in 1991, even though a similar technique was debuted in the 1960s by Iler.[59] It applicability stems from the variety of materials that can be assembled through this technique, which requires only a material with multiple charges such as charged nanoparticles, polyelectrolytes, and biological molecules. Additionally, films grown through the LbL process can be tailored on the nanoscale, show self-limiting growth, and are typically very thin. It's a simple and inexpensive process that builds well-controlled, reproducible thin films.[40, 41] LbL films are not restricted to crosslinking bonds by electrostatic forces. Hydrogen-bonding is also well documented for forming LbL films.[60-66] Non-planar geometries can also be used for film substrates.[40]

The charge density necessary for LbL film growth was studied by Sun et al.[67] using a copolymer polyelectrolyte by varying the mole fraction of the charged group in the copolymer. Below a certain charge density, the polyelectrolyte cannot form a layer because it is no longer

charged enough to deposit, or will get removed in the rinsing process because the electrostatic attraction between the few charged groups left is not enough to hold it together.

1.4 Tailoring ISAM film morphology through solution properties

There are several ways that ISAM or LbL films can be tailored on a molecular level. Fully charged polyelectrolytes deposit in relatively flat, straight chains. Changing the number of charges available for binding adjusts how the depositing layer arranges itself. Deposition solution concentration, pH, charge density, ionic screening, molecular weight, all affect the final film. But pH and salt concentration, which governs ionic screening, are accepted as the most impactful parameters.[43, 61, 68-73]

Charge density of strong polyelectrolytes is not significantly affected by changes in pH.[69, 74] There are a large number of sites on the polymer chain that can bind electrostatically, and charge density is most strongly affected by ionic screening. The polymer chain conformation and resulting thickness of the layer can be modified by changing the concentration of binding sites by adding a salt such as sodium chloride to reduce the number of sites. The salt inhibits some of those sites from binding to the underlying layer, and the chain between charged sites arranges itself in a loopy, thicker layer, since the electrostatic reduced repulsion between charges no longer forces the chain to straighten.[43, 75-77] At low salt concentrations, this causes an increase in layer thickness, which is called screening-enhanced adsorption. As the addition of salt continues, charged binding sites become so few and far between that film growth is restricted, and eventually stops altogether, in a process called screening-reduced adsorption.[43, 75]

However for weak polyelectrolytes, changing the solution pH is enough to affect the charged sites available for binding. For weak polyelectrolytes, even a small change in pH is enough to drastically change the degree of ionization of the polymer chain.[69, 72, 78]

1.5 Linear and Exponential ISAM Film Growth

ISAM films usually grow linearly with each increasing bilayer adsorption, though usually the first few layers may deviate from this pattern as a result of substrate effects.[79] However, several groups have reported ISAM films that show that the adsorbing bilayer thickness increases with each deposition step, so that the film grows exponentially with increasing layer deposition.[80-84] Exponential growth occurs as a result of the adsorbing layer diffusing through the multilayer film, instead of just depositing on the surface. More material is deposited with

each layer, resulting in exponential film thickness growth.[81, 85, 86] The strength of the bonding interactions between polyelectrolytes is acknowledged as a large contributor to determining the growth mode.[87] Dipping time also affects the film growth. If the time length is too short for the adsorbing layer to diffuse throughout the film, then more linear growth is observed.[88] Molecular weight[89] and steric hindrance[48, 87] are also factors governing polyelectrolye diffusion and therefore the growth regime. Further, the grown mode can change even using the same polyelectrolytes by modulating interaction strength with salt[90, 91] or pH adjustments.[89, 92]

1.6 Summary and Thesis Contents

Ionic polymer-metal composite actuators with highly porous conductive network composite electrodes show promise for application in a number of technologies. Their low weight and large bending under low voltages are characteristics that are highly desirable in many fields. Additionally, IPCNC actuators with CNCs fabricated via electrostatic self-assembly are even more attractive because of the low cost of the simple fabrication process, as well as the thin layers resulting from the easily automated and repeatable layer-by-layer self-assembly process. These actuators have been shown to provide larger bending capability and higher strain than other types of IPCNCs fabricated via the direct assembly process or even electroless plating. While much progress has been made in improving these traits, further improvements must be made in order to understand the ion transport in such structures, and its effect on the bending and strain production capability. Also further research is needed to improve the lifetime and energy conversion efficiency in these devices. Improvements in these areas will provide optimization of the CNC in IPMC actuators.

Nafion based IPMC actuators have shown promising results in terms of bending curvature and time, and the addition of a CNC improves these characteristics. Thin CNCs fabricated through the ISAM process enhance actuation further. However, since LbL CNCs have not previously contained ion conducting polymers, we hypothesized that their inclusion could further enhance actuator performance in bending speed and curvature.

PAMPS and Nafion are well known ion conducting polymers, and have been used in other LbL film applications to enhance ionic conductivity. As a result of their success elsewhere, we anticipated that including them in the CNC might contribute to bending curvature and speed. This thesis presents the results of IPMC actuators with CNCs containing PAMPS and Nafion. 30 bilayers of PAH/AuNPs was replaced with 15 quadlayers of

PAH/AuNPs/PAH/PAMPS or PAH/AuNPs/PAH/Nafion. The AuNPs could not be completely eliminated since they serve the important function of providing a high surface area electrode with high porosity. The ISAM CNC film was optimized by varying the pH of PAH in the PAMPS-containing films, and the NaCl concentration in both PAMPS and Nafion, and testing the resulting films.

CNCs were evaluated by thickness measurements and ionic liquid uptake of actuator samples, both of which provide indications of the structure of the ISAM film on a molecular level. Further testing of the actuator bending was completed using a homemade setup as pictured and described in Section 2.6. Actuator samples were cut into strips and placed under constant DC voltage for several minutes. Bidirectional bending was recorded as a function of curvature versus time. Several samples of each type of CNC were fabricated and compared. PAMPS-containing samples were compared to each other, as were Nafion containing samples. Finally, the largest and fastest bending samples of each ion conducting material were compared. In both materials, we saw that thicker CNCs showed reduced cation bending speed but increased curvature. Thicker CNCs include those with larger pH and/or increased salt concentration for ionic screening. Thinner CNCs, such as those produced at pH 4.0 PAH with little or no salt produced enhanced anionic bending curvature as well as both increased cationic and anionic bending speed. Improvements over the control CNC samples (PAH/AuNPs only, no salt) were shown in both PAMPS and Nafion containing samples. These results indicate that the introduction of ion conducting polyelectrolytes within the CNC does improve actuator function under the proper LbL assembly conditions.

When the samples displaying the largest cationic and anionic bending for PAMPS and Nafion were compared, the PAMPS-containing sample showed larger and faster bending deformation overall. Cationic bending curvatures for the two polymer types were closer, indicating the anionic bending may be more strongly affected by the differences between PAMPS and Nafion.

Another major focus of this thesis is on IPMC actuator samples with PAH/AuNP CNCs, and their long-term current response under a constant applied voltage and varied relative humidity conditions for possible hygrometer applications. Humidity was controlled in the test chamber, voltage was controlled and current was measured through an impedance analyzer. The IPMC actuator's detectable humidity range was explored by determining the steady-state

electrolysis current through both a wide range of relative humidity as well as a narrow range. Current values from at least 10-80 percent relative humidity (%RH) in 10% increments can be clearly differentiated, and differentiation between smaller %RH differences appear readily obtainable. A range of test voltages were studied at low and high %RH to identify a test voltage that would prevent actuator currents from exceeding the detection range of the impedance analyzer, but would be large enough for water electrolysis. 2.5 V was chosen for all subsequent tests.

The effects of ionic liquid concentration in the IPMC actuator-based hygrometer was studied, as well as the effect of PAH pH, and the resulting CNC thickness. While the device worked under all sample conditions, greater ionic liquid content allowed for faster ion motion, and therefore a faster steady-state current response. Samples with no ionic liquid however had a slightly more stable steady-state current, and a larger current difference between low and high %RH. The pH of PAH in the CNC did not have an apparent strong effect.

Finally, the response speed for large changes in %RH were studied and compared to the response speed of a commercial fast hygrometer used to determine relative humidity in the chamber for all experiments. The relative speed showed very promising results, with an ionic liquid containing IPMC actuator sample responding approximately 4 times faster than the capacitive fast digital hygrometer. Samples with no ionic liquid responded slightly slower, but still more than 3 times faster than the digital hygrometer. The CNC also contributed to the response speed, since the IPMC actuator samples with a CNC had an increased response speed over those without a CNC. Results on the ion conducting polymers in the CNC of an IPMC actuator as well as IPMC actuators for humidity sensing are very promising for future work. Further details and results are discussed in the following chapters.

1.7 References

1. B. J. Akle, M. D. Bennett and D. J. Leo, Sensors and Actuators A: Physical **126** (1), 173-181 (2006).
2. B. J. Akle, M. D. Bennett, D. J. Leo, K. B. Wiles and J. E. McGrath, Journal of Materials Science **42** (16), 7031-7041 (2007).
3. B. J. Akle, W. Habchi, T. Wallmersperger, E. J. Akle and D. J. Leo, Journal of Applied Physics **109** (7), 074509 (2011).
4. B. J. Akle and D. J. Leo, Smart Mater Struct **16** (4), 1348-1360 (2007).

5. A. J. Duncan, S. A. Sarles, D. J. Leo, T. E. Long, B. J. Akle and M. D. Bennett, presented at the SPIE Electroactive Polymers and Devices 2008 (unpublished).
6. R. Gao, D. Wang, J. R. Heflin and T. E. Long, Journal of Materials Chemistry **22** (27), 13473 (2012).
7. M. D. Green, D. Wang, S. T. Hemp, J. H. Choi, K. I. Winey, J. R. Heflin and T. E. Long, Polymer **53** (17), 3677-3686 (2012).
8. Inamuddin, A. Khan, M. Luqman and A. Dutta, Sensor Actuat a-Phys **216**, 295-300 (2014).
9. C. Jangu, J.-H. H. Wang, D. Wang, S. Sharick, J. R. Heflin, K. I. Winey, R. H. Colby and T. E. Long, Macromol Chem Phys **215** (13), 1319-1331 (2014).
10. K. B. Joshi, B. J. Akle, D. J. Leo and S. Priya, Proc Spie **7975** (2011).
11. S. W. Lee, J. W. Kim, Y. H. Kim, S.-H. Lee and J. Y. Jho, Macromolecular Research **21** (6), 699-703 (2012).
12. S. W. Lee, S. N. You, S.-H. Lee and J. Y. Jho, Macromolecular Research **21** (6), 704-708 (2012).
13. Y. Liu, S. Liu, J. H. Lin, D. Wang, V. Jain, R. Montazami, J. R. Heflin, J. Li, L. Madsen and Q. M. Zhang, Appl Phys Lett **96** (22), 223503 (2010).
14. A. A. A. Moghadam, W. Y. J. Hong, A. Kouzani, A. Kaynak, R. Zamani and R. Montazami, Sensor Actuat a-Phys **217**, 168-182 (2014).
15. R. Montazami, S. Liu, Y. Liu, D. Wang, Q. Zhang and J. R. Heflin, Journal of Applied Physics **109** (10), 104301 (2011).
16. M. Shahinpoor and K. J. Kim, Sensor Actuat a-Phys (2002).
17. L. Supriya and R. O. Claus, Ieee Sensor, 619-622 (2004).
18. T. Wallmersperger, B. J. Akle, D. J. Leo and B. Kroplin, Compos Sci Technol **68** (5), 1173-1180 (2008).
19. M. D. Bennett, D. J. Leo, G. L. Wilkes, F. L. Beyer and T. W. Pechar, Polymer **47** (19), 6782-6796 (2006).
20. A. A. A. Moghadam, W. Hong, A. Kouzani and A. Kaynak, Sensors and Actuators A: Physical **212**, 168-182 (2014).
21. T. Wu, D. Wang, M. Zhang, J. R. Heflin, R. B. Moore and T. E. Long, ACS applied materials & interfaces **4** (12), 6552-6559 (2012).
22. K. B. Joshi, B. J. Akle and D. J. Leo, Proc. SPIE 7975 **7975** (2011).
23. M. Shahinpoor and K. J. Kim, Sensors and Actuators A: Physical (2002).
24. S. Liu, R. Montazami, Y. Liu, V. Jain, M. Lin, J. R. Heflin and Q. M. Zhang, Appl Phys Lett **95** (2), 023505 (2009).
25. S. Liu, R. Montazami, Y. Liu, V. Jain, M. Lin and X. Zhou, Sensors and Actuators A: Physical **157** (2), 267-275 (2010).
26. Y. Liu, R. Zhao, M. Ghaffari, J. Lin, S. Liu and H. Cebeci, Sensors and Actuators A: Physical **181**, 70-76 (2012).
27. R. Gao, D. Wang, J. R. Heflin and T. E. Long, Journal of Materials Chemistry **22** (27), 13473-13476 (2012).
28. B. Jeong and A. Gutowska, TRENDS in Biotechnology **20** (7), 305-311 (2002).
29. A. J. Duncan, S. A. Sarles and D. J. Leo, Proc. SPIE 6927 (2008).
30. I. Must, V. Vunder, F. Kaasik, I. Põldsalu, U. Johanson, A. Punning and A. Aabloo, Sensor Actuat B-Chem **202**, 114-122 (2014).
31. B. J. Akle and D. J. Leo, J Intel Mat Syst Str **19** (8), 905-915 (2008).

32. M. D. Bennett and D. J. Leo, Sensors and Actuators A: Physical **115** (1), 79-90 (2004).
33. Y. Liu, C. Lu, S. Twigg, M. Ghaffari, J. Lin, N. Winograd and Q. M. Zhang, Scientific Reports **3**, 973 (2013).
34. D. S.-d. la Cruz, M. D. Green, Y. Ye, Y. A. Elabd, T. E. Long and K. I. Winey, Journal of Polymer Science Part B: Polymer Physics **50** (5), 338-346 (2012).
35. Y. Liu, S. Liu, J. Lin, D. Wang, V. Jain, R. Montazami, J. R. Heflin, J. Li, L. Madsen and Q. M. Zhang, Appl Phys Lett **96** (22), 223503 (2010).
36. R. Montazami, D. Wang and J. R. Heflin, International Journal of Smart and Nano Materials **3** (3), 204-213 (2012).
37. W. Hong, C. Meis, J. R. Heflin and R. Montazami, Sensor Actuat B-Chem **205**, 371-376 (2014).
38. J. Hou, Z. Zhang and L. A. Madsen, The Journal of Physical Chemistry B **115** (16), 4576-4582 (2011).
39. K. J. Kim and M. Shahinpoor, Smart Materials and Structures **12** (1), 65-79 (2003).
40. P. T. Hammond, Adv Mater **16** (15), 1271-1293 (2004).
41. G. Decher and J.-D. Hong, Makromol Chem-M Symp **46** (1), 321-327 (1991).
42. S. Liu, R. Montazami, Y. Liu, V. Jain, M. R. Lin, X. Zhou, J. R. Heflin and Q. M. Zhang, Sensor Actuat a-Phys **157** (2), 267-275 (2010).
43. D. M. DeLongchamp and P. T. Hammond, Chem Mater **15** (5), 1165-1173 (2003).
44. T. Zeng, R. Claus, F. Zhang and W. Du, Smart Materials and Structures **10** (4), 780 (2001).
45. J. N. Ashcraft, A. A. Argun and P. T. Hammond, Journal of Materials Chemistry **20** (30), 6250-6257 (2010).
46. Y. Xiang, S. Lu and S. P. Jiang, Chemical Society Reviews **41** (21), 7291-7321 (2012).
47. S. P. Jiang, Z. Liu and Z. Q. Tian, Adv Mater **18** (8), 1068-1072 (2006).
48. S. P. Jiang and H. Tang, Colloid Surface A **407**, 49-57 (2012).
49. S. Yılmaztürk, H. Deligöz, M. Yılmazoğlu, H. Damyan, F. Öksüzömer, S. N. Koç, A. Durmuş and M. Ali Gürkaynak, Journal of Power Sources **195** (3), 703-709 (2010).
50. S. Yılmaztürk, H. Deligöz, M. Yılmazoğlu, H. Damyan, F. Öksüzömer, S. N. Koç, A. Durmuş and M. A. Gürkaynak, Journal of Membrane Science **343** (1–2), 137-146 (2009).
51. C. Guo, H. Sun and X. S. Zhao, Sensor Actuat B-Chem **164** (1), 82-89 (2012).
52. V. Srinivasaraghavan, J. Strobl, D. Wang, J. R. Heflin and M. Agah, Biomed Microdevices **16** (5), 689-696 (2014).
53. D. DeLongchamp and P. T. Hammond, Adv Mater **13** (19), 1455-1459 (2001).
54. J. A. Janik, J. R. Heflin, D. Marciu, M. B. Miller, H. Wang, H. W. Gibson and R. M. Davis, 2001 (unpublished).
55. R. Montazami, V. Jain and J. R. Heflin, Electrochim Acta **56** (2), 990-994 (2010).
56. P.-G. Su and K.-H. Cheng, Sensor Actuat B-Chem **137** (2), 555-560 (2009).
57. P.-G. Su, W.-C. Li, J.-Y. Tseng and C.-J. Ho, Sensor Actuat B-Chem **153** (1), 29-36 (2011).
58. G. Decher and J. D. Hong, Berichte der Bunsengesellschaft für physikalische Chemie **95** (11), 1430-1434 (1991).
59. R. K. Iler, J Colloid Interf Sci **21** (6), 569-594 (1966).
60. E. Kharlampieva, V. Kozlovskaya and S. A. Sukhishvili, Adv Mater **21** (30), 3053-3065 (2009).
61. J. L. Lutkenhaus and P. T. Hammond, Soft Matter **3** (7), 804-816 (2007).

62. J. L. Lutkenhaus, K. D. Hrabak, K. McEnnis and P. T. Hammond, Journal of the American Chemical Society **127** (49), 17228-17234 (2005).
63. M. Z. Markarian, M. D. Moussallem, H. W. Jomaa and J. B. Schlenoff, Biomacromolecules **8** (1), 59-64 (2007).
64. W. B. Stockton and M. F. Rubner, Macromolecules **30** (9), 2717-2725 (1997).
65. S. Yang, Y. Zhang, Y. Guan, S. Tan, J. Xu, S. Cheng and X. Zhang, Soft Matter **2** (8), 699-704 (2006).
66. S. A. Sukhishvili and S. Granick, Macromolecules **35** (1), 301-310 (2002).
67. Q. Sun, Z. Tong, C. Wang, B. Ren, X. Liu and F. Zeng, Polymer **46** (13), 4958-4966 (2005).
68. S. Boddohi, C. E. Killingsworth and M. J. Kipper, Biomacromolecules **9** (7), 2021-2028 (2008).
69. J. Choi and M. F. Rubner, Macromolecules **38** (1), 116-124 (2005).
70. S. T. Dubas and J. B. Schlenoff, Macromolecules **34** (11), 3736-3740 (2001).
71. A. Garg, J. R. Heflin, H. W. Gibson and R. M. Davis, Langmuir **24** (19), 10887-10894 (2008).
72. S. S. Shiratori and M. F. Rubner, Macromolecules **33** (11), 4213-4219 (2000).
73. Z. Sui, D. Salloum and J. B. Schlenoff, Langmuir **19** (6), 2491-2495 (2003).
74. N. S. Zacharia, M. Modestino and P. T. Hammond, Macromolecules **40** (26), 9523-9528 (2007).
75. H. G. M. Van de Steeg, M. A. Cohen Stuart, A. De Keizer and B. H. Bijsterbosch, Langmuir **8** (10), 2538-2546 (1992).
76. Y. Lvov, G. Decher and H. Moehwald, Langmuir **9** (2), 481-486 (1993).
77. S. L. Clark, M. F. Montague and P. T. Hammond, Macromolecules **30** (23), 7237-7244 (1997).
78. D. Yoo, S. S. Shiratori and M. F. Rubner, Macromolecules **31** (13), 4309-4318 (1998).
79. N. S. Zacharia, D. M. DeLongchamp, M. Modestino and P. T. Hammond, Macromolecules **40** (5), 1598-1603 (2007).
80. D. L. Elbert, C. B. Herbert and J. A. Hubbell, Langmuir **15** (16), 5355-5362 (1999).
81. L. Richert, P. Lavalle, E. Payan, X. Z. Shu, G. D. Prestwich, J.-F. Stoltz, P. Schaaf, J.-C. Voegel and C. Picart, Langmuir **20** (2), 448-458 (2004).
82. T. J. Halthur and U. M. Elofsson, Langmuir **20** (5), 1739-1745 (2004).
83. P. Kujawa, P. Moraille, J. Sanchez, A. Badia and F. M. Winnik, Journal of the American Chemical Society **127** (25), 9224-9234 (2005).
84. C. Picart, P. Lavalle, P. Hubert, F. J. G. Cuisinier, G. Decher, P. Schaaf and J. C. Voegel, Langmuir **17** (23), 7414-7424 (2001).
85. C. Picart, J. Mutterer, L. Richert, Y. Luo, G. D. Prestwich, P. Schaaf, J.-C. Voegel and P. Lavalle, Proceedings of the National Academy of Sciences **99** (20), 12531-12535 (2002).
86. P. Lavalle, V. Vivet, N. Jessel, G. Decher, J.-C. Voegel, P. J. Mesini and P. Schaaf, Macromolecules **37** (3), 1159-1162 (2004).
87. L. Xu, D. Pristinski, A. Zhuk, C. Stoddart, J. F. Ankner and S. A. Sukhishvili, Macromolecules **45** (9), 3892-3901 (2012).
88. N. Hoda and R. G. Larson, The Journal of Physical Chemistry B **113** (13), 4232-4241 (2009).
89. B. Sun, C. M. Jewell, N. J. Fredin and D. M. Lynn, Langmuir **23** (16), 8452-8459 (2007).

90. G. Liu, J. Zhao, Q. Sun and G. Zhang, The Journal of Physical Chemistry B **112** (11), 3333-3338 (2008).
91. S. T. Dubas and J. B. Schlenoff, Macromolecules **32** (24), 8153-8160 (1999).
92. K. Itano, J. Choi and M. F. Rubner, Macromolecules **38** (8), 3450-3460 (2005).

Chapter 2: Methods for ISAM Film Growth, Actuator Fabrication, and Testing

The following subsections detail typical ISAM film deposition for fabricating actuator samples for testing. Films are also grown on glass substrates for thickness characterization. Following ISAM film growth, actuator samples are soaked in ionic liquid and have gold electrodes added. After sample preparation is complete, they are tested using a setup designed to determine bending curvature as a function of time.

2.1 Substrate Preparation

Glass substrates were prepared for film growth by rinsing and wiping with acetone, followed by a quick isopropyl alcohol rinse with subsequent reverse osmosis (RO) water. Then the substrate was dried with nitrogen before mounting onto the sample holder. Frames for film mounting are cleaned with isopropyl alcohol, rinsed with RO water, and dried with nitrogen gas. Nafion film substrates were mounted onto the edges of a thin polycarbonate frame using double stick tape. No additional process is needed to induce negative charges on the substrates in order to begin film growth with a cationic polyelectrolyte.

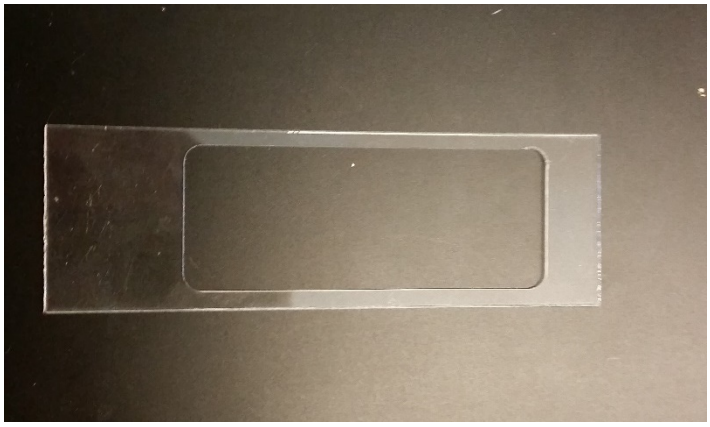

Figure 2.1: Plastic frame used for mounting Nafion films during LbL film deposition.

2.2 Ionic Self-Assembled Multilayer Film Deposition

ISAM (also known as polyelectrolyte multilayer or PEM) film growth was completed in a Nanostrata Stratosequence VI programmable dipping robot. The dipping robot holds eight 120 mL beakers that typically contain either polyelectrolyte solutions or water. It includes a pump that can be used to replace and refill water for each rinsing step, so that each rotation is provided with clean water. The sample holder rotates during each deposition and rinsing step, and the

time length for each is individually programmable. However, there is a mismatch between the time measured by the program controller and real time, so deposition times are approximate, but consistent.

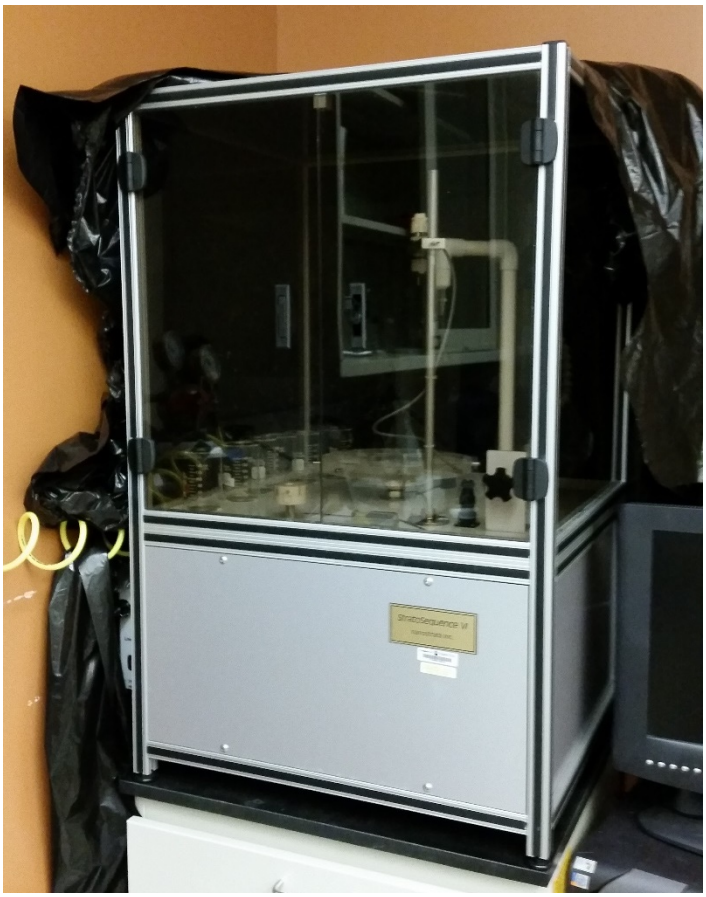

Figure 2.2: Nanostrata programmable dipping robot.

Bilayers of poly(allylamine hydrochloride) (PAH) (~58,000 M_w, Sigma Aldrich) and ~3 nm gold nanoparticles (AuNPs) (Purest Colloids, Inc.) were deposited for 3 min 40 s on Nafion NR-211 membrane (Ion Power, Inc.). Between each polyelectrolyte (PE) deposition step, samples were rinsed in 3 beakers of RO water for approximately 1 minute each. No drying was used between dipping steps. After PEM film formation, samples were left exposed to the ambient air overnight in order to give time for any residual water within the film left over from formation to equilibrate. Some residual water is still present within the film since Nafion retains water even after drying.[1]

2.3 Thickness Determination

In order to measure the thickness of the partially complete layer structure, a sample on a glass substrate was removed from the dipping robot after every 10 bilayers or 5 quadlayers, in order to determine how film thickness was affected by increasing layer number. The robot was then immediately restarted to minimize film drying before growth was finished.

Thickness measurements were completed using a Veeco Dektak 150 surface profiler. Samples on glass substrates only were measured by making a scratch in the multilayer film by hand, with plastic tweezers, in order to prevent scratching the underlying glass, and therefore a misleading thickness measurement. The step height of the scratch was measured in several places for each sample, and the results were averaged. Roughness values were obtained through this process as well.

2.4 Ionic Liquid Soaking

After film thickness was measured, the Nafion film coated with the CNC was soaked in 1-ethyl-3-methylimidazolium trifluoromethanesulfonate (EMI-Tf) ionic liquid (Sigma Aldrich). EMI-Tf was chosen as the ionic liquid because Liu *et al*.[2] found it to have a greater strain response in IPMC actuators with a CNC. Weight percent uptake (wt %, technically w/w%) was determined by cutting a sample of the Nafion/CNC, weighing it, then placing it in the ionic liquid for a period of time. Next, the sample was taken out of the ionic liquid, and excess liquid on the outside was patted dry, which was followed by weighing the sample again. Weight percent uptake was then determined according to the equation below:

$$wt\ \% = \frac{m_{after\ soak} - m_{before\ soak}}{m_{before\ soak}} * 100$$

As the ions contributed by the ionic liquid are the major source of bending motion for the actuator, generally the increased ionic liquid uptake also increases bending.[3-5] For samples that had a goal weight percent uptake, if the uptake was not enough after one soak period, then it was put back in the ionic liquid again in order to get closer, and following that the same steps were repeated.

2.5 Electrode Fabrication

The final step in IPMC actuator fabrication occurs after the ionic liquid soaking. Thin gold (120 nm, L.A. Gold Leaf) electrodes are manually hot pressed on either side at

approximately 900 psi, at 95°C, for 40 seconds. The gold is attached to a paper backing for strength and stability before the gold is attached to something else, which requires removal after hot pressing. The IPMC is allowed to cool, before the backing from the gold foil is removed by carefully peeling it away from the sample. This can be difficult. Smaller samples tend to be imparted with a high degree of bending from this peeling step. They can roll up, and then must be flattened before they can be tested. The curling direction is difficult to keep track of after flattening. However, multiple samples of each set of fabrication parameters were always tested, in order to randomize any particular affinity to bending direction, so that an idea of the potential bending for both sides can be obtained.

2.6 Bending Characterization

Bending measurements are completed in the homemade environmental test chamber shown in Figure 2.3. Relative humidity in the chamber is controlled by an ultrasonic humidifier and nitrogen gas. Humidity is monitored by the Fluke 971 temperature/humidity meter, which is kept inside the chamber close to where the sample is mounted and is kept within ±1.5%RH during testing. Time is always allowed for the humidity in the chamber to equilibrate and for residual voltage in the sample to go down. Samples are typically cut in 1x10 mm^2 strips, and mounted between the two electrodes below the magnifying glass, then conditioned by applying a DC voltage of 4 V and switching the polarity several times after the actuator has reached its maximum cationic bending. This improves the bending in IPMC actuators with a CNC, which is thought to occur through the ion motion creating channels for easier mobility.[6] After conditioning, bending measurements are done under constant DC voltage of 4 V, and the bending is recorded with a Sony HRX-MC1 video camera.

While some of the properties governing bending like ionic solution viscosity and ionic conductivity are dependent on temperature, the temperature in the laboratory stays consistently between about 18-21°C year round.

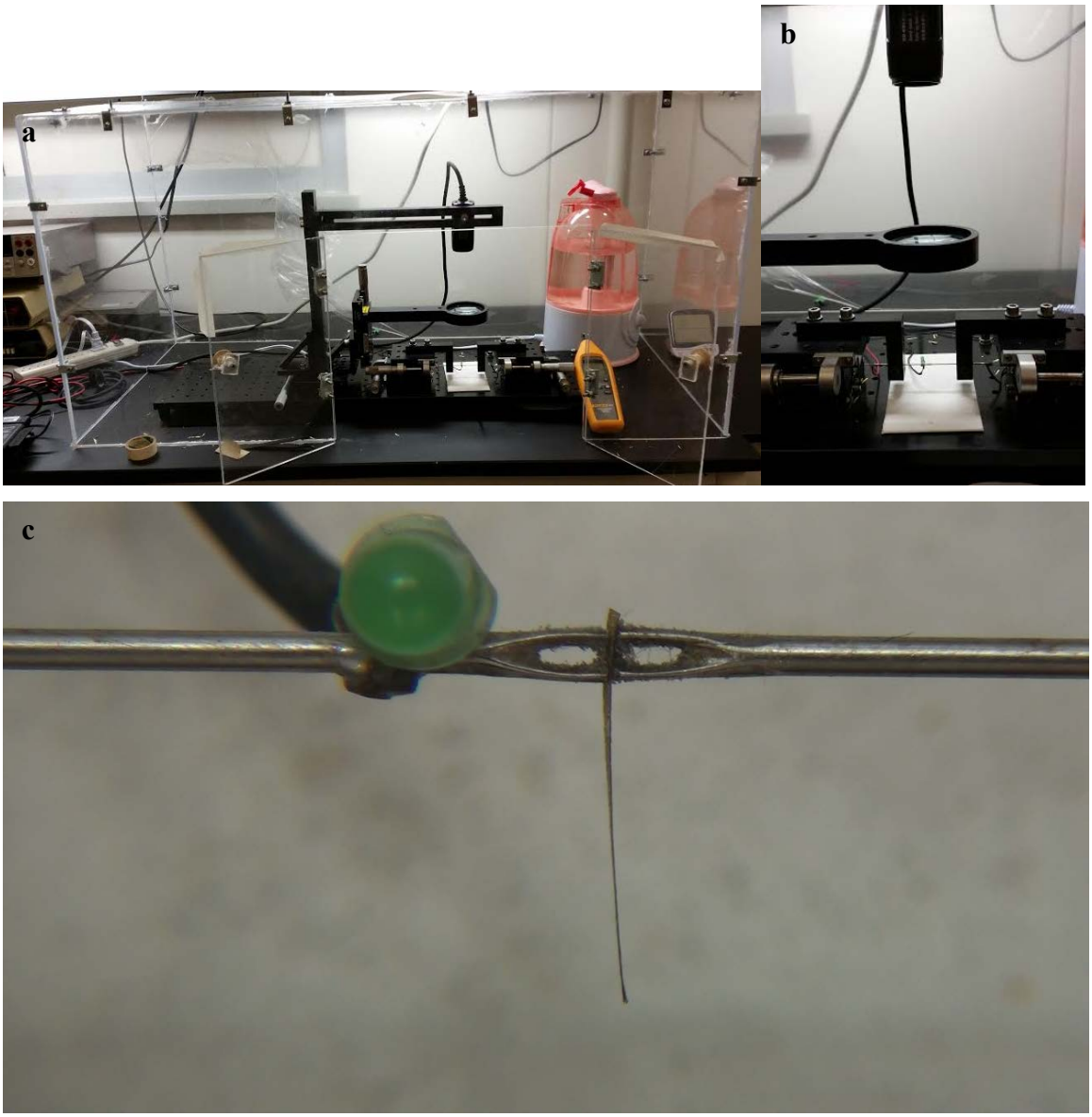

Figure 2.3: (a) Environmentally controlled test chamber, containing mounting station, camera, digital hygrometer, humidifier, and nitrogen gas input. (b) Close-up of sample mounting area, with camera and electrodes. (c) Example of image provided by extracting frames from the HD video.

Bending analysis proceeds by extracting images from the recorded video. Bending curvature (the inverse of radius of curvature) is measured as a function of time. Actuator bending is approximated to the circumference of a circle, which allows for solving for the radius of using the total straight length of the actuator, and the distance between the endpoints when it is bent. This is shown in Figure 2.4 below.

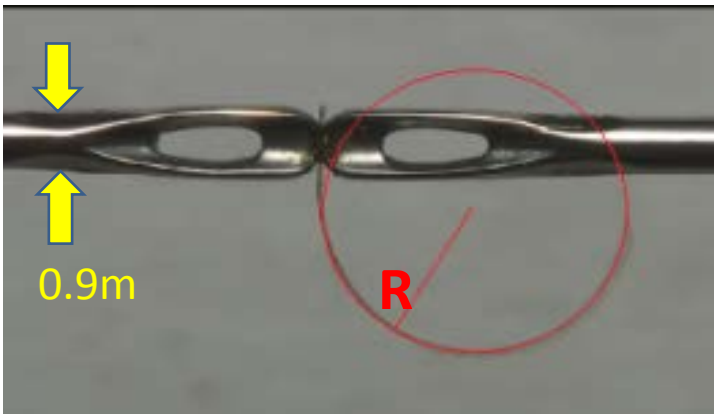

Figure 2.4: The actuator strip follows the overlaid circle during bending.

Two input parameters, l and d are needed. l is the original length of the actuator (segment of circle if the radius is equal to infinity). d is the length of the chord across the segment l when it is curved. If θ is the angle between lines starting at the endpoints of the segment l to the center of the circle (each of length r = radius), then we know that rθ = l. From trigonometry, sin(θ/2) = (d/2)/R. This provides a method for determining the radius of curvature using the original length of the segment and the distance between the endpoints of the segment. However, this is a nonlinear equation that must be solved numerically. Wolfram Mathematica's build in FindRoot function was used in order to solve for this. It is a numerical equation solver that uses Newton's Method.

The first few images in a bending measurement are usually blurry, as the actuator sample moves too quickly for the frame rate of the camera to resolve. The actuator end point of these first few images must be analyzed by hand. Endpoints of subsequent images were detected automatically using Mathematica's ImageFeatureTrack function, which is capable of determining the coordinate of a given point in a series of images. This process was overseen in order to make sure the tip of the sample was accurately tracked. The time for each point is obtained through the image's frame number and the camera's frame rate.

2.7 Initial optimization of pH PAH in actuator samples containing CNCs of PAH/AuNPs

Before any experiments were conducted using new materials, the original CNC ingredients were tested using different pH values for PAH. First, LbL films were fabricated on glass substrates for thickness measurements, as well as on Nafion. Thickness results are shown in Figure 2.5, which indicate film thickness increases with increasing pH PAH. The Nafion

sample was then soaked in EMI-Tf. These samples all had a very high ionic liquid content – approximately 45 wt%, which is about the maximum absorption possible.

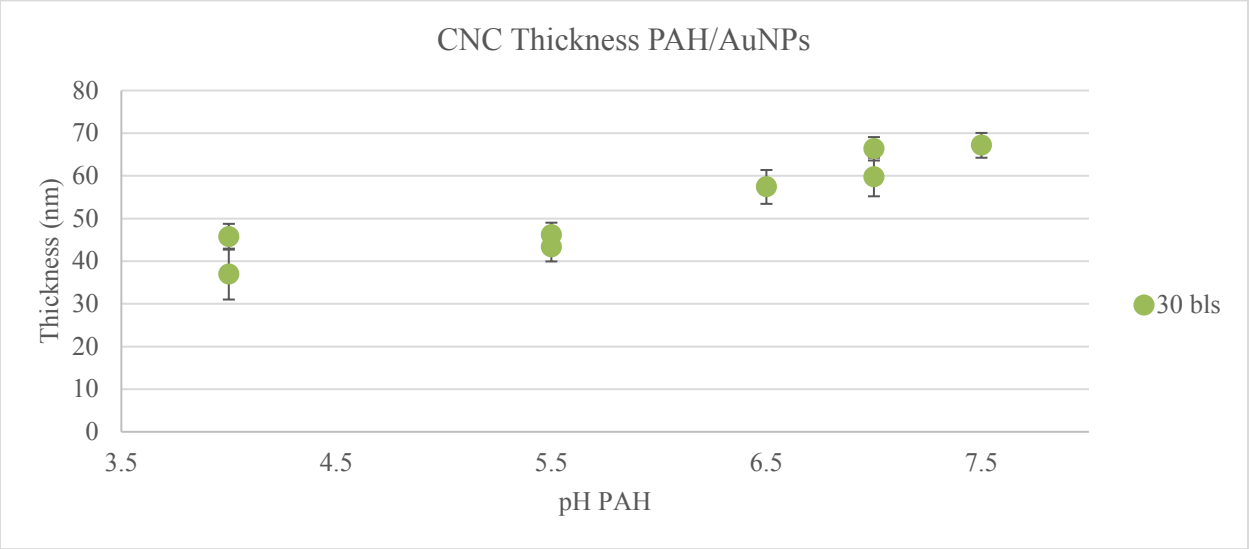

Figure 2.5: Profilometry thickness measurements for 30 bilayers (bls) of PAH/AuNPs at varying pH PAH. Error bars are given by the standard deviation.

After ionic liquid soaking, samples were hot pressed and fabricated into actuator samples. Then bending as a function of time was determined as described in Section 2.6. Several strips of the hot pressed sample were tested. Bending results are plotted in Figure 2.6 on separate plots for each pH. Large variation in the largest positive and negative bending curvatures occurred particularly in pH 4.0 and pH 7.0 samples. Samples with negative curvatures less than -1 indicate that the sample has made a full loop during bending. The largest positive and negative curvature values are also highlighted with data labels for easier differentiation between curves when the data is close together.

In some of the curves with larger maximum positive bending curvature, negative bending is reduced from the other samples. This may be because peeling the gold foil backing after hot pressing causes the sample to roll and then gives it a preferred bending direction. At all pH values, there was less spread in the positive bending curvature, while negative bending showed a much wider range from sample to sample. Several pH 4.0 samples had very large negative bending curvatures, while only one pH 7.0 sample showed a large negative curvature.

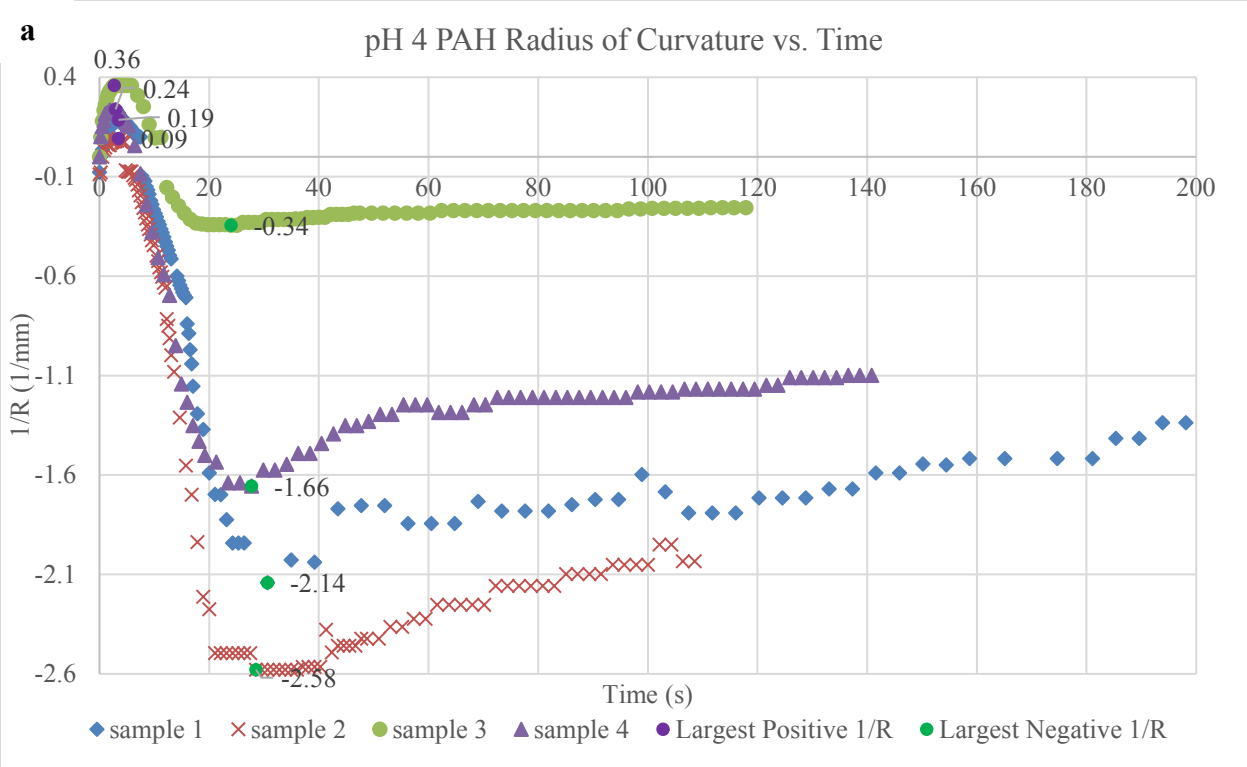
a
pH 4 PAH Radius of Curvature vs. Time
0.36
0.24
0.19
0.09
0.34
-1.66
-2.14
-2.58
1/R (1/mm)
Time (s)
sample 1
sample 2
sample 3
sample 4
Largest Positive 1/R
Largest Negative 1/R

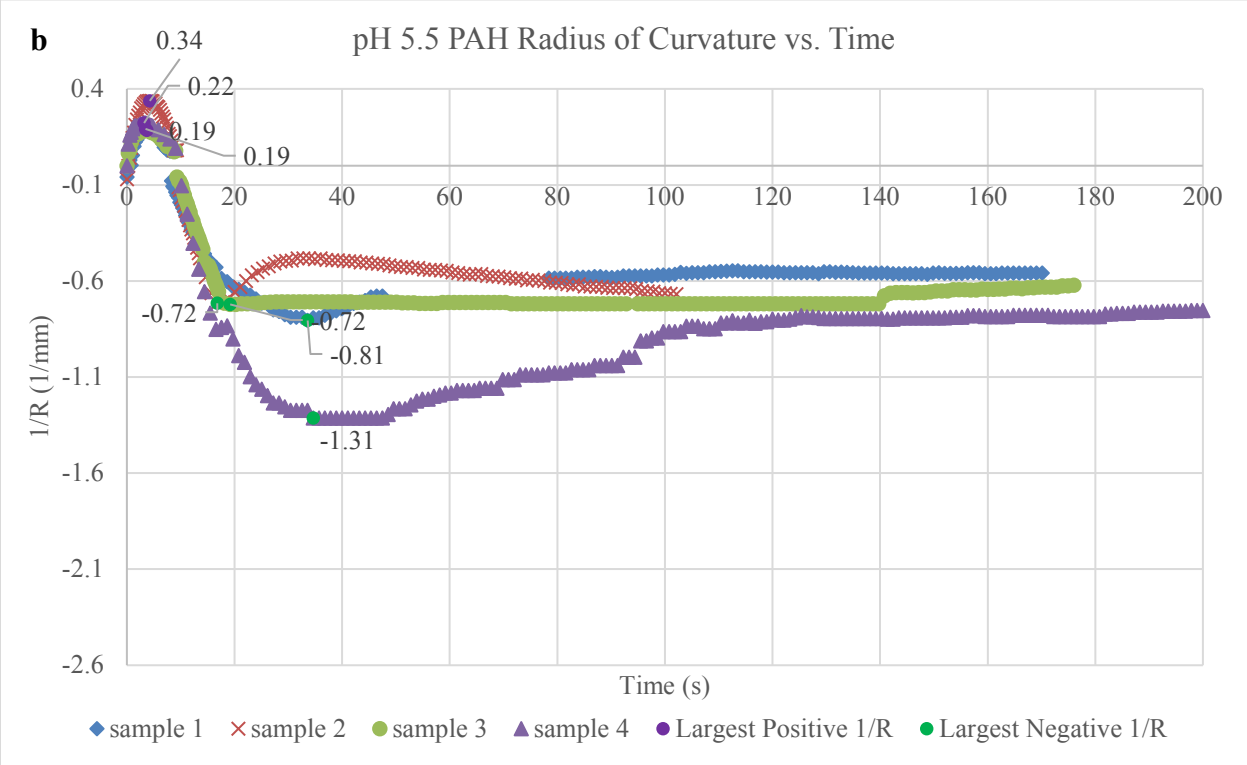
b
pH 5.5 PAH Radius of Curvature vs. Time
0.34
0.22
0.19
0.19
-0.72
-0.72
-0.81
-1.31
1/R (1/mm)
Time (s)
sample 1
sample 2
sample 3
sample 4
Largest Positive 1/R
Largest Negative 1/R

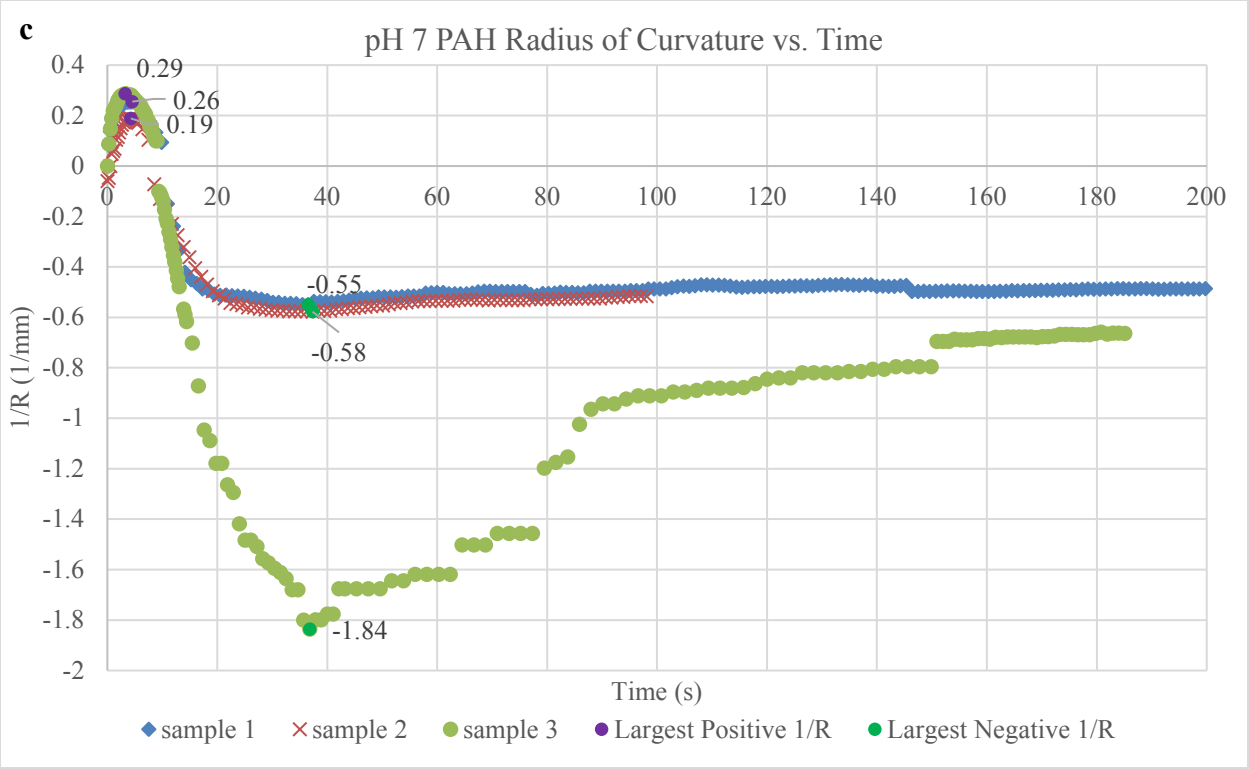

Figure 2.6: Plots showing bending curvature as a function of time for all samples of PAH/AuNPs at different pH values for PAH. All samples had approximately 45 wt% EMI-Tf.

Relative bending speeds and curvatures are more easily viewed in Table 1, which has cells color coded in accordance to the relative value. Dark green indicates values that correspond to higher performance, while red shows less desirable results. Samples made with PAH at pH 4.0 showed largest negative bending curvatures, but pH 5.5 samples had the fastest negative bending time. Additionally the pH 4.0 PAH run had the largest of all the positive bending curvatures, with pH 5.5 also having one sample with large positive curvature. However, from the averages, there was essentially no difference in positive bending. pH 4.0 samples had the best bending characteristics overall in these terms. In conjunction with the thickness data, thinner (pH 4.0) CNCs had significantly larger negative bending, and fast positive bending. Thicker CNCs provided larger positive bending, but at a slower rate.

PAH/AuNP Actuator Sample Bending Curvatures 45 wt%					
pH PAH	sample #	Time	Largest Positive Radius of Curvature	Time	Largest Negative Radius of Curvature
pH 4	sample 1	3.47	0.19	30.67	-2.14
pH 4	sample 2	3.47	0.09	28.53	-2.58
pH 4	sample 3	2.67	0.36	24.00	-0.34
pH 4	sample 4	2.93	0.24	27.73	-1.66
pH 5.5	sample 1	3.47	0.19	33.60	-0.81
pH 5.5	sample 2	4.27	0.34	16.80	-0.72
pH 5.5	sample 3	3.73	0.19	19.20	-0.72
pH 5.5	sample 4	3.20	0.22	34.67	-1.31
pH 7	sample 1	4.53	0.26	36.53	-0.55
pH 7	sample 2	4.27	0.19	37.33	-0.58
pH 7	sample 3	3.20	0.29	36.80	-1.84

Table 1: Maximum and minimum bending curvatures and their corresponding times for all samples tested. Dark green highlighting indicates a more desirable value while dark red cells have undesirable values.

Average PAH/AuNP Actuator Sample Bending Curvatures 45 wt%								
pH PAH	Time	Time Std. Dev.	Largest Positive 1/R	Largest Positive 1/R Std. Dev.	Time	Time Std. Dev.	Largest Negative 1/R	Largest Negative 1/R St. Dev.
4	3.13	0.40	0.22	0.11	27.73	2.78	-1.68	0.97
5.5	3.67	0.46	0.23	0.07	26.07	9.38	-0.89	0.29
7	4.13	0.63	0.20	0.09	34.33	5.12	-0.94	0.61

Table 2: Averages of the above table of maximum and minimum bending curvatures and respective times.

2.8 Summary

To summarize, the CNC film is prepared through LbL deposition on glass and Nafion film substrates. Film thicknesses are measured on the glass substrate, while actuator samples are fabricated by soaking the Nafion membrane in ionic liquid, which provides the ion source. Electrodes are added, and actuator bending is recorded and analyzed to determine bending curvature over time.

In IPMC actuator samples with PAH/AuNPs, the pH of PAH affects the resulting bending curvature and speed. Although there was significant variation in the measurements, thinner CNC layers at pH 4.0 PAH, appear to allow for fast cationic and anionic bending, with large negative curvature. In contrast, thick CNC layers appear to cause larger but slower cationic bending, and decreased anionic bending.

2.9 References

1. D. R. Morris and X. Sun, J Appl Polym Sci **50** (8), 1445-1452 (1993).
2. S. Liu, R. Montazami, Y. Liu, V. Jain, M. Lin, J. R. Heflin and Q. M. Zhang, Appl Phys Lett **95** (2), 023505 (2009).
3. W. Hong, C. Meis, J. R. Heflin and R. Montazami, Sensor Actuat B-Chem **205**, 371-376 (2014).
4. R. Montazami, S. Liu, Y. Liu, D. Wang, Q. Zhang and J. R. Heflin, Journal of Applied Physics **109** (10), 104301 (2011).
5. R. Montazami, D. Wang and J. R. Heflin, International Journal of Smart and Nano Materials **3** (3), 204-213 (2012).
6. D. Wang, Dissertation/Thesis, Virginia Tech 2015.

Chapter 3: Introduction of the Ion-Conducting Polyelectrolyte PAMPS into the CNC of an IPMC Bending Actuator

3.1 Introduction

Ion conducting polymers have recently become popular for their wide applicability in polymer-based electrochemical devices such as fuel cells and sensors, and have favorable properties such as low weight, and mechanical and chemical stability.[1] As will be discussed in the next section, adding ion conducting polyelectrolytes has improved ionic conductivity in various applications, including some making use of thin LbL films.

Their success in other films and applications suggested to us that incorporating an ion conducting polymer into the CNC of the IPMC actuator could have benefits in bending speed and curvature. Nafion, another ion conducting polyelectrolyte has been previously used in IPMC actuator CNCs through the direct assembly process. However, the non-ion conducting polymer LbL grown films showed increased speed over actuators processed through the direct assembly method since they are thinner.[2] Ion conducting polymer films fabricated through the ISAM process have not previously been produced for CNC layers on an IPMC actuator. Based on the success of ion conducting polymers in many applications discussed next in Section 3.2, it was important to examine how they would affect actuator bending and speed when included in a thin ISAM film.

One criterion for the ISAM application proposed was water solubility, since ISAM films are typically deposited in water-based solutions. Another deciding factor was the ion conducting polyelectrolytes available. Polyacids (negative polyelectrolytes) are more common than positively charged ion conducting polymers. The anionic gold nanoparticles, however, could not be completely removed from the CNC, as they increase the effective surface area of the electrode and provide porosity, allowing ion motion and storage.[3, 4] As a result, the strong polyacid poly(2-acrylamido-2-methyl-1-propanesulfonic acid) (PAMPS or polyAMPS), was chosen as a good candidate, but in order to keep the gold nanoparticles, a 15 quadlayer structure of PAH/AuNPs/PAH/PAMPS was proposed to compare to 30 bilayers of PAH/AuNPs.

3.2 Literature Review

PAMPS is an ion conducting polymer with a history of use in electrochromic devices[5, 6] as well as other applications such as actuators[7], humidity sensors[8, 9], and in LbL films.[1, 10]

Additionally, its sulfonic acid groups make it water soluble, making it suitable for use in the electrostatic LbL film growth process. PAMPS has been successfully used in enhancing proton and ionic conductivities in various types of ion conducting devices.[1, 6, 7, 11] A few examples of these are discussed in the following paragraphs.

Dai *et al*.[7] used solution cast blends of PVA (poly(vinyl alcohol)) and PAMPS to make and test an IPMC actuator made from the polymer blend membranes. Varying ratios of PAMPS to PVA were tested, and they found that increasing the PAMPS content increased the ionic conductivity, ion exchange capacity, water uptake, thermal stability, bending deformation, force generation, and caused faster bending speed, as a result of increasing the sulfonic acid content. The optimal actuator length of 1 cm gave a maximum tip force, but it was less than that of a Nafion-based IPMC actuator.[7]

In a study by DeLongchamp and Hammond,[1] the ionic conductivity of bilayers of LPEI (linear poly(ethylene imine))/PAMPS and LPEI/Nafion under different polyelectrolyte solution assembly conditions and hydration conditions was measured. Their goal was to enhance ion mobility through reducing the crosslink density between polyelectrolyte multilayers, as well as replacing electrostatic crosslinks with weaker interactions. Of the films tested, the LPEI/PAMPS film with no salt had the highest ionic conductivity at intermediate RH values, and was among the highest at full RH saturation (100%RH). The screened PAMPS had lower conductivity than unscreened at low and middle range RH conditions. They speculated that the lower salt concentrations in PAMPS allowed for weaker crosslinks between layers, thereby allowing for more rearrangement of bonds within the film.[1]

The polyelectrolytes used were adjusted in order to produce a film with the greatest ion conductivity possible with these materials. The weak polyelectrolyte LPEI was first pH adjusted to find the optimal degree of ionization, and PAMPS and Nafion had their ionic strength adjusted by adding varying levels of NaCl. The screening-enhanced adsorption of strong polyelectrolytes with salt causes large changes in the film structure when thicker layers with more open space and loops are deposited. These two factors together have strong effects on the crosslink density of the resulting film, since they individually adjust the polymer's charge and conformation, as discussed in the introductory chapter.[1]

They found an unusual relationship between salt concentration and film thickness in the LPEI/PAMPS film. There were two separate peaks, shown on the plot in Figure 3.1 below of

film thickness versus salt concentration in PAMPS. This was attributed to weak hydrogen bonding interactions between the amide groups in PAMPS and LPEI, which were screened a low salt concentrations, followed by the electrostatic interaction screening at higher salt concentrations.[1]

Overall contributions by DeLongchamp and Hammond[1] include the information that in order to increase ionic conductivity, reducing crosslink density will benefit ion mobility. In addition, mobility in LbL films saturated with plasticizer is limited by the crosslinks in the network, but with less plasticizer, the limiting factor is the ions available for conduction.[1]

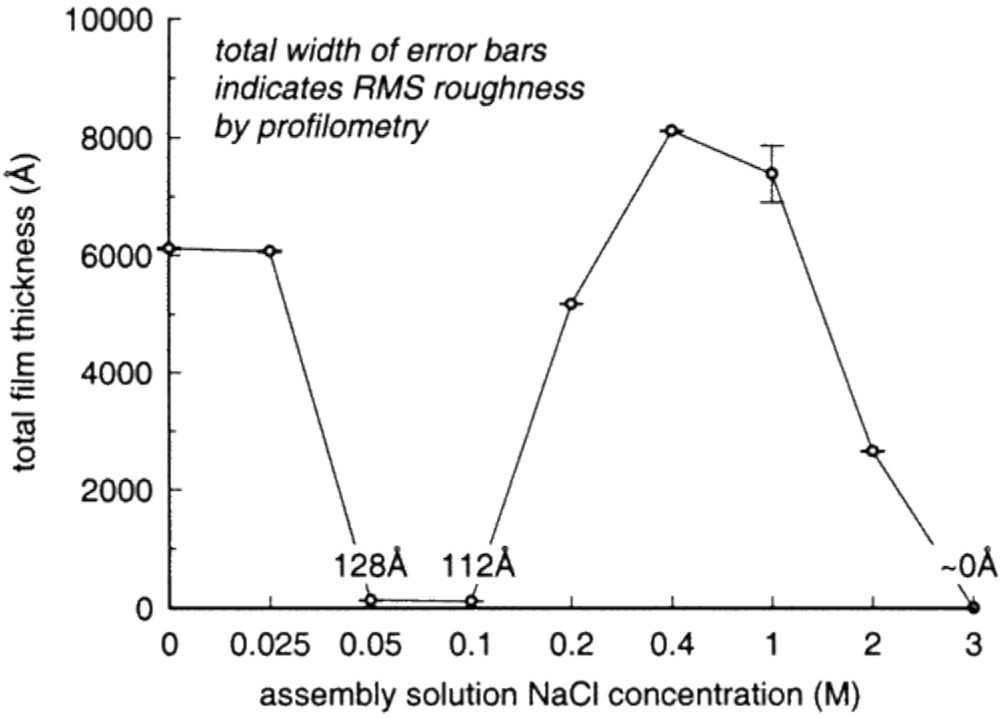

Figure 3.1: 30 bilayer film thickness of LPEI and PAMPS. LPEI pH was held constant while NaCl concentration in PAMPS was varied. The two maxima indicate two separate crosslinking interactions that were screened with different NaCl concentrations. The first was attributed to hydrogen bonding and the second the more typical electrostatic binding interactions. Reprinted with permission from D. M. DeLongchamp and P. T. Hammond, Chem Mater 15 (5), 1165-1173 (2003). Copyright 2003 American Chemical Society.[1]

Farhat and Hammond[12] used LbL films containing PAMPS in their study on using LbL to build electrodes that were both electrically and ionically conducting while containing a platinum catalyst. PAMPS is a hydrophilic conducting polymer, which was beneficial to the conductivity in this case, since acids are not lost by evaporation from the LbL film. In this example, the group

tried different pH values for their polyelectrolyte assembly solutions, and found that the higher pH values of their polymers constructed films that were more porous, which allowed for increased ionic conductivity measurements compared to lower pH, less porous films. In other words, porous, less dense films allow for easier ion motion.[12]

A humidity sensor was developed by Su *et al*.[9] using an LbL film containing PAMPS doped with two salts, based on measuring impedance through the device. They studied the effects and improvements to the sensor caused by the number of layers, the concentration of the polyelectrolytes during film growth, the salt concentration, temperature effects, response and recovery time, and stability.[9] They optimized the deposition concentration of PAMPS first, followed by the number of layers. An intermediate concentration of PAMPS (10 mM) worked best for humidity sensing, which they attributed to the fact that at lower concentrations, the polymer deposits quickly and spreads out in order to maximize charge compensation with few polymer chains. This leaves little room for ion motion within the film. At high concentrations, more molecules are present, and more polymer chains are added to the system, which also restrict ion motion. They found that increasing the number of bilayers containing PAMPS also increased impedance, since ion conduction occurred mainly in the outer PAMPS layer.[9]

Jean-Paul Randin[6] used Nafion, poly-AMPS (PAMPS), and other ion conducting polymers in an electrochromic device. PAMPS performance surpassed that of Nafion and the other polymers, as a result of its superior water solubility and stability. Nafion also had good stability, but was less water-soluble, which limited the contact with the underlying material.[6] Ionic conductivity was increased with the water content of the polymer, as a result of hydrogen bridges forming between ionic groups. Ionic conductivity increased with increasing sulfonic acid groups, as expected.

The possibility of various PEM films reducing methanol permeability through Nafion films for direct methanol fuel cell applications was evaluated by Jiang and Tang.[10] Proton conductivity was also an important factor for their LbL films. They found that the resulting film growth mechanism strongly impacts the methanol permeability, but not proton conductivity. Exponential growth in PEM films better blocked methanol penetration, which is desirable for this application, as exponential growth in LbL films requires much of the open space to be taken up as each subsequent layer is deposited. Diffusion of the adsorbing polymer occurs through the film, thereby increasing the density and reducing permeability to other molecules.[10] Of the

polyelectrolytes they tried, the found that the growth regime related to the structure of the polyelectrolytes. Smaller side groups allowed for exponential growth, because they were more easily able to diffuse throughout the film. PAH/PAMPS multilayer films grew in the linear regime, as a result of PAMPS large side groups, which have lower flexibility than polymers with smaller side chains.[10]

PAMPS has also been used to increase proton conductivity in proton exchange membrane fuel cells, such as in the work done by Feng *et al*.[11] Their goal was to reduce the humidity dependence of the proton conduction for their device by adding PAMPS to titanate nanotubes. This was achieved since the PAMPS brushes that were grafted onto the nanotubes were saturated with water at much lower relative humidity, thereby causing constant proton conductivity at RH values greater than 30%, unlike traditional perfluorosulfonated ionomer proton conductivity.[11]

3.3 Materials and Methods

3.3.1 Materials

Electrostatic LbL films were fabricated from 15 quadlayers of poly(allylamine hydrochloride) (PAH), anionic gold nanoparticles (AuNPs), and a PAMPS solution (15 wt % in H_2O, Sigma Aldrich, M_w ~ 2,000,000 g/mol). The LbL process description was previously mentioned. Films were grown on glass substrates for thickness determination and Nafion membrane (Ion Power Inc. Nafion^{TM} NR-211, EW 1100) for IPMC fabrication. 10 mM PAH (Sigma Aldrich, M_w ~ 58,000 g/mol) was used as the starting polyelectrolyte, followed by colloidal anionic ~3 nm AuNPs (Purest Colloids), which were used as purchased. PAH was used as the second layer of polycationic solution after the gold nanoparticles, and the quadlayer structure was completed with a layer of 10 mM PAMPS solution, which was diluted with RO water.

After film growth, the electrolyte/plasticizer is added to the IPMC by soaking in 1-ethyl-3-methylimidazolium trifluoromethanesulfonate (EMI-Tf) (≥98%, Sigma Aldrich), used as purchased. Following ionic liquid soaking, 120 nm gold electrodes (L.A. Gold Leaf, 23K/95.83 % Au) are manually hot pressed on the outside of the polyelectrolyte multilayer/Nafion composite film.

3.3.2 Methods

PAH, PAMPS, and AuNPs were deposited for ~3 min 40 s. Between each PE deposition step, samples were rinsed in a single beaker of RO water for approximately 3 minutes. No

drying was used between dipping steps. Control samples were fabricated with the same dipping times and solution concentrations, but only PAH and AuNP layers were fabricated, leaving room for 3 rinsing steps, each for about 1 minute. pH of PAH was adjusted to values of 4.0, 6.5, 7.5 within ±0.1 immediately before the dipping process was started. Salt containing solutions were prepared at least 12 hours in advance of film growth in order to allow for adequate stirring.

In order to measure the thickness of the partially complete layer structure, a sample on a glass substrate was removed from the dipping robot after every 5 quadlayers. This allowed for determining how film thickness was affected by increasing layer number. The robot was then immediately restarted to minimize film drying before growth was finished.

3.4 Experimental Planning

Based on DeLongchamp and Hammond's[1] work in optimizing LbL film solution conditions to yield the greatest ionic conductivity, the pH of PAH in conjunction with NaCl concentration in PAMPS was optimized to create an IPMC actuator with the strongest and fastest bending. It is well known in the field that for weak polyelectrolytes like PAH, the pH of the solution most strongly affects the degree of ionization of the polymer, which in turn affects how individual polymer chains are deposited on the growing PEM film surface.[13] The pH values used for PAH were based on the work of Choi and Rubner,[14] who found that PEM film thicknesses transition from very thin, flat chain deposits to much thicker loopy chain deposits when a weak polyelectrolyte has between 70-90% of its charged groups ionized. While these values change even at a single pH from solution to once they are deposited in a film, they found PAH is about 90% ionized at pH 6.5 in solution, and is about 70% ionized at pH 8.0 in solution.[14] This prompted choosing values of 6.5 and 7.5, as well as 4.0, where it is almost completely ionized in solution.

Salt concentrations for PAMPS solutions were determined based on the work of DeLongchamp and Hammond.[1] They observed two separate bonding interactions forming multilayers in PAMPS, using NaCl concentrations between 0 and 3 M. Values of 0, 0.04, 0.1, 0.4, and 2 M NaCl, were chosen, as they seemed mostly likely to be effective in producing desired CNC properties.

The PAMPS experiment used multiple pH values even after the previous determination from Chapter 2: that PAH at pH 4.0 provides superior bending results overall. Assessing the pH effect was important with the addition of a new material, as well as incorporating salt to vary

ionic screening. These two parameters had the potential to affect the film multilayer morphology, so examining the pH effect on the resulting actuator was again important. Optimal film characteristics were expected to arise when some open space was present in the film as a result of some charge screening, so at an intermediate salt concentration.

A total of 15 runs was planned, varying the pH of PAH and NaCl concentration in PAMPS. Initially, 3 runs with pH 4.0, 6.5, and 8 PAH, and no salt in PAMPS were completed, to ensure the process worked before purchasing fresh materials. Later pH 7.5 instead of 8.0 was decided, since it was expected there would be no significant difference in properties with that change. The initial trial was completed to ensure that it would work, before starting an extended experiment. The order was randomized in order to reduce variations caused improvement in technique.

Full Factorial PAMPS Actuator Sample Fabrication Plan			
Run #	pH PAH	[NaCl] in PAMPS	X
11	4	0	X1
10	4	0.04	X2
2	4	0.1	X3
15	4	0.4	X4
13	4	2	X5
14	6.5	0	X6
9	6.5	0.04	X7
1	6.5	0.1	X8
5	6.5	0.4	X9
7	6.5	2	X10
12	7.5	0	X11
4	7.5	0.04	X12
3	7.5	0.1	X13
8	7.5	0.4	X14
6	7.5	2	X15

Table 3: Experimental plan for fabricating multilayer films.

3.5 Results and Discussion

3.5.1 Initial trial run: Thickness and Ionic Liquid Soaking Parameters

Film thicknesses were measured on the first three sets of trial films, containing quadlayers of PAH/AuNPs/PAH/PAMPS. Film thickness increased with increasing pH PAH (decreasing degree of ionization), as expected. Plot (a) of Figure 3.2 shows the total film thickness at 5, 10, and 15 quadlayer intervals for each pH value. Part (b) shows the average

thickness for a single quadlayer, based on the total thickness and number of quadlayers deposited.

Determining the film growth regime in terms of the linear versus exponential growth from only three data points is difficult when studying the total film thickness. It is clear however, that as the degree of ionization of PAH decreases with increasing pH, significantly thicker films are grown, as shown in part (a) of Figure 3.2 below.[14] By dividing the total film thickness by the number of quadlayers, the growth regime is more obvious. For the linear growth regime, average single quadlayer thicknesses as in plot (b) of Figure 3.2 should be approximately equal no matter the number of layers that have been deposited. The pH 4.0 data set appears to be in the linear growth regime, as expected since the PAH is nearly fully charged. However, the pH 6.5 and 7.5 are less linear, and are likely within the exponential growth phase.

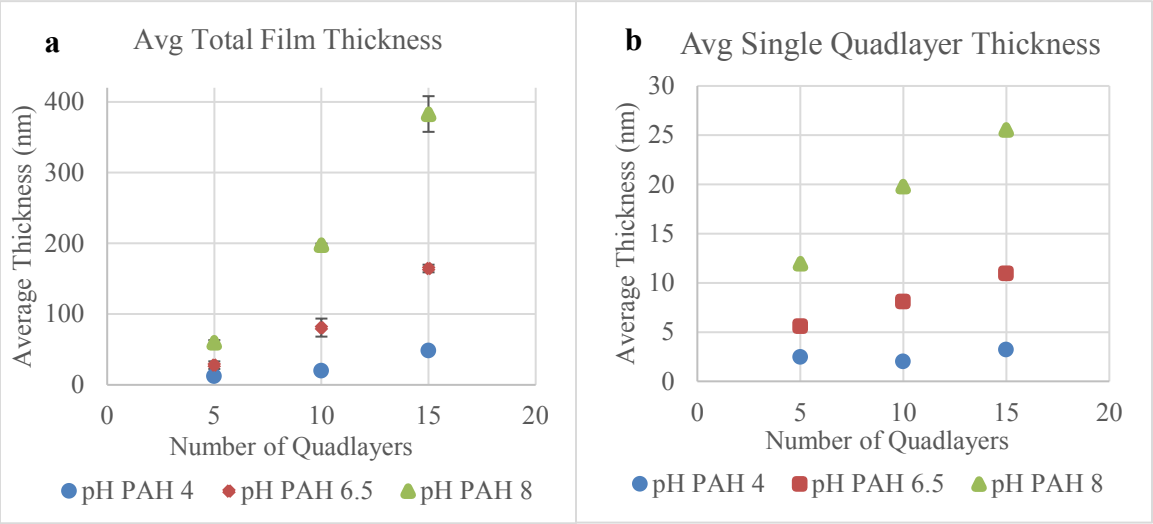

Figure 3.2: Film thicknesses of trial runs of PAMPS-containing CNCs. Thickness increases with increasing pH PAH for this range. Error bars in plot a show the standard deviation and for most points are too small to be visible.

After initial trials with PAMPS-containing samples, ionic liquid soaking in EMI-Tf was started at the previous standard temperature of 80 °C. There was some CNC degradation at 80 °C, however, especially in samples with the larger pH of PAH. After this initial discovery, trials at different temperatures and time lengths were completed to determine the limits before ruining the CNC or losing mass.

Ionic liquid soaking tests started with soaking from 50-80 °C in 10 °C increments, for 30 minutes, and images of the samples after soaking are shown in Figure 3.3 below. As the temperature increased, the CNC film suffered from increased degradation and mass loss. This

was more obvious in thicker CNC films, since they are initially thicker and darker in color. The mass loss also makes weight percent uptake difficult to determine because while ionic liquid is being absorbed, increasing the mass, some of the CNC is lost.

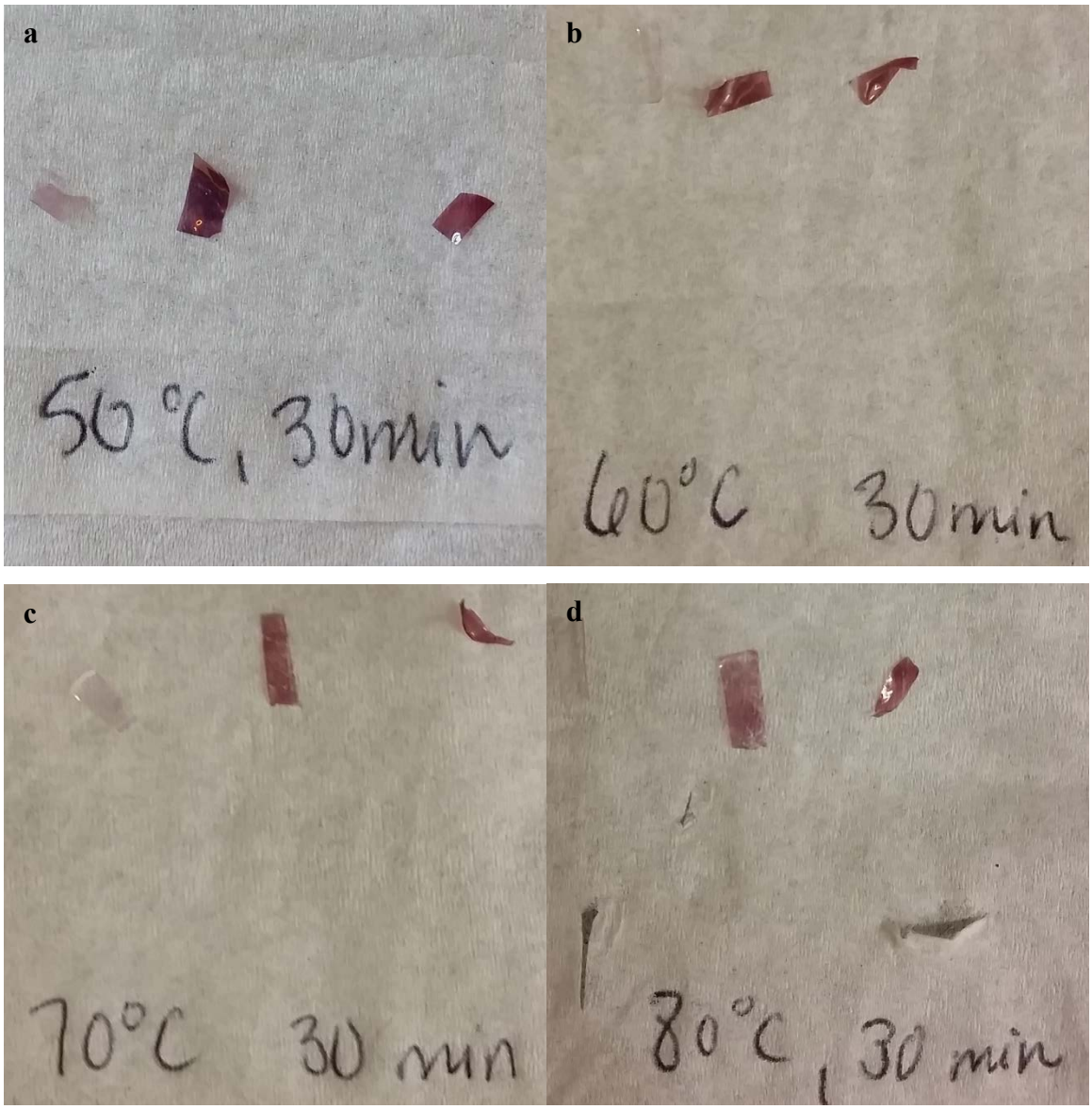

Figure 3.3: Pictures of PAMPS-containing samples after 30 minutes at various temperatures in EMI-Tf. For each image, pH 4.0 PAH is on the left, followed by pH 6.5 in the center, and pH 7.5 on the right. Notice the lighter color as the temperature increase, which is especially noticeable in the samples with larger pH of PAH. This color change indicates loss or degradation of the multilayer film.

The weight percent uptake was also measured for all of these samples, which further confirms that degradation and mass loss occurred. This is most obvious at pH 8.0, where the sample soaked at 50 °C had a negative weight percent uptake. The overall mass loss means the

temperature was too high for the CNC, but wasn't enough for the ionic liquid uptake from the Nafion substrate to overshadow the missing mass from the CNC. The CNC was originally thickest at pH 8.0, so this effect would also be more obvious at pH 8.0. At the other temperatures tested for the pH 8.0 samples, ionic liquid uptake increases with increasing temperature. The Nafion base is still stable at all temperatures tested, and accounts for the majority of ionic liquid uptake. At pH 4.0 and 6.5, the increasing ionic liquid uptake with increasing temperature is not observed. These samples had thinner CNCs initially, and therefore had less mass to lose. In thin CNC films, competition between mass loss and ionic liquid uptake is less clear.

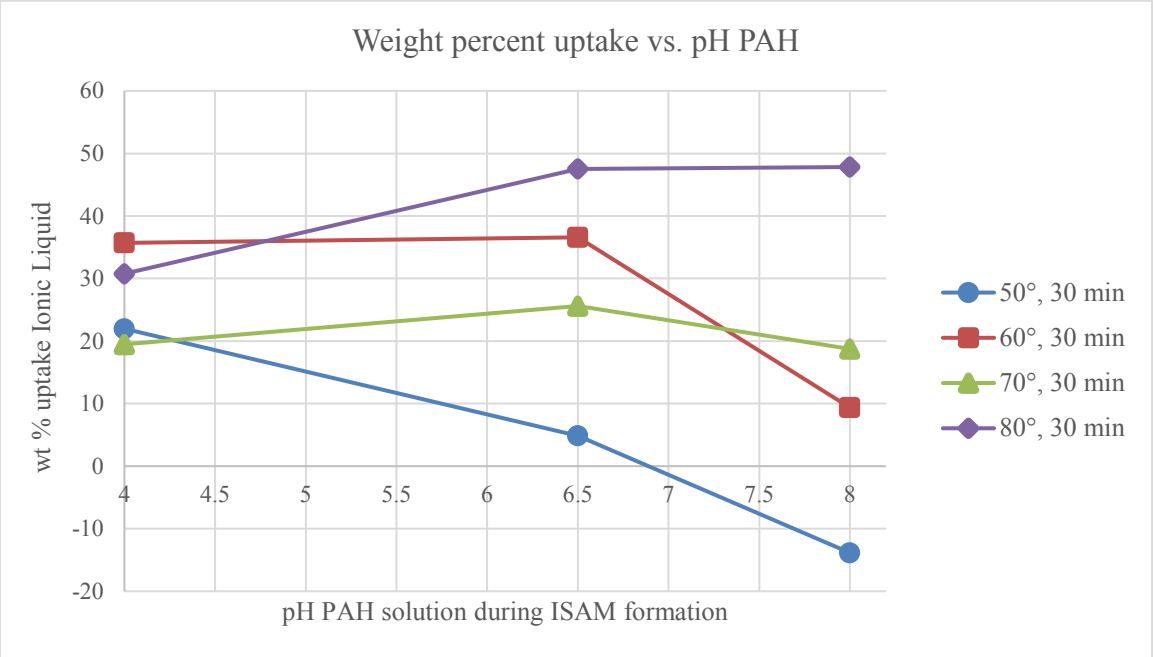

Figure 3.4: Ionic liquid uptake at various temperatures in samples with different pH of PAH after 30 minutes of soaking.

Based on the fact that at 50 °C, mass was lost, any higher temperature was too hot for the film to stay intact. Additional testing for longer time lengths was completed at 40 °C, with no indication of damage, so all subsequent samples were soaked at 40 °C. The time length was increased when necessary to enhance ionic liquid uptake.

3.5.2 Full scale test: Thickness measurements

After these 3 initial film fabrications were tested, the full test matrix fabrication was completed. Film thicknesses were measured by profilometry, and the average thicknesses of the

15 quadlayer films are shown below in Figure 3.5. Thicknesses for the 0 M NaCl with pH 4.0 and 6.5 for PAH are both less than those from the initial trial tests with the same solution values, but this could be a result of fresh PAMPS being more highly charged.

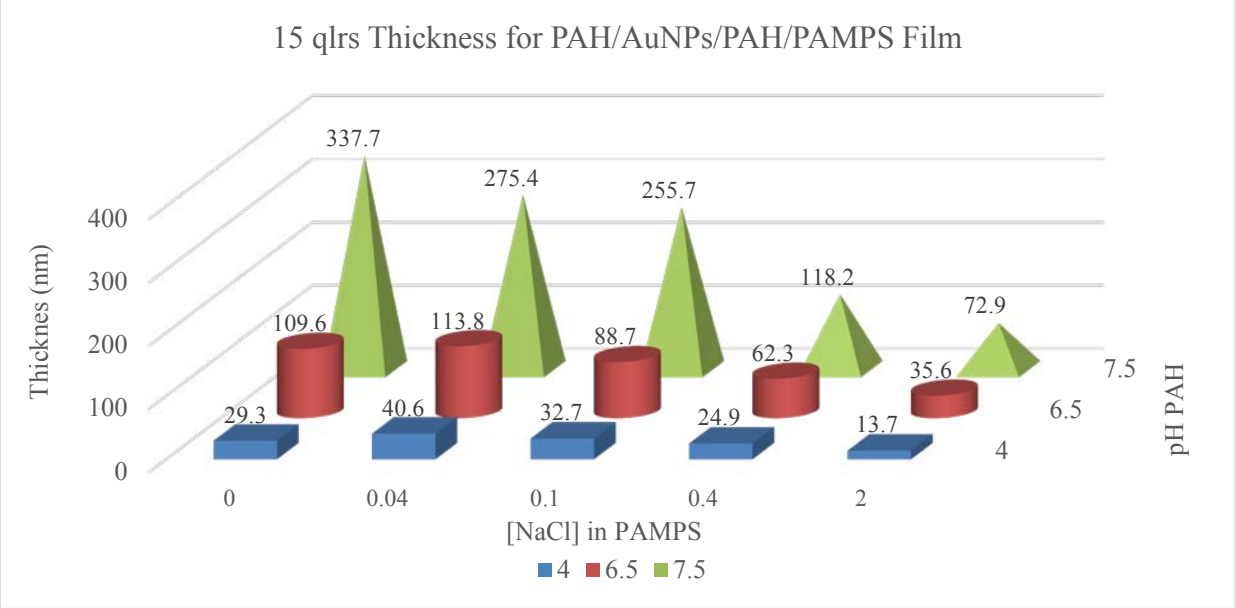

Figure 3.5: Thickness results for PAMPS CNC films. These results and their standard deviations are also shown in Table 4.

Results generally follow the expectations of thickness increases cause by degree of ionization reduction and screening-enhanced adsorption. Thicknesses rise with increasing pH at all NaCl concentrations. Additionally, salt concentration appears to have the same effect as standard ionic screening. Thickness increases with increasing salt content up to a point, after which further increasing salt content reduces thickness as a result of fewer charges on the depositing polymer that can contribute to growth. This is clear at pH 4.0 and 6.5. However, at pH 7.5, the thickness is continually reduced with increasing salt concentration, likely as a result of changing the degree of ionization of both polymers significantly, which masks the effect that can be seen when changing only pH or salt concentration.

The bimodal peak thickness effect seen by DeLongchamp and Hammond[1] in films with LPEI/PAMPS was not observed. This may be because there are other factors contributing to the thickness in this LbL film, such as being quadlayers of PAH/AuNPs/PAH/PAMPS instead of bilayers of LPEI and PAMPS and consisting of a different polycation. The bimodal peak could

also be disguised by using fewer data points, since hydrogen bonding is still possible between PAH and PAMPS, based on their nitrogen containing side groups.

Confirmation of film growth from the PAH/PAMPS layers is important to ensure film growth proceeded as expected. The average thickness of the 10 bilayer film of PAH/AuNPs was compared to those for 10 quadlayer films of PAH/AuNPs/PAH/PAMPS. PAMPS-containing quadlayer films should be significantly thicker than their bilayer counterparts at each pH PAH since they should contain twice the total number of layers. The 10 quadlayer PAMPS-containing films were thicker than the 10 bilayer films for all cases, though the difference in the case of pH 6.5 PAH, 2 M NaCl in PAMPS film is small. Perhaps this smaller difference was caused by screening reduced adsorption preventing much PAMPS film growth in the 2 M NaCl containing PAMPS. The fact that nearly all thicknesses of PAMPS-containing quadlayer films are significantly thicker than PAH/AuNPs only bilayer films is enough to determine that PAMPS was incorporated into the film as expected.

Comparison of PAMPS CNC Thickness to PAH/AuNP CNC Thickness				
pH PAH	**[NaCl] (M) in PAMPS**	**# layers**	**Thickness (nm)**	**Thickness St. Dev. (nm)**
4	-	10 bls	7.92	1.20
4	0	10 qlrs	14.63	77.06
4	0.04	10 qlrs	23.52	7.09
4	0.1	10 qlrs	17.08	15.21
4	0.4	10 qlrs	17.44	5.58
4	2	10 qlrs	12.33	4.63
6.5	-	10 bls	20.68	0.99
6.5	0	10 qlrs	65.81	17.61
6.5	0.04	10 qlrs	53.28	52.12
6.5	0.1	10 qlrs	45.96	48.37
6.5	0.4	10 qlrs	39.29	22.53
6.5	2	10 qlrs	22.64	9.72
7.5	-	10 bls	23.96	3.08
7.5	0	10 qlrs	144.96	49.73
7.5	0.04	10 qlrs	102.23	29.21
7.5	0.1	10 qlrs	80.59	22.96
7.5	0.4	10 qlrs	70.57	15.33
7.5	2	10 qlrs	40.35	26.05

Table 4: Thickness comparison for PAMPS-containing quadlayers of PAH/AuNPs/PAH/PAMPS and bilayers of PAH/AuNPs (shaded blue). Each set of films with varied NaCl concentration in PAMPS should be compared to the PAMPS free film at the same pH PAH.

Average RMS roughness was also measured using profilometry and is shown in Figure 3.6. The thickest films, with pH 7.5 and lower salt concentrations have the largest roughness values. Shiratori and Ruber[13] showed LbL film roughness tends to follow film thickness when

the pH of polyelectrolytes is adjusted, which in general is also seen in the PAMPS-containing films.

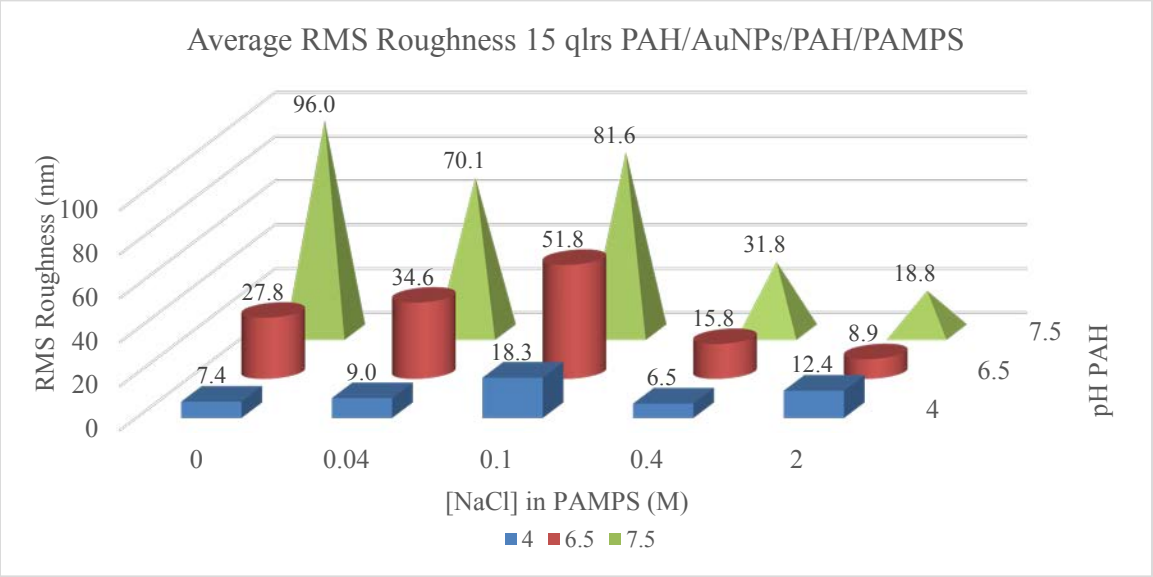

Figure 3.6: Average RMS roughness determined by profilometry. These results and their standard deviations are also shown in Table 17 in Appendix A.

3.5.3 Full scale test: Ionic liquid uptake

After determination that 40 °C was the temperature limit for ionic liquid soaking, a sample from each fabrication was soaked at that temperature for 20 minutes. The uptake results are shown in Figure 3.7. The constant time length soak provided an initial idea for how long they would need to be soaked comparatively and for a goal ionic liquid uptake for all samples.

In order to make an accurate comparison between samples with different CNCs, approximately the same ionic liquid uptake was necessary, since bending depends on ion concentration. In general, pH 4.0 samples showed the greatest and fastest ionic liquid uptake, followed by the pH 6.5 samples with greater NaCl concentration that had similar uptakes, all of which had thin CNCs. Based on this test, the pH 7.5 samples were the limiting cases in terms of the maximum possible ionic liquid uptake. These limiting cases were first soaked for extended time periods to determine the largest uptake possible.

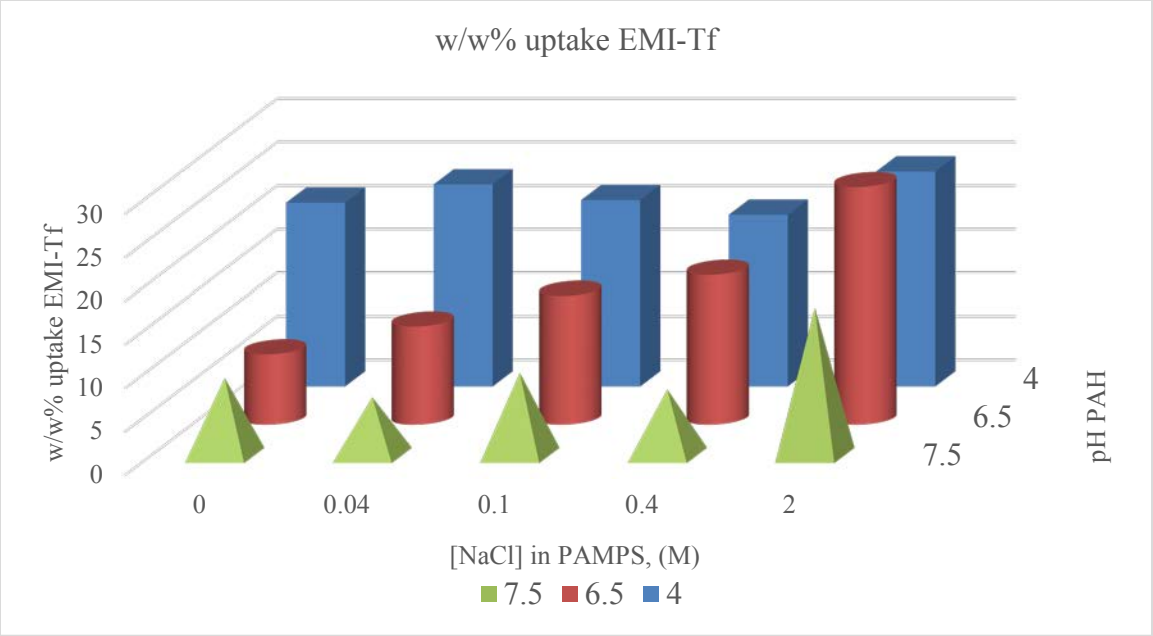

Figure 3.7: Ionic liquid uptake of the samples after 20 minutes each in 40 °C.

The ionic liquid uptake information allowed for a goal weight percent uptake for all samples, which was selected as 17.0 wt%. A range of ± 3.0 wt% was allowed since materials were limited. Most sample runs were successfully made into samples close to 17.0 wt%. There were a few that repeatedly failed, however, due to the hot pressed gold electrode not sticking properly after extended ionic liquid soaking. These were Run 13 and 14, PAH pH 4.0 and 2 M NaCl and pH PAH 6.5 and 0 M NaCl, respectively. These samples were among the last fabricated, leaving the most time between the CNC film deposition and sample fabrication. Perhaps, the older the samples were, the less ionic liquid they could absorb, which required longer and longer soaking in an attempt to reach the goal weight percent uptake. But there was also a competing factor with the gold sticking during hot pressing. The longer the sample was in the ionic liquid, and the more frequently it was taken out to determine the current weight uptake, the less likely the gold was to stick during hot pressing. Extended time length seemed to be less of a problem than drying the excess ionic liquid before weighing. Additional complications included the limited amount of each sample run.

For the final comparison, all samples except for Run 13, PAH pH 4.0 with 2 M NaCl, and Run 14, PAH pH 6.5 with 0 M NaCl were within the 17.0 ± 3.0 wt% uptake. A 24.7 wt% uptake sample was tested for Run 13 instead, and a 13.2 wt% uptake sample of Run 14, since those were

the closest working samples obtained. The weight percent uptakes of the samples tested and analyzed are shown in Table 5 below.

Ionic Liquid Weight Percent Uptake for Each Fabrication Condition				
Run #	**pH PAH**	**[NaCl] in PAMPS**	**Tested wt %**	**X**
1	6.5	0.1	14.8	X8
2	4	0.1	16.5	X3
3	7.5	0.1	17.0	X13
4	7.5	0.04	17.4	X12
5	6.5	0.4	17.2	X9
6	7.5	2	17.0	X15
7	6.5	2	14.4	X10
8	7.5	0.4	17.7	X14
9	6.5	0.04	17.6	X7
10	4	0.04	14.5	X2
11	4	0	15.3	X1
12	7.5	0	15.2	X11
13	4	2	24.7	X5
14	6.5	0	13.2	X6
15	4	0.4	19.7	X4

Table 5: Weight percent uptake of EMI-Tf ionic liquid for each sample. The goal was 17.0 ± 3.0 wt%. All but run 13 and 14 fell within that range.

3.5.4 Bending tests

Approximately 3 sample actuator strips of each fabrication run were tested and analyzed for bending using the procedure described in the introductory chapter. The humidity for all bending tests was kept between 50 ± 1.5 %RH. For most samples, the three bending measurements have significant variation, with some samples having a larger positive bending, and little bending on the negative side. In other samples, the opposite was observed. This likely occurs as a result of peeling off the gold backing after hot pressing, which leaves smaller samples with noticeable inherent curling. Samples were flattened by unrolling and pressing under a book. Less curling after peeling seems to occur in samples with larger area. However, small samples were necessary when determining the temperature and time limits for ionic liquid soaking, so that material would last throughout the trial and error in the ionic liquid soaking process. Because of the preferred bending direction issue, comparisons of each run were plotted in terms of the largest maximum bending as well as the most negative bending curvature.

First the measurements for samples with the largest bending curvature at each pH were compared. For the pH 4.0 PAH samples, shown in Figure 3.8 (a), there is not much of a trend based on NaCl concentrations for producing faster and strongly bending actuators. The 2 M NaCl sample was fastest (though this can be discounted since it had a greater ionic liquid

content), while the 0.1 M NaCl sample had the largest bending, but both were improvements over the non-PAMPS-containing control. For the pH 6.5 PAH samples, intermediate levels of NaCl caused greater performance than the control in both speed and bending curvature. With pH 7.5 PAH, the 0.04 M and 2 M NaCl samples had nearly equal bending curvatures and speeds, with curvatures greater than any of the other samples. At pH 7.5, however, the control sample containing no PAMPS also had significant positive bending, but was a little faster.

The largest negative bending curvatures were compared separately in Figure 3.8 d-f. For pH 4.0, there is not an obvious trend. The 0 M NaCl sample shows the strongest bending, and is followed by the control sample with PAH/AuNPs, then the 0.4 M NaCl sample, which is similar. For pH PAH 6.5, the middle range salt concentration containing samples, 0.1 M and 0.4 M NaCl have the most desirable bending characteristics both of which displayed larger and faster bending than the control sample. In the pH 7.5 samples, the control had the largest bending, and the rest of the samples were similar, with those containing less salt being slightly better.

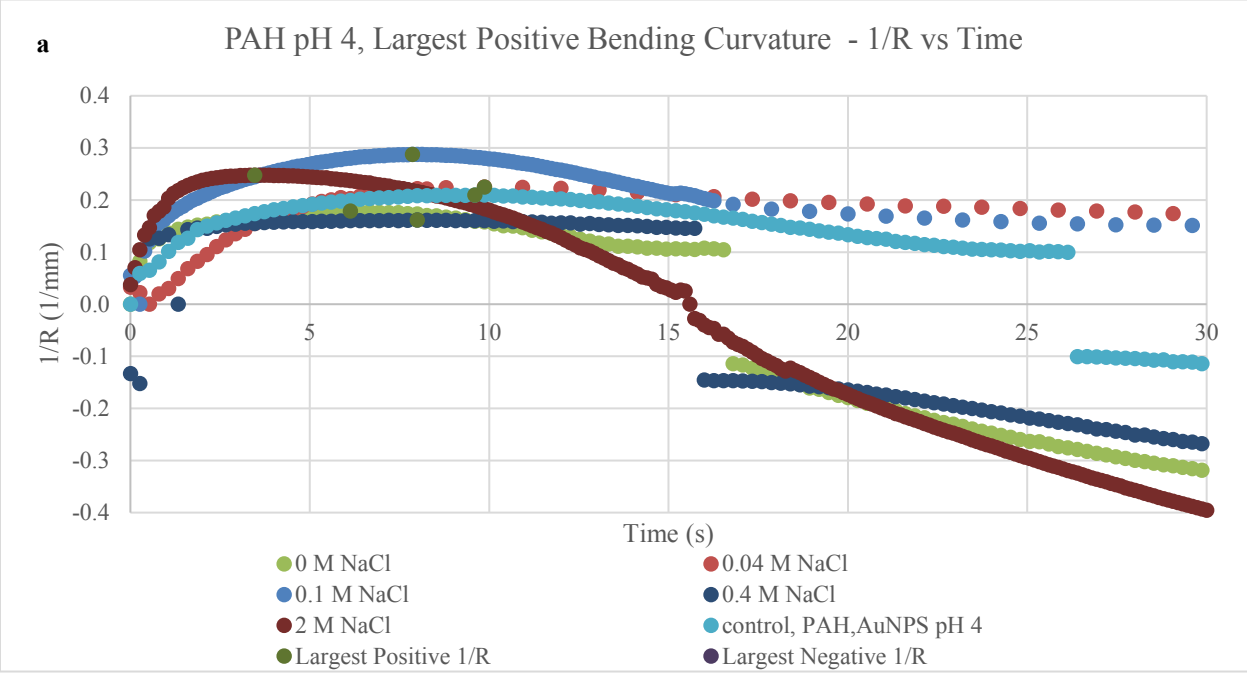

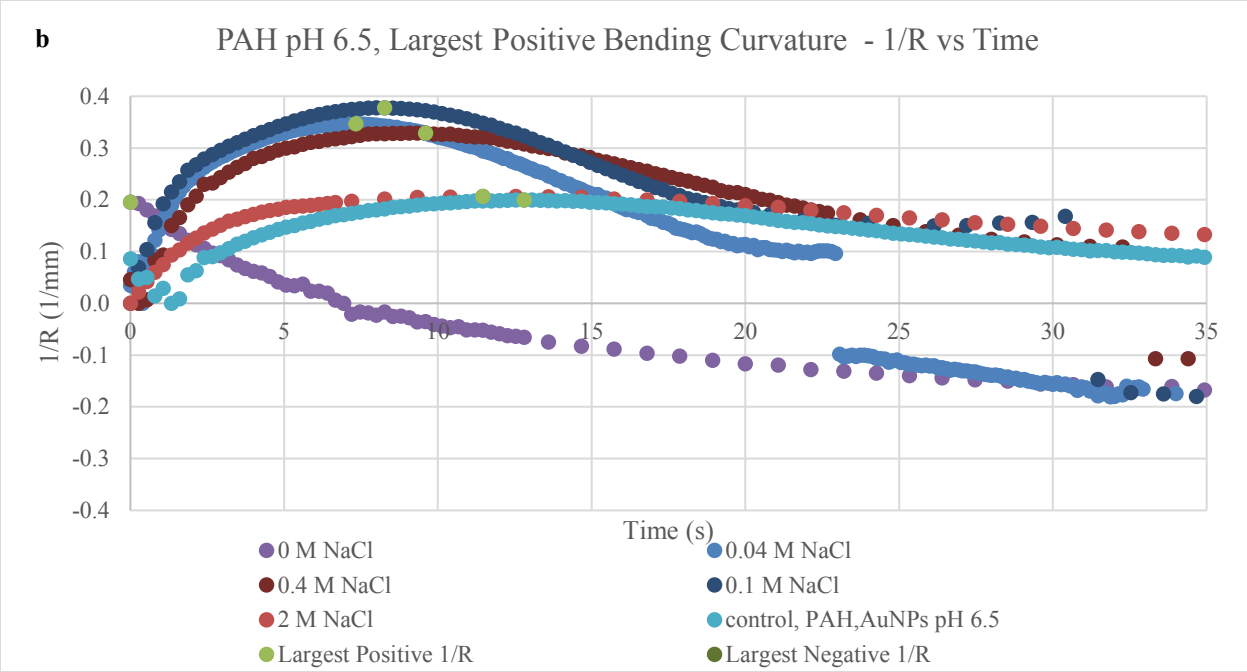
b
PAH pH 6.5, Largest Positive Bending Curvature - 1/R vs Time
1/R (1/mm)
Time (s)
0 M NaCl
0.04 M NaCl
0.4 M NaCl
0.1 M NaCl
2 M NaCl
control, PAH,AuNPs pH 6.5
Largest Positive 1/R
Largest Negative 1/R

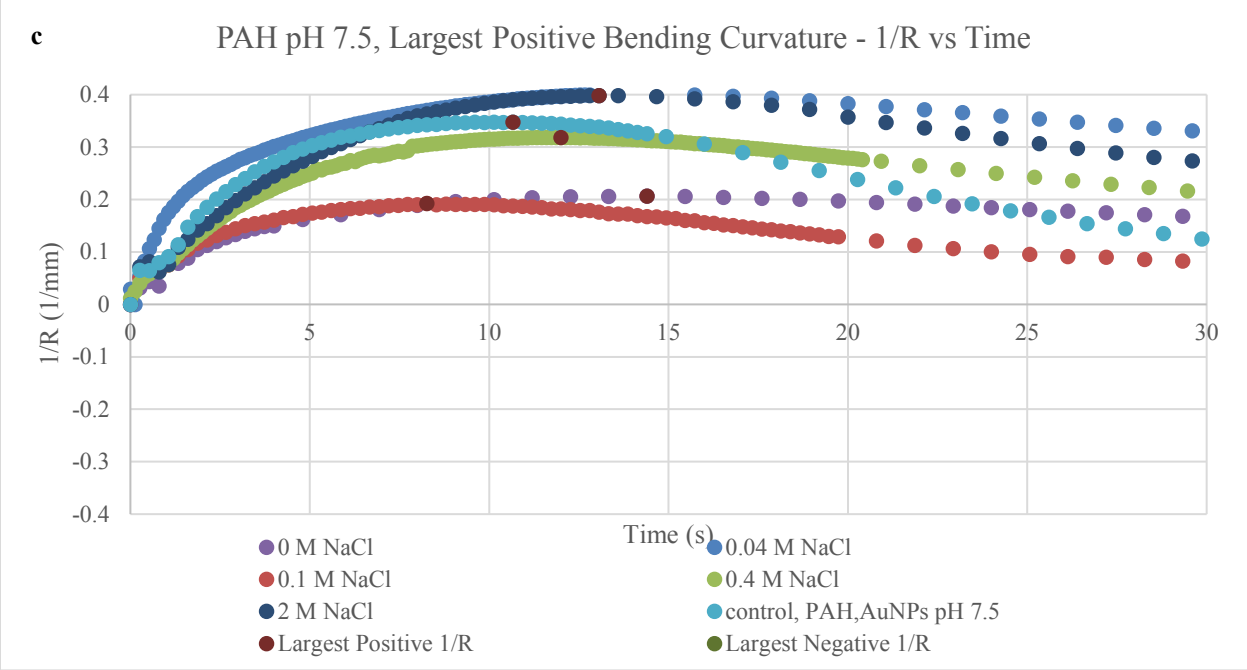
c
PAH pH 7.5, Largest Positive Bending Curvature - 1/R vs Time
1/R (1/mm)
Time (s)
0 M NaCl
0.04 M NaCl
0.1 M NaCl
0.4 M NaCl
2 M NaCl
control, PAH,AuNPs pH 7.5
Largest Positive 1/R
Largest Negative 1/R

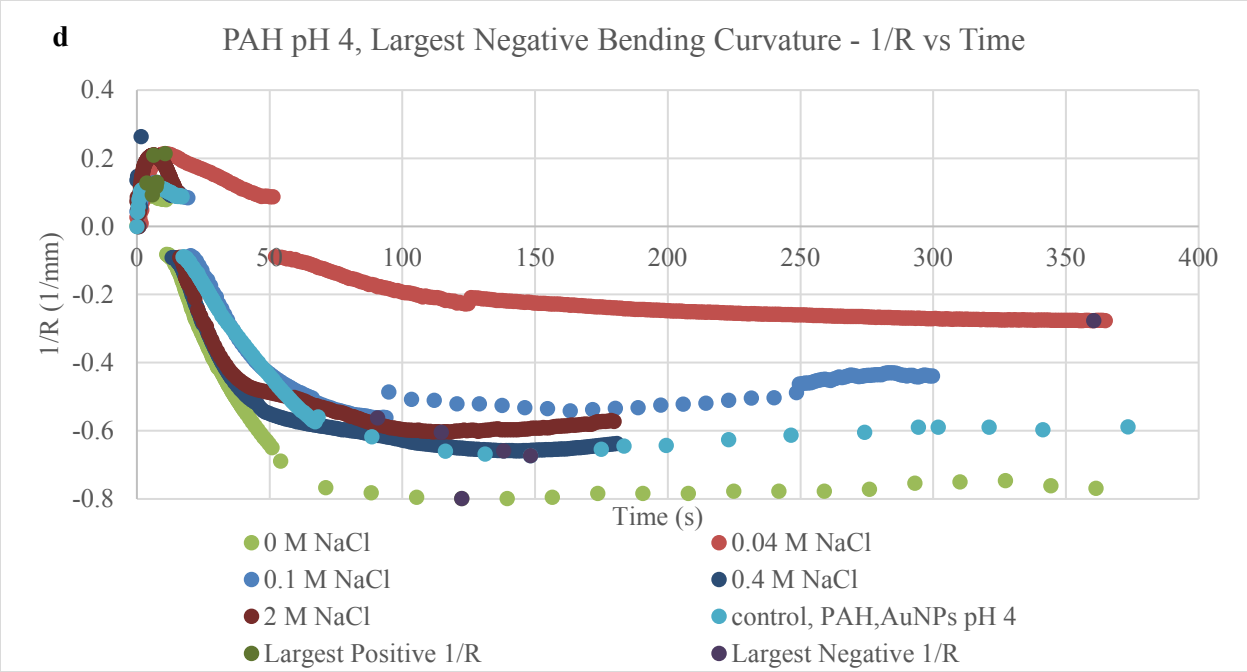
d
PAH pH 4, Largest Negative Bending Curvature - 1/R vs Time
1/R (1/mm)
Time (s)
0 M NaCl
0.04 M NaCl
0.1 M NaCl
0.4 M NaCl
2 M NaCl
control, PAH,AuNPs pH 4
Largest Positive 1/R
Largest Negative 1/R

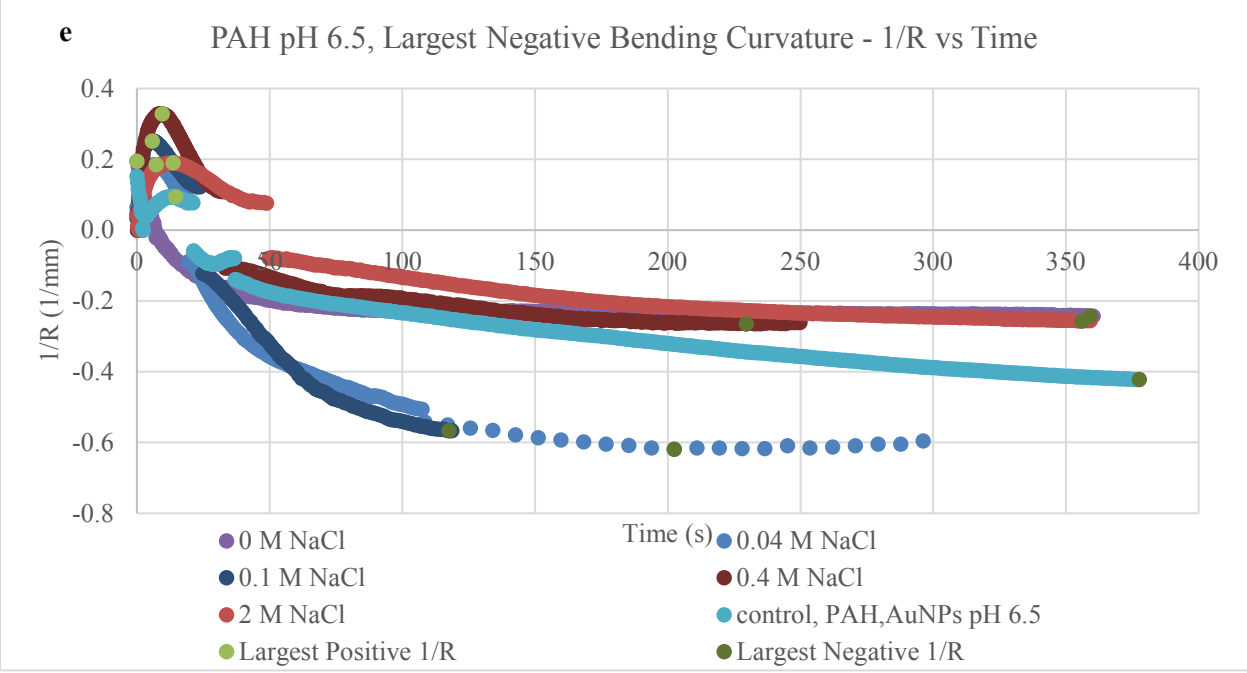
e
PAH pH 6.5, Largest Negative Bending Curvature - 1/R vs Time
1/R (1/mm)
Time (s)
0 M NaCl
0.04 M NaCl
0.1 M NaCl
0.4 M NaCl
2 M NaCl
control, PAH,AuNPs pH 6.5
Largest Positive 1/R
Largest Negative 1/R

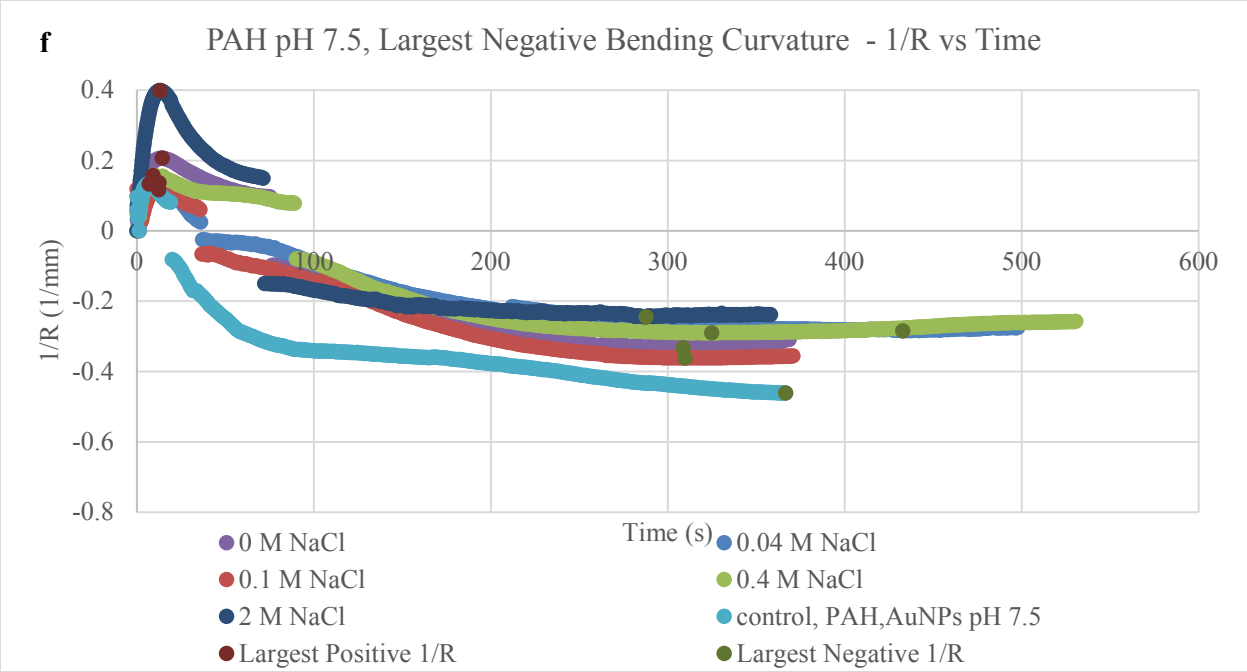

Figure 3.8: a-f Largest maximum and minimum bending curvatures for each, which are divided by pH of PAH to enhance readability.

Samples from each pH value with the largest and fastest negative radius of curvature were chosen and plotted together, as shown below in Figure 3.9. For both pH 4.0 and 6.5 PAMPS-containing samples met these requirements, while at pH 7.5, the PAMPS-free control sample showed the largest and fastest negative bending. The salt-free, pH 4.0 sample has the most desirable bending characteristics overall, followed by the pH 6.5, 0.04 M NaCl sample, then the pH 7.5 control. Overall, the lower pH values and salt concentrations provide negative bending characteristics closest to the goal in terms of improving bending deformation and speed.

For the largest and fastest maximum or positive bending curvature, the pH 7.5, 0.04 M NaCl sample had the largest curvature, but it was very closely followed by the pH 6.5, 0.1 M NaCl sample, which was faster. The pH 4.0, 0.1 M NaCl sample had a large positive bending curvature, but barely moved in the negative direction. PAMPS-containing actuator samples showed larger and faster negative bending than the control samples for all pH values. Lack of motion in the negative direction likely indicates damage, as the other samples that bent less (not shown) had the typical bidirectional bending.

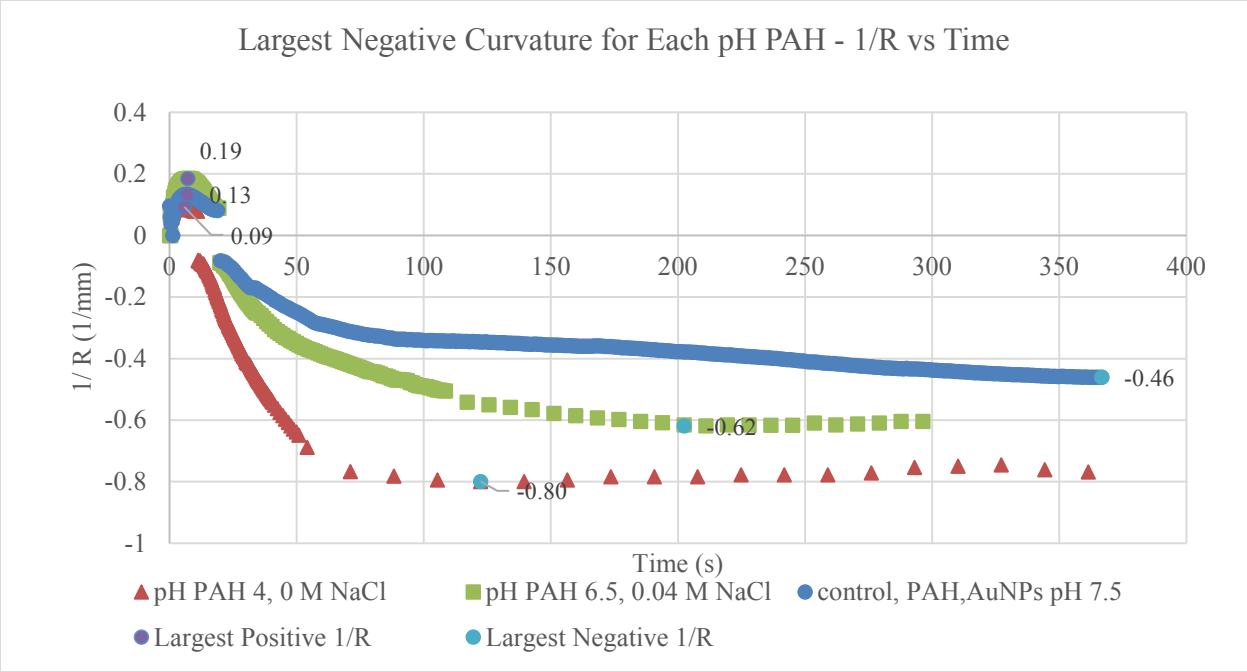

Figure 3.9: Sample from each pH value with largest negative curvature.

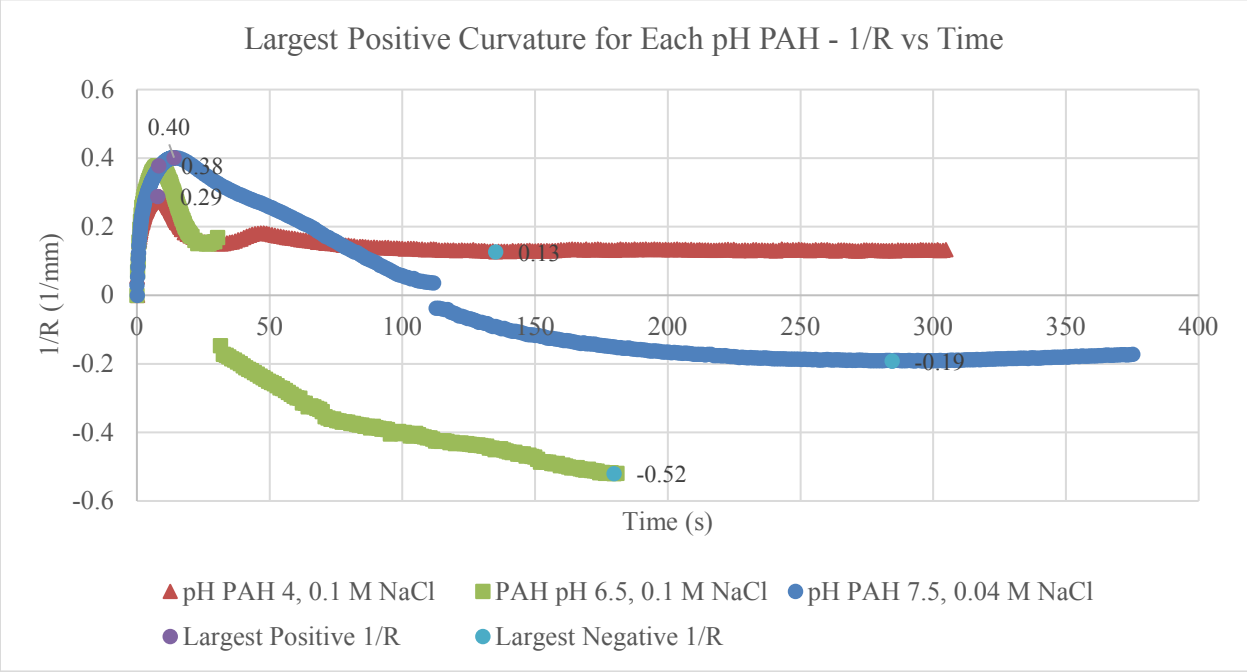

Figure 3.10: Sample from each pH value with largest positive curvature.

In summary, the lower pH values for PAH with low concentrations of salt (0-0.04 M) had the largest and fastest anionic (negative) bending deformation. These were all samples with thin CNCs. The largest positive bending curvatures were shown by samples with larger pH values

for PAH and slightly greater salt concentrations (0.04-0.1 M NaCl), which provide thicker CNCs. The trend shown by thicker CNCs adding to the cationic bending but slowing it, and thinner CNCs improving anionic bending is likely a result of the effects of pH and NaCl concentration on film thickness instead of the film morphology due to charge density. Similar results were observed by Liu *et al*.[3], who discovered that thicker CNC layers increase the long ion transport time which decreases bending speed.

Comparisons between samples with the same salt concentration are shown below in Figure 3.11 and Figure 3.12. The samples with the largest positive bending curvatures are shown in the first set of plots, while samples with the largest negative bending curvatures are shown in the second set.

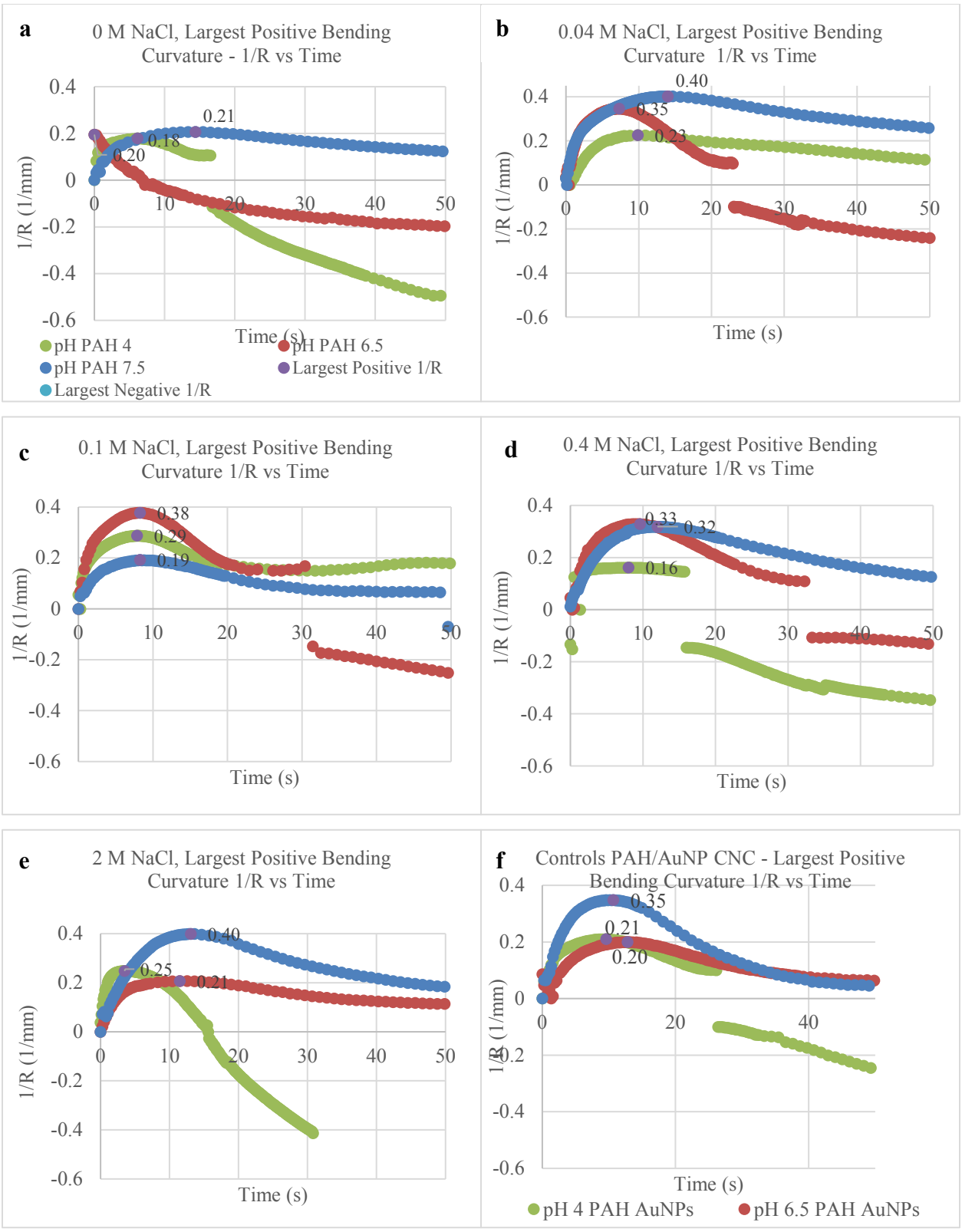

Figure 3.11: Sample with maximum positive bending curvature for each NaCl concentration value

For the samples with no NaCl in the PAMPS layer, the pH 4.0 PAH sample was the fastest, while the pH 7.5 had the largest positive bending deformation. The control samples also show the same trend. At 0.04 M NaCl, pH 6.5 shows the fastest and largest bending, but pH 4.0 and 7.5 follow the same general trend as in the 0 M NaCl sample with pH 4.0 being quick, but pH 7.5 being slower but having greater curvature overall. The middle NaCl concentration samples of 0.1 M bent all at approximately the same speed, so increased pH does not slow down the bending, as in the lower salt concentration samples. pH 7.5 had the smallest curvature and pH 6.5 had the largest curvature. 0.4 M NaCl pH 4.0 samples were the fastest, but had the smallest curvature again. pH 7.5 was the slowest, but only slightly since it was very similar to pH 6.5. Again at 2 M NaCl, the same trend is seen. pH 4.0 for PAH gives the fastest sample (though this sample had more ionic liquid than the others), while pH 7.5 gives the largest curvature and slowest bending. From these observations, pH 4.0 usually had the fastest positive bending (cationic), except at 0.04 M NaCl. At 0.1 M NaCl, pH was not a significant factor for bending speed. The pH 7.5 sample usually attained the largest positive curvature, except at 0.1 M NaCl, where the pH 6.5 sample surpassed the others, and at 0.4 M NaCl, pH 6.5 had very similar results as pH 7.5.

These trends all follow the observations by Liu *et al*.[3] Thicker CNC films cause larger strain and curvature but slower bending deformations. Thicknesses for the results discussed here indeed follow expectations based on literature results of increasing thickness with increasing pH PAH, and salt concentration's influence of thickness.[1, 13]

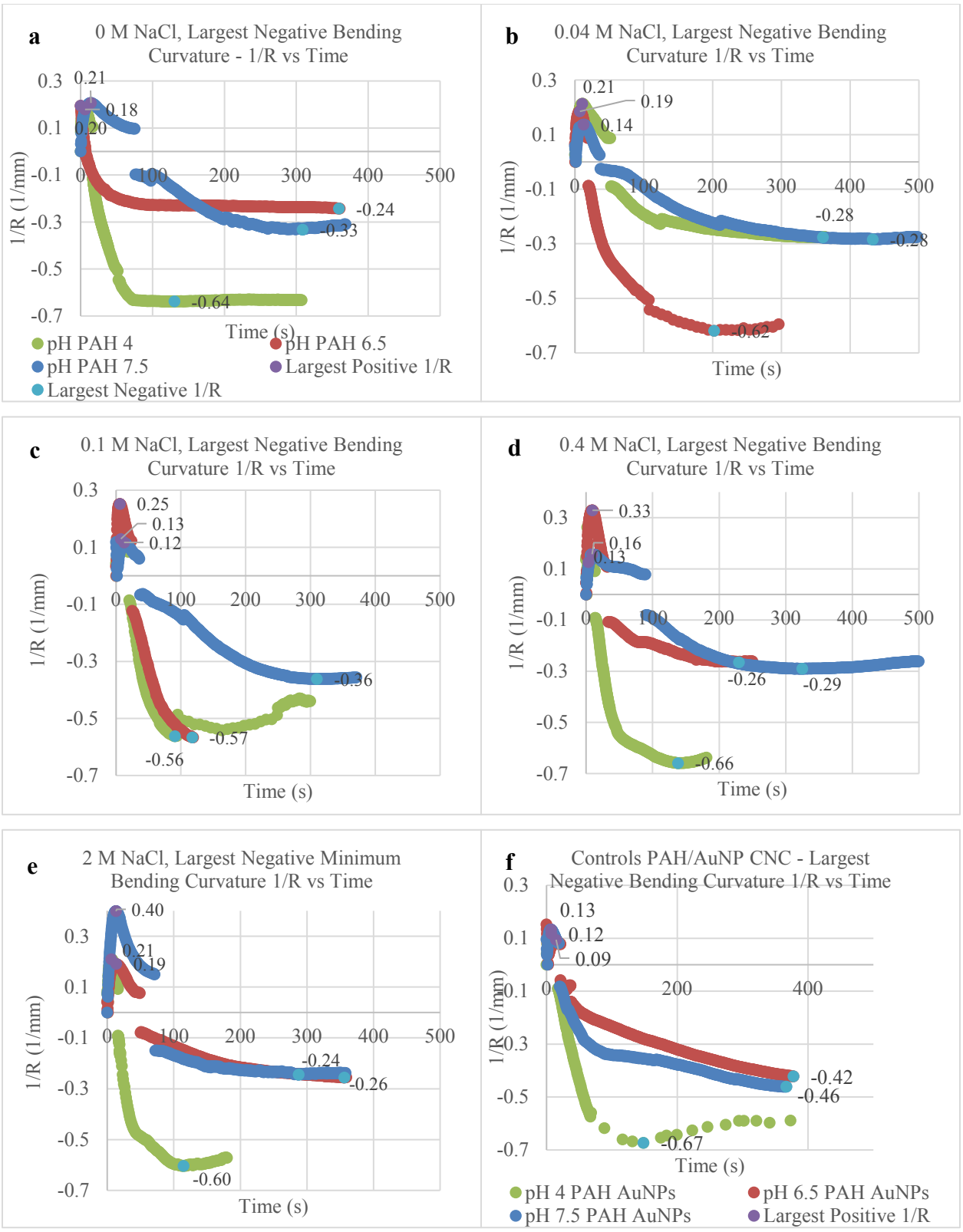

Figure 3.12: Plot of bending curvature as a function of time for each NaCl concentration. Each plot displays the bending curvature for the sample that had the largest negative bending deformation.

The samples with the largest negative bending curvature followed similar trends as those in the samples with the largest positive curvature. In samples with no salt, the pH 4.0 sample was undoubtedly the fastest with largest bending. In the 0.04 M NaCl sample, the pH 6.5 sample had the largest curvature, as it was when comparing the positive bending curvature. For the other three salt concentrations, pH 4.0 samples had the largest curvature and were the fastest bending. pH 7.5 samples were consistently the slowest in these last three sets. pH 6.5 also did well at 0.1 M NaCl and was comparable to the pH 4.0 sample. Generally, at low NaCl concentrations, the pH 4.0 sample was significantly better than other pH values in terms of both bending speed and curvature. The greatest pH value tested consistently had the slowest negative bending times and took a long time to reach peak negative (anionic) bending, again probably a result of the thicker layers requiring long ion transport times.[3] At 0.04 M NaCl, the results did not follow this trend. Instead, the pH 6.5 sample had significantly better bending characteristics. At 0.04 M NaCl, the pH 4.0 sample was the thinnest, so those results do not follow the thickness versus speed observation by Liu *et al*.[3] The control sample showed similar trends with respect to pH as PAMPS-containing samples with 0, 0.4, and 2 M NaCl, with pH 4.0 bending significantly more than pH 6.5 and 7.5.

Table 6 below shows the largest positive and negative bending curvature for each sample along with their corresponding times. They have been shaded according to their values, with dark green indicating more desirable values. Red highlights show less optimal values. Faster times are desired, as well as larger positive and negative curvatures. The fastest cationic bending (positive bending) occurs largely in samples with pH 4.0 for PAH. They are the thinnest samples, so this is consistent with observations by Liu *et al*.[3] The salt free/pH 4.0 sample and pH 4.0/0.04 M NaCl sample have very fast bending—faster than the control samples. The fastest anionic bending (negative bending) also occurs largely in samples with pH 4.0 for PAH, where salt concentration appears to be less of a factor, since nearly all salt concentration values have fast anionic bending. Anionic bending in pH 4.0 PAH/AuNPs/PAH/PAMPS samples are also largely faster than the pH 4.0 control samples. One measurement that does not follow the same trend is the pH 6.5/0.1 M NaCl sample. Two of those samples had very fast anionic bending, but the other two were rather slow.

In terms of the positive bending curvature, samples with greater film thicknesses produced larger but slower bending deformation. Samples with pH 7.5 PAH had large bending,

including those from the control set, while pH 6.5/0.1 M also showed significant bending, but these all were on the slower side. The largest negative bending was seen mostly in samples with pH PAH 4.0, including the control, though the samples with pH 6.5/0.04 M NaCl also had similar bending curvature. Generally, thinner films are faster in both cationic and anionic bending regimes, and the thicker films produced larger but slower cationic bending deformations. These results demonstrate that tuning film thickness is a good way to ensure the actuators have the desired bending speeds and times for either cationic or anionic bending. This could be chosen based on the application, and which bending direction it relies on more heavily.

PAMPS-Containing Actuator Sample Bending Curvature Measurements								
Run	pH PAH	[NaCl] (M)	Sample number	Wt % EMI-Tf	Largest Positive 1/R time	Largest Positive 1/R	Largest Negative 1/R time	Largest Negative 1/R
11	4	0	1	15.3	6.4	0.159	82.4	-0.51
11	4	0	2	15.3	5.867	0.093	122.4	-0.8
11	4	0	3	15.3	6.133	0.179	130.4	-0.64
10	4	0.04	1	14.5	11.73	0.192	174.9	-0.12
10	4	0.04	2	14.5	10.67	0.213	360.5	-0.28
10	4	0.04	3	14.5	12	0.059	351.7	-0.04
10	4	0.04	4	14.5	9.867	0.225	358.7	-0.21
2	4	0.1	1	16.5	107.7	0.045	329.6	-0.04
2	4	0.1	2	16.5	7.467	0.129	90.67	-0.56
2	4	0.1	3	16.5	6.8	0.218	131.7	-0.37
2	4	0.1	4	16.5	12.27	0.058	166.9	-0.47
2	4	0.1	5	16.5	7.867	0.288	135.2	0.126
15	4	0.4	2	19.7	7.467	0.117	132	-0.53
15	4	0.4	3	19.7	8	0.162	176.5	-0.46
15	4	0.4	5	19.7	3.733	0.127	138.1	-0.66
13	4	2	1	24.7	6.267	0.209	114.7	-0.6
13	4	2	2	24.7	6	0.246	99.87	-0.46
13	4	2	3	24.7	3.467	0.248	108.3	-0.54
14	6.5	0	1	13.2			359.2	-0.24
14	6.5	0	2	13.2			364.5	-0.14
14	6.5	0	3	13.2			395.7	-0.13
9	6.5	0.04	1	17.6	7.2	0.185	202.4	-0.62
9	6.5	0.04	2	17.6	8.267	0.208	306.7	-0.62
9	6.5	0.04	3	17.6	5.333	0.167	209.6	-0.56
9	6.5	0.04	4	17.6	7.333	0.346	231.3	-0.48
1	6.5	0.1	1	14.8	5.867	0.252	117.6	-0.57
1	6.5	0.1	2	14.8	9.867	0.203	90.93	-0.13
1	6.5	0.1	3	14.8	8.267	0.378	179.7	-0.52
1	6.5	0.1	4	14.8	8	0.348	238.7	-0.27
1	6.5	0.1	4	14.8	92.53	0.348	N/A	N/A
5	6.5	0.4	1	17.2	8.533	0.244	224.5	-0.19
5	6.5	0.4	2	17.2	16	0.188	260.8	-0.17
5	6.5	0.4	3	17.2	9.6	0.329	229.6	-0.26
7	6.5	2	1	14.4	7.467	0.178	436.8	-0.25
7	6.5	2	2	14.4	13.6	0.191	356	-0.26
7	6.5	2	3	14.4	11.47	0.207	443.5	-0.09
12	7.5	0	1	15.2	15.2	0.162	361.9	-0.18
12	7.5	0	2	15.2	14.4	0.207	308.8	-0.33
12	7.5	0	4	15.2	13.6	0.207	363.5	-0.19
4	7.5	0.04	1	17.4	12.53	0.137	432.8	-0.28
4	7.5	0.04	2	17.4	14	0.401	284.5	-0.19
4	7.5	0.04	3	17.4	8.8	0.213	360.5	-0.24
3	7.5	0.1	1	17	12.27	0.117	309.9	-0.36
3	7.5	0.1	2	17	8.267	0.192	255.5	-0.2
3	7.5	0.1	3	17	13.07	0.207	354.4	-0.27
8	7.5	0.4	1	17.7	9.067	0.157	324.8	-0.29
8	7.5	0.4	2	17.7	9.333	0.167	280.4	-0.23
8	7.5	0.4	3	17.7	12	0.319	256.5	-0.09
6	7.5	2	1	17	14.4	0.25	315.2	-0.12
6	7.5	2	2	17	13.07	0.399	287.7	-0.24
6	7.5	2	2	17	71.2	0.34	344.3	0.093
6	7.5	2	3	17	14.13	0.124	272.3	-0.23

PAH/Au NPs	4	-	2	14.3	7.2	0.117	148.3	-0.67
PAH/Au NPs	4	-	3	14.3	9.6	0.21	134.7	-0.56
PAH/Au NPs	4	-	4	14.3	11.2	0.087	167.7	-0.53
PAH/Au NPs	6.5	-	1	16.4	12.8	0.2	366.7	-0.34
PAH/Au NPs	6.5	-	3	16.4	14.67	0.094	377.6	-0.42
PAH/Au NPs	6.5	-	4	16.4	13.87	0.05	237.1	-0.31
PAH/Au NPs	7.5	-	1	16.5	11.47	0.311	362.1	-0.31
PAH/Au NPs	7.5	-	2	16.5	10.67	0.348	400	-0.26
PAH/Au NPs	7.5	-	3	16.5	6.933	0.133	366.7	-0.46

Table 6: Largest positive and negative bending curvature with corresponding times. The time columns are highlighted from green to red with dark green showing the fastest times and red showing the longest times. The largest positive 1/R column shows smaller numbers in red and larger numbers in green, while the reverse is true for the largest negative 1/R column. For all columns dark green indicates more desirable qualities, which fades to dark red, to mark less optimal values.

The trends are especially apparent in the table below that shows the averages of bending time and largest positive and negative bending curvatures. pH 4.0 samples displayed the fastest bending in both directions, as well as the largest negative bending. Larger pH values showed larger cationic (positive) bending.

pH PAH	[NaCl] (M)	Wt % Uptake EMI-Tf	Largest Positive 1/R time	Largest Positive 1/R Time Std. Dev.	Largest Positive 1/R	Largest Positive 1/R Std. Dev.	Largest Negative 1/R time	Largest Negative 1/R Time Std. Dev.	Largest Negative 1/R	Largest Negative 1/R Std. Dev.
4	0	15.3	6.13	0.27	0.14	0.05	111.73	25.72	-0.65	0.15
4	0.04	14.5	11.07	0.99	0.17	0.08	311.47	91.10	-0.16	0.10
4	0.1	16.5	28.43	44.39	0.15	0.10	170.83	92.80	-0.27	0.29
4	0.4	19.7	6.40	2.32	0.14	0.02	148.89	24.14	-0.55	0.10
4	2	24.7	5.24	1.55	0.23	0.02	107.60	7.42	-0.53	0.07
6.5	0	13.2					373.16	19.73	-0.17	0.06
6.5	0.04	17.6	7.03	1.23	0.23	0.08	237.50	47.72	-0.57	0.06
6.5	0.1	14.8	24.91	37.83	0.31	0.07	156.73	66.09	-0.37	0.21
6.5	0.4	17.2	11.38	4.04	0.25	0.07	238.31	19.64	-0.21	0.05
6.5	2	14.4	10.84	3.11	0.19	0.01	412.09	48.69	-0.20	0.10
7.5	0	15.2	14.40	0.80	0.19	0.03	344.71	31.11	-0.23	0.09
7.5	0.04	17.4	11.78	2.68	0.25	0.14	359.29	74.14	-0.24	0.05
7.5	0.1	17	11.20	2.57	0.17	0.05	306.58	49.55	-0.28	0.08
7.5	0.4	17.7	10.13	1.62	0.21	0.09	287.22	34.67	-0.20	0.11
7.5	2	17	28.20	28.67	0.28	0.12	304.87	31.70	-0.13	0.16
4	-	14.3	9.33	2.01	0.14	0.06	150.22	16.62	-0.59	0.08
6.5	-	16.4	13.78	0.94	0.11	0.08	327.11	78.17	-0.36	0.06
7.5	-	16.5	9.69	2.42	0.26	0.11	376.27	20.68	-0.34	0.11

Table 7: Bending curvature and speed averages for each sample. For the time columns green indicates faster response time, while red indicates longer times. For the 1/R columns, large numbers are green in the Largest Positive /R column while more negative numbers are green in the Largest Negative 1/R column.

While variation in bending direction preference is undesirable from sample to sample, this could likely be alleviated by using larger samples of the composite film for soaking and hot pressing. This is also more feasible now that temperature and soaking times are known. Most of the samples that were made were used in testing ionic liquid soaking parameters, and trying to get the gold to stick during hot pressing. By analyzing the samples with the largest bending in both directions, the realization that thicker CNC layers allowing greater cationic bending, while the largest anionic bending occurred in much thinner CNC layer samples may have gone unnoticed.

3.6 Conclusion

The results presented do not indicate that a CNC incorporating PAMPS displays better bending characteristics in all aspects. However, this analysis presents information that is helpful in determining the CNC growth parameters, based on the goals of the application. It also showed that forming quadlayers of PAH/AuNPs/PAH/PAMPS can improve bending speed and curvature for both directions. For applications making use of the fast cationic bending, but do not require large deformation, lower salt concentrations in conjunction with low pH provide the desired response. On the other hand, if larger cationic bending is required, but the speed is less important, then large salt concentrations in PAMPS and high pH PAH provide the matching results. Fast cationic bending in thinner layers is likely the result of faster ion transport since less material was present.

The largest anionic bending deformation, with additionally fast motion occurred in samples with thin CNCs (those with pH 4.0), making them good candidates for anionic bending applications. The most promising results were found in samples with PAH at pH 4.0 and no salt in PAMPS. This combination produces the very thin layers of polyelectrolyte, thereby reducing total film thickness. pH 4.0 samples with large salt concentrations produced even thinner films, but likely, the salt-induced screening reduced adsorption affects ion motion through CNC so that bending is slowed and reduced. PAMPS successfully contributed toward bending enhancement.

3.7 References

1. D. M. DeLongchamp and P. T. Hammond, Chem Mater **15** (5), 1165-1173 (2003).
2. B. J. Akle, M. D. Bennett, D. J. Leo, K. B. Wiles and J. E. McGrath, Journal of Materials Science **42** (16), 7031-7041 (2007).
3. S. Liu, R. Montazami, Y. Liu, V. Jain, M. R. Lin, X. Zhou, J. R. Heflin and Q. M. Zhang, Sensor Actuat a-Phys **157** (2), 267-275 (2010).
4. R. Montazami, S. Liu, Y. Liu, D. Wang, Q. Zhang and J. R. Heflin, Journal of Applied Physics **109** (10), 104301 (2011).
5. M.-C. Bernard, A. Hugot-Le Goff and W. Zeng, Electrochim Acta **44** (5), 781-796 (1998).
6. J. P. Randin, Journal of The Electrochemical Society **129** (6), 1215-1220 (1982).
7. C.-A. Dai, C.-J. Chang, A.-C. Kao, W.-B. Tsai, W.-S. Chen, W.-M. Liu, W.-P. Shih and C.-C. Ma, Sensors and Actuators A: Physical **155** (1), 152-162 (2009).
8. P.-G. Su and S.-C. Huang, Sensor Actuat B-Chem **113** (1), 142-149 (2006).
9. P.-G. Su, W.-C. Li, J.-Y. Tseng and C.-J. Ho, Sensor Actuat B-Chem **153** (1), 29-36 (2011).
10. S. P. Jiang and H. Tang, Colloid Surface A **407**, 49-57 (2012).
11. J. Feng, Y. Huang, Z. Tu, H. Zhang, M. Pan and H. Tang, Scientific Reports **4**, 6225 (2014).
12. T. R. Farhat and P. T. Hammond, Chem Mater **18** (1), 41-49 (2006).
13. S. S. Shiratori and M. F. Rubner, Macromolecules **33** (11), 4213-4219 (2000).
14. J. Choi and M. F. Rubner, Macromolecules **38** (1), 116-124 (2005).

Chapter 4: Introduction of the Ion-Conducting Polyelectrolyte Nafion into the CNC of an IMPC Bending Actuator

4.1 Introduction

While actuation times and bending curvature have both been improved from bare Nafion through the addition of a CNC, actuation speed, efficiency, lifetime for a sample, and bending strain can still be improved.[1, 2] Some of these improvements may occur through improving ion conduction through the CNC, ideally by incorporating ion conducting polyelectrolytes in the LbL built CNC film.

Porosity, and the internal structure in the CNC are known to affect actuation performance in IPMC type actuators.[1, 3] Ion motion through the CNC depends on the open space and channels within the CNC structure. Interactions between the mobile ions and the molecules in the CNC are also factors affecting the ionic conductivity and therefore bending of the actuator.[3] Therefore, by adding ionically conductive materials, further improvement may be made. When the CNC is highly porous, ion transport is promoted as a result of increasing the effective surface area of the electrode, due to the porosity.[4, 5]

Film porosity or open space, traversed by mobile ions can be tailored through the LbL self-assembly by adjusting solution properties during deposition, as discussed in the introductory chapter. In short, changing the number of charged groups on a polyelectrolyte influences how it will deposit in a PEM (polyelectrolyte multilayer) film.

Additionally, studying the solution assembly conditions can generate increased ionic conductivity in an LbL film through identification of the most conducive crosslinking characteristics for ion conduction.[6]

4.2 Literature Review

Nafion is an ionomer fabricated by DuPont formed by copolymerizing fluorotetraethylene (TFE) with perfluorinated vinyl either, with sulfonate end groups.[7-10] The fluorocarbon backbone is hydrophobic, while the terminating sulfonate or sulfonic acid (acid form) groups are hydrophilic, which causes a phase-separated structure of ion clusters and channels in the presence of water, which is crucial for the highly ion conducting properties of Nafion.[4, 7, 11] As a result of its ion conduction, combined with its chemical and thermal stability,

Nafion has been widely used in sensors, IEAP and IPMC actuators, and polymer fuel-cells.[4, 5, 7-10, 12]

Nafion has been successfully incorporated into the CNC of an IMPC actuator with a Nafion substrate through the direct assembly process (DAP), which was discussed in Chapter 1.[13] The DAP method is designed to fabricate a Nafion/RuO_2 nanocomposite CNC, for an IPMC actuator. DAP-produced IPMC actuators showed good bending results, but ultimately, the LbL CNC fabrication process produces better elastic moduli, peak-to-peak strain, electromechanical conversion efficiency, and bending speed compared to the DAP process.[1, 14] Improvements were attributed to the significantly thicker CNC layer formed by the DAP method—3 μm, compared to 0.4 μm for the self-assembled CNC. Thicker layers decrease actuator speed by increasing the ion motion time, but can in general increase bending strain.[1, 14] The success of the thicker DAP fabricated actuators containing Nafion in the CNC, indicate that thinner Nafion layers, such as those that would be formed from the LbL process, could provide further improvement in bending.

Additional benefits of including Nafion in LbL films were found by Daiko *et al*.[15] Proton conductivity of phenylsilsesquioxane particles was improved 4 orders of magnitude by adding ultra-thin layers of polydiallyldimethylammonium chloride and Nafion by LbL to the surface. Fabricating more Nafion layers also increased the proton conductivity.[15]

Before starting LbL film growth with Nafion in this work, a survey of previous LbL films using Nafion dispersion was completed. It has been used in a number of applications, but it is rather expensive, so information on concentrations others used and their corresponding dipping times was gathered. Usually lower polyelectrolyte concentration can be compensated using a longer dipping time for LbL films. One literature article indicated the stock solution concentration of 5 wt%, or 42 mM was used.[16] We considered 5 wt% to be excessively high, so we first confirmed that deposition could work with 0.5 wt% (4.2 mM) or 0.25 wt % (2.1 mM), which were values reported in several other articles.[17, 18] Other concentrations reported were approximately the same wt% values, but in terms of molarity instead[6] or 1 mg/mL (.909 mM).[19-21]

4.2.1 Effects of solvent type on Nafion

There were variations in what was used to dilute the Nafion solution in the literature. Ping *et al*.[18] used pure ethanol as a diluent, while DeLongchamp and Hammond[6] and Abebe and

Farhat[17] used deionized water instead. Others used a mixture of ethanol and water or methanol and water.[19-21] Studies that used Nafion in solution, but were using it outside of building LbL films were also examined, such as the work by Sun *et al*,[22] who used pure ethanol. Although Nafion is partially water-soluble, many studies used different alcohols as a diluent, especially those who used it in LbL films, which are mostly commonly fabricated in aqueous solutions.[23, 24]

This prompted further research on the solubility of Nafion in water versus the solubility of Nafion in methanol and ethanol. Vishnyakov and Neimark[25] studied a simulation of the molecular dynamics using an equimolar methanol water mixture as the solvent for Nafion. In the simulation, they found that methanol had a slightly higher concentration around the polytetrafluororethylene (PTFE) backbone due to Van der Waals interactions between Nafion's PTFE backbone and the methyl group. Water slightly preferred the sulfate groups, as a result of hydrogen bonds. The simulated polymer chain had a similar folding geometry in the mixture as it does in pure water. The uptake of the mixture was greater than the uptake for either water or methanol alone, with maximum solvation in an equimolar ratio.[25]

Riven *et al*.[26] studied the transport and solubility of water and 3 lower weight alcohols in Nafion membranes, and discovered that the alcohol solubility in Nafion was increased by adding some water to the alcohol. Additionally, the alcohol solubility was a few times greater than pure water. This group's results gave some indication on how water and alcohols interact with the Nafion polymer. The group concluded that alcohols likely dissolve the PTFE backbone, which the water interacts with the sulfonic acid groups, since alcohol alone has a significant solubility in Nafion.[26]

Work by Elliott *et al*.[27] focused on swelling of Nafion membranes in an ethanol/water mixture. They also found evidence of the ethanol helping to solvate or plasticize the fluorocarbon backbone, which allows for rearrangement of the matrix. The degree of swelling of the Nafion polymer is affected by the polarity of the solvent. SAXS and XRD data indicated that polar solvents gravitate toward the charged groups while less polar solvents interact with the fluorocarbon areas.[27]

Thin LbL films capped with a Nafion layer were studied by Sangribsub *et al*.[28] to increase the hydrophobicity of multilayers of combinations of PAH, poly(ethyleneimine), and polystyrene particles. They studied polyelectrolyte solution ionic strength and ratio of water to ethanol as the diluent for the Nafion solution, and its effects on resulting hydrophobicity in the

LbL film. As long as there was some of both the ethanol and water in the solution, the exact ratio did not significantly affect film growth or contact angle.[28] A water-only solution showed the lowest contact angle, which indicated that the ethanol does play an important role in solvation, as suggested by these other literature articles.[28]

Results from the studies discussed above all indicate that alcohol plays an important role in solvating the Nafion PTFE backbone.[25-28] Since both methanol and ethanol improve solvation effect, a methanol/water mixture was chosen as the diluent for the Nafion dispersion used for the CNC. As Vishnyakov and Neimark[25] showed through simulation that uptake was highest in equimolar methanol/water, a 50/50 vol% mixture of the two was chosen for simplicity's sake.[25] As the molecular weights of the two are very similar, this is close to equimolar.

4.2.2 Solvent quality in LbL films

Further literature review on the effect solvent type has in LbL constructed films was conducted. Poptoshev *et al*.[29] studied how ethanol added to polyelectrolyte solutions affected the resulting film grown by LbL. They used PAH and PSS, to form their multilayer films. Solvent quality for the hydrophilic polyelectrolyte solutions was decreased by adding ethanol to the aqueous solution. Increasing ethanol to water ratio increased the thickness of the resulting multilayer film by changing the conformation of the polymer chains. More coiled, less extended polymer chains deposit and increase the thickness of an individual layer.[29]

Solvent effects are clearly important for LbL film growth since polymer conformation is affected. In Nafion's case, the PTFE backbone prefers alcohol, so the end result for LbL films containing Nafion solvated in different ratios of alcohol and water would experience different effects as multilayers of PAH/PSS did in results from Poptoshev *et al*.[29]

4.2.3 Internal morphology of Nafion and ionic conductivity

As-received Nafion membranes were compared to solution cast Nafion membranes by Zaluski and Xu.[30] They studied the water adsorption, ac impedance, dc conductivity, and structure through WAXD. Ionic clustering in Nafion has been shown to be present by small-angle x-ray scattering by Gierke *et al*.[31] and Moore and Martin[32] and is an important factor contributing to Nafion's high ionic conductivity.[30] The solution cast films showed significantly different properties than the as-received membranes, so they do have some morphological differences, perhaps since casting was completed below the glass transition temperature, there wasn't enough thermal energy to form the clusters. The cast films adsorbed much less water, has

a much lower ionic mobility, and at room temperature, the conductivity was 10^4 times lower than the as-received film. Wide-angle x-ray diffraction (WAXD) and differential scanning calorimetry (DSC) data showed some ionic cluster evidence, but it was reduced compared to the as-received membrane, which simply indicates that the morphology of the cast films is somewhat present but less developed.[30]

4.3 Materials and Methods

4.3.1 Materials

Quadlayer films of poly(allylamine hydrochloride) (PAH), anionic gold nanoparticles (AuNPs), and a Nafion™ dispersion were fabricated via the electrostatic layer-by-layer (LbL) deposition process, as explained in the introductory chapter. Films were grown on glass substrates and Nafion membrane (Ion Power Inc. Nafion™ NR-211, EW 1100). 10 mM PAH (Sigma Aldrich, M_w ~ 58,000 g/mol) was used as the starting polyelectrolyte, followed by colloidal ~3 nm AuNPs (Purest Colloids), which were used as purchased. Another layer of PAH is included after the gold nanoparticles, which was then followed by a Nafion dispersion (EW 1100, Fuel Cell Store). Originally, the Nafion dispersion comes as a 5 wt% solution in a mixture of lower molecular weight alcohols and water. The Nafion-alcohol-water stock solution was diluted to 0.25 wt% with RO water in order to perform the deposition, so that the final solution contained 2.5 % alcohol.

After film growth, mobile ions are imparted into the film interior by soaking at an elevated temperature in 1-ethyl-3-methylimidazolium trifluoromethanesulfonate (EMI-Tf) (≥98%, Sigma Aldrich), used as purchased. Following ionic liquid soaking, 120 nm gold electrodes (L.A. Gold Leaf, 23K) are hot pressed on the outside of the PEM film coated Nafion film.

4.3.2 Methods

PAH and AuNPs were deposited for ~3 min 40 s and Nafion was deposited for ~ 16 min. Between each polyelectrolyte deposition step, samples were rinsed in a single beaker of RO water for approximately 3 minutes. No drying was used between dipping steps.

In order to measure the thickness of the partially complete layer structure, a sample on a glass substrate was removed from the dipping robot after every 5 quadlayers, in order to determine how film thickness was affected by increasing layer number. The robot was then immediately restarted to minimize film drying before growth was finished.

4.4 Key Issues

4.4.1 Deposition time vs Nafion concentration

The wide range of Nafion solution concentrations used in the literature prompted examination of solution concentration versus deposition time. Ideally, conserving Nafion solution by using a low concentration but longer dipping time during ISAM growth would result in equally thick films as a film grown with a more concentrated solution for a shorter time.

First, the time length for film deposition needed to be determined to ensure complete multilayer growth occurred even at low solution concentrations. Multilayer films of equal thickness were attempted by using different solution concentration through adjusting the growth time. To test this, two solutions were prepared, one at 0.5 wt% (4.2 mM) and one at 0.25 wt% (2.1 mM), diluted with an equal volume mixture of 50% RO water/50% methanol. First films were grown only on glass substrates in order to determine if comparable film thicknesses could be obtained using the two different concentrations of Nafion solution at different deposition times. The greater concentration was left to deposit for 10 minutes, and 15 minutes was used for the lower concentration. Both time lengths were values reported in the literature for deposition times for Nafion solutions of similar concentrations.[6, 17] PAH and AuNP layers were both set to deposit for about 3 minutes and 40 seconds; a much shorter time was possible because of their much greater concentrations.

During the first two film growths, PAH at pH 7.0 was used for both PAH layers, thicknesses were measured to determine the final fabrication parameters. Thickness results with RMS roughness error bars are shown in the Figure 4.1 below.

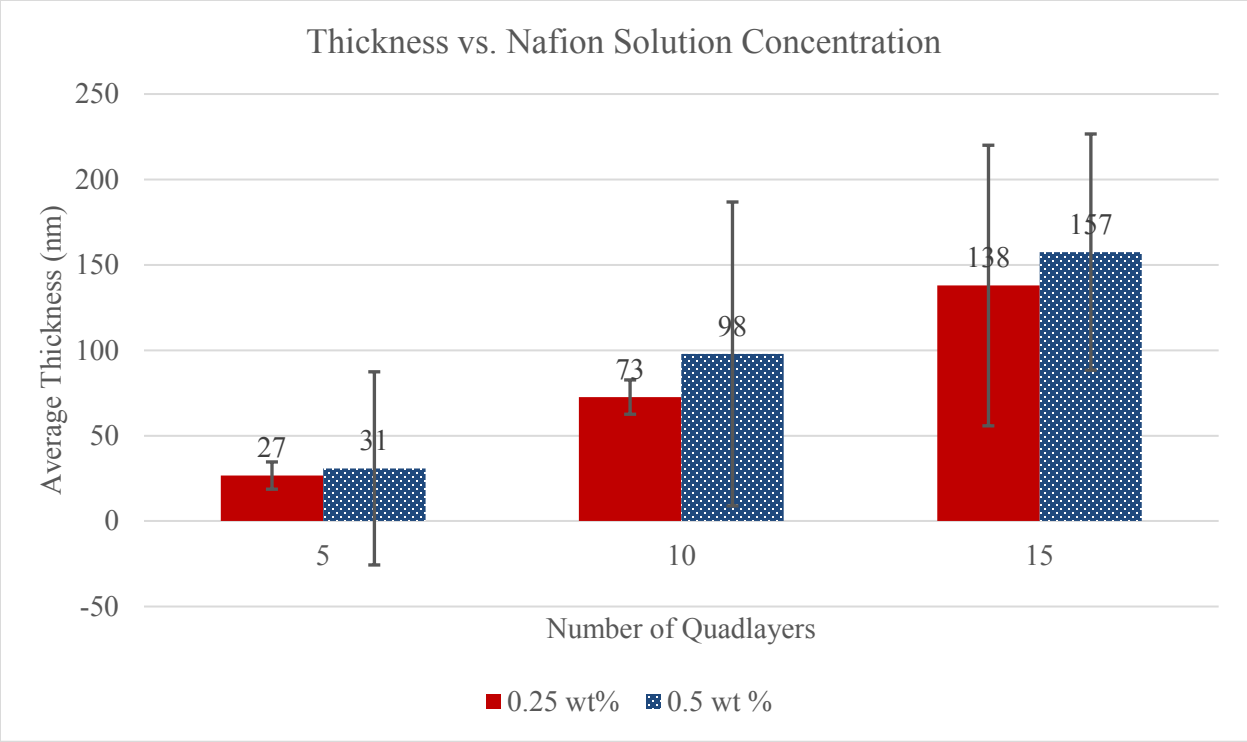

Figure 4.1: Thickness of resulting quadlayer films of PAH/AuNPs/PAH/Nafion as a function of Nafion solution concentration measured by profilometry. Error bars are obtained via R_q, or RMS roughness, also obtained through profilometry. Values with corresponding standard deviations are also found in Table 20.

Originally, using the greater concentration, 0.5 wt% Nafion, was planned since the resulting films were a little thicker, and it required shorter deposition time. The first planned run was Nafion-containing 0.05 M NaCl. Solutions were made at least 12 hours in advance of the fabrication and left stirring in order to ensure homogeneity. Substrates were prepared as detailed in Section 2.1, by mounting the film onto a polycarbonate frame with double sided tape.

During the first fabrication on Nafion film, the Nafion film stuck to the pump that removes water, and had no visible ISAM coating. The film separated from the tape, which was had never been previously observed after many times using the same LbL process on Nafion film substrates. The obvious initial conclusion was that perhaps that sample was never very well attached to the frame. So a retrial was planned. Extra care was taken to ensure the film was well attached to the frame. But during the second trial deposition process the Nafion film also detached from the frame.

After the Nafion film separated from the tape twice, it seemed more likely that something in one of the solutions was interacting with the tape, causing the Nafion film to be released. The

only things different about these runs rather than any other film growths was the presence of the Nafion polymer and alcohol in the solution. Quick stability experiments were completed by placing part of the tape between glass slides and part of it exposed to the solution. The taped slides were then tested in varying Nafion, methanol, and water solution conditions. In all cases, the exposed part of the tape turned from transparent to translucent white and became less sticky after several hours in the solution. The part of the tape sandwiched between the glass lost its adhesive and turned white only in the Nafion/water/methanol solution and the methanol/water solution. The sample that was placed in water was still stuck tightly. This indicated that the methanol was reacting with the tape and making it less sticky.

Since the methanol was reacting with the tape, a method to suspend the film on the frame without using the tape was needed. Other methods have been used by previous group members, including stapling the film between two frames, and sandwiching the film between the grooves Ziploc strips glued to the frame. Dong Wang discovered that the steel in the staples reacts poorly with the gold nanoparticle colloid, so the Ziploc attachment method was used, after testing the glue for stability in methanol and Nafion solution.[33]

The next dipping fabrication was prepared using 0.5 wt% Nafion solution and the films looked very light and thin compared to the previous deposition, where the Nafion film detached from the frame. Additionally, the gold nanoparticle colloid had turned blackish-purple from bright magenta, indicating degradation.[33] After ruling out that the glue was damaging the AuNPs, it seemed the double layered frame prevented complete rinsing. Each solution was contaminated by previous polyelectrolyte remaining on the frame, which was brought into the next polyelectrolyte solution. Only one rinsing step occurred between each polyelectrolyte layer, while previous uses of the Ziploc frame were done with the standard fabrication materials PAH and AuNPs. This leaves room for 3 rinsing beakers before going on to the next polyelectrolyte solution. In this case, cross contamination of the polyelectrolyte solutions was problematic.

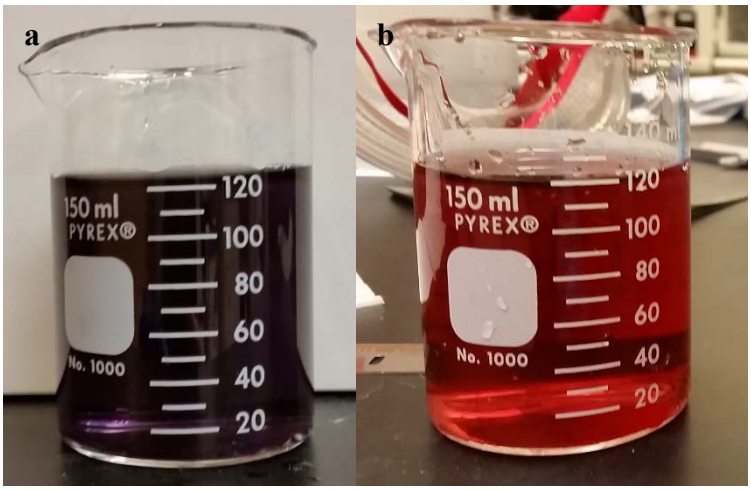

Figure 4.2: AuNP colloid after use for 5 quadlayers in the deposition using a double-layered Ziploc frame. Notice from the image on the left that it is a dark purple, almost black color, compared to the original color, which is a bright magenta, as shown by the image on the right.

Increasing the rinse time would not help if the double layer frame was bringing too much solution with it each time, so instead, the tape method was resumed, and as much alcohol as possible was eliminated from the Nafion solution in order to preserve the tape's integrity. Alcohol was removed by diluting the Nafion stock solution with pure RO water, to 0.25 wt% Nafion. The smaller concentration was chosen since the Nafion stock solution is about half alcohol. After testing in the new Nafion solution, the tape was stable, and the tape mounting method seemed likely to hold the Nafion film during the ISAM film growth. New solutions were prepared, and subsequent depositions produced intact LbL films on Nafion.

Aqueous Nafion solutions with large salt concentrations however, formed agglomerates upon addition of the salt. After vigorous stirring, agglomeration was reduced enough to perform the multilayer film growth, but this agglomeration was not a problem in methanol/water based Nafion solution at the same NaCl concentrations. A similar problem was observed by DeLongchamp and Hammond, who also diluted Nafion stock solution with pure water.[6] They observed the ionic screening caused thickness increase and decrease with a salt concentration range from 0-0.4 M NaCl. They observed a "visible cloudiness" in a water-based 2 mM Nafion solution with 4% alcohol, and solid precipitates at concentrations of 1 M and greater. In the Nafion solution in this work, however, cloudiness was seen at 0.1 M NaCl and greater, which resulted in very rough Nafion films. DeLongchamp and Hammond concluded that water was a

poor solvent for Nafion, so the ionic screening thickness variation resulted over a smaller NaCl concentration range than in other polyelectrolytes.[6]

4.5 Results and Discussion

4.5.1 Experiment plan

During experiment planning for incorporating Nafion into the CNC, the number of different fabrication conditions was reduced to 5 from 15, by restricting PAH's pH to 4.0. The most desirable bending characteristics for other IPMC actuators were produced using pH 4.0 PAH in the CNC. This was true for CNC multilayers composed only of PAH and AuNPs, as well as within quadlayer CNCs containing a sulfonic acid polymer, PAMPS, PAH, and AuNPs. The same type of experiment as the PAMPS-containing CNC was designed, but using Nafion dispersion instead. Nafion is a strong polyelectrolyte, so its degree of ionization was modified using NaCl added to the solution.

Because of the overall success of pH 4.0 PAH in CNCs, pH effects on PAH were excluded and only pH 4.0 PAH was used. The goal was to determine the fabrication parameters for a PAH/AuNPs/PAH/Nafion CNC that enhanced IPMC actuator performance the most, by varying NaCl concentration in the Nafion solution. This allowed the ISAM film morphology and thickness to be tailored using NaCl screened Nafion. Standard PAH/AuNPs are composed of 30 bilayers of the multilayer film, so 15 quadlayers was again chosen for the Nafion-containing CNC. The same dipper setup was used as in the PAMPS-containing CNC fabrication. PAH was the first layer deposited, followed by rinsing for approximately 3 minutes in one beaker of water. Gold nanoparticles are then deposited, followed by another layer of PAH. Finally a layer of Nafion is deposited. Rinsing occurs after each layer deposition, and the process is repeated 15 times. The total number of layers is the same for both the standard CNC composed of PAH and AuNPs and this version.

The literature was reviewed to determine a range of NaCl concentrations in Nafion that would cause thickness and film morphology change. DeLongchamp and Hammond[6] provided very useful information on the range of NaCl concentrations in Nafion where screening-enhanced and screening-reduced adsorption occurs. Thickness of Nafion-containing LbL films can be varied widely between 0 and 0.2 M NaCl in 0.002 M Nafion aqueous solution.[6] Others who performed LbL with Nafion solution also used values within this range.[16-21] This led to choosing 0, 0.025, 0.05, 0.1, and 0.2 M NaCl in 0.25 wt% (2.1 mM) Nafion solution as values

for fabricating and testing Nafion CNC actuators. Based on this, the following test matrix was developed. Originally, pH 7.0 PAH was planned, but after further information, pH 4.0 was confirmed to produce better CNCs.

Nafion-Containing Actuator Sample Fabrication Plan				
Run #	pH PAH	[NaCl] in Nafion	Nafion solution	g NaCl for 120 mL
2	7	0	0.5 wt% = 4.2 mM	0
3	4	0	0.25 wt% = 2.1 mM	0
4	4	0.025	0.25 wt% = 2.1 mM	0.17532
5	4	0.05	0.25 wt% = 2.1 mM	0.35064
6	4	0.1	0.25 wt% = 2.1 mM	0.70128
7	4	0.2	0.25 wt% = 2.1 mM	1.40256

Table 8: Plan for fabricating quadlayer CNC with PAH/AuNPs/PAH/Nafion with varying concentrations of NaCl to vary ionic screening in the Nafion solution.

4.5.2 CNC thickness

Film thickness of each sample was measured after fabrication. Average measurements and RMS roughness are shown below in Figure 4.3. Error bars are obtained from the RMS roughness values. NaCl concentrations greater than 0.1 M produced very rough multilayer films, which was clearly visible to the naked eye. Spots and streaks were present over the entire multilayer film in samples containing large salt concentrations. Additionally, increasing film thickness with increasing layer number was not present in films containing Nafion with sodium chloride concentrations greater than 0.1 M. This is likely a result of the roughness values being so large, that accurate film thicknesses were unobtainable with this method, or the NaCl produced enough ionic screening that nonuniform films were produced.

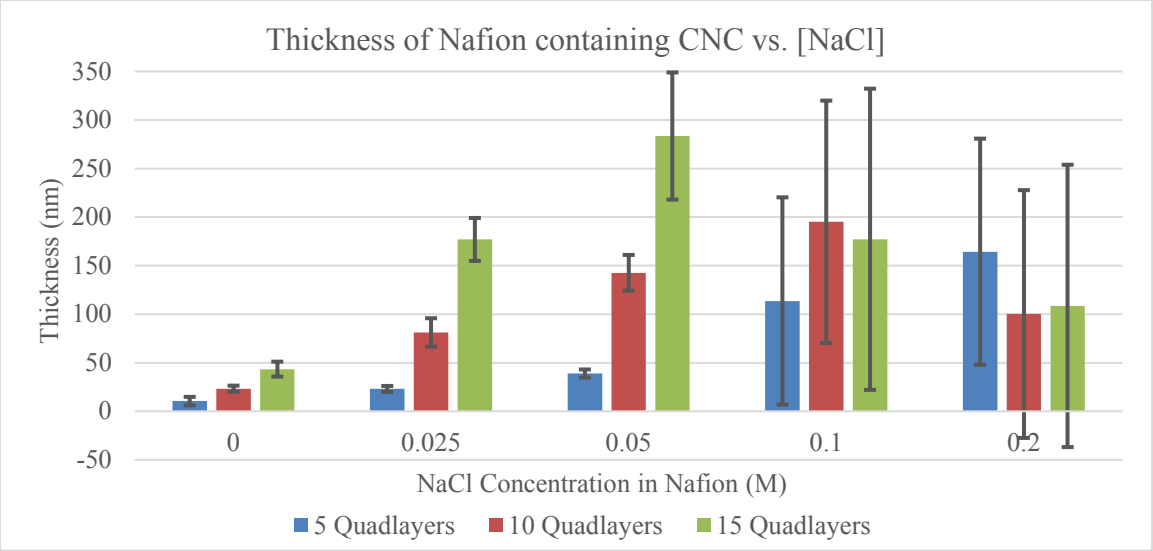

Figure 4.3: Thickness of the CNC on glass substrates. Error was obtained from RMS roughness. 0.1 M and 0.2 M NaCl in Nafion made for high roughness values, and inconsistency in film growth as more quadlayers were added. Values with corresponding standard deviations are also found in Table 20.

Table 9 shows thickness comparison of a 10 bilayer film of PAH and AuNPs with 10 quadlayer films of PAH/AuNPs/PAH/Nafion at various NaCl in Nafion concentrations. Nafion was indeed deposited, since the Nafion quadlayers (containing twice as many layers) are significantly thicker for each NaCl concentration.

Comparison of Nafion CNC Thickness to PAH/AuNP CNC Thickness				
pH PAH	**[NaCl] (M) in Nafion**	**# layers**	**Thickness (nm)**	**Thickness St. Dev. (nm)**
4	-	10 bls	7.92	1.20
4	0	10 qlrs	23.26	0.82
4	0.025	10 qlrs	81.23	3.73
4	0.05	10 qlrs	142.61	4.26
4	0.1	10 qlrs	195.13	16.51
4	0.2	10 qlrs	100.16	44.77

Table 9: Thickness comparison for Nafion-containing quadlayer films and PAH/AuNP bilayer (shaded blue) films.

The 15 quadlayer ISAM films on both Nafion and glass substrates are shown in Figure 4.4. Some of the features, especially those on the larger NaCl concentration samples are visible to the naked eye.

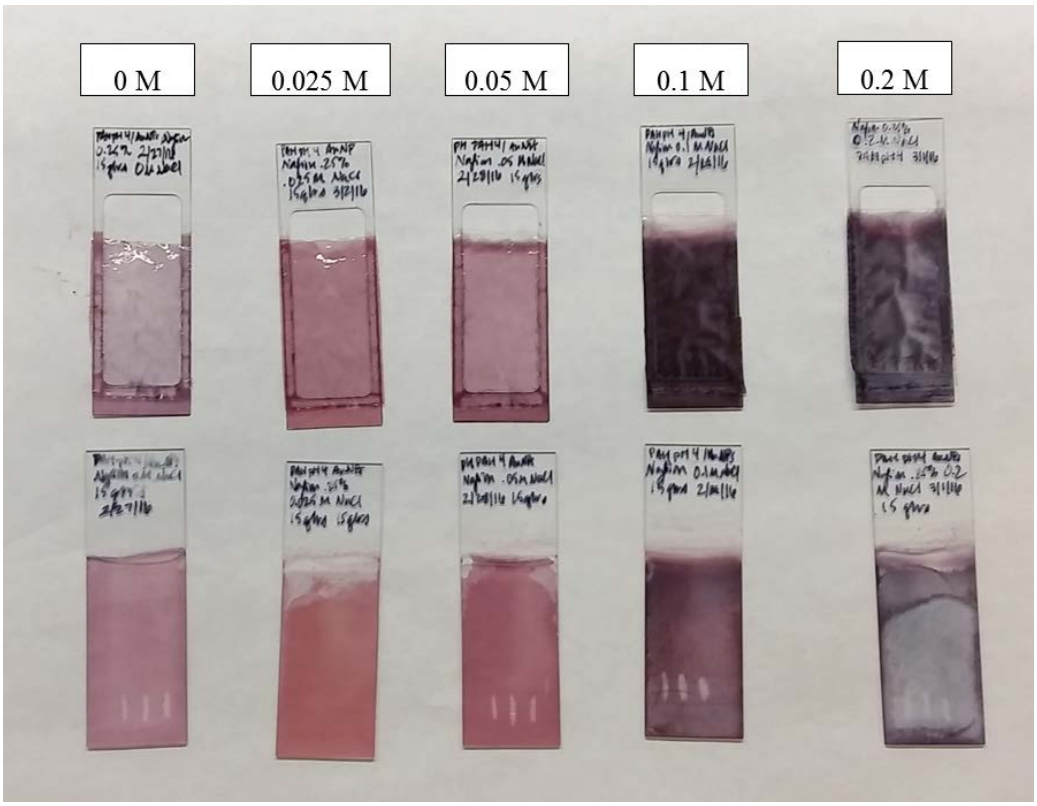

Figure 4.4: 15 quadlayer PAH/AuNPs/PAH/Nafion multilayer films. Nafion substrates are shown at the top with glass substrates at the bottom. NaCl in the Nafion layer increases from 0 to 0.2 M from left to right. Notice the films look uniform (apart from the edges) on the 0, 0.025, 0.05 M NaCl samples, but the two on the right, 0.1 and 0.2 M NaCl appear quite inhomogeneous in the center.

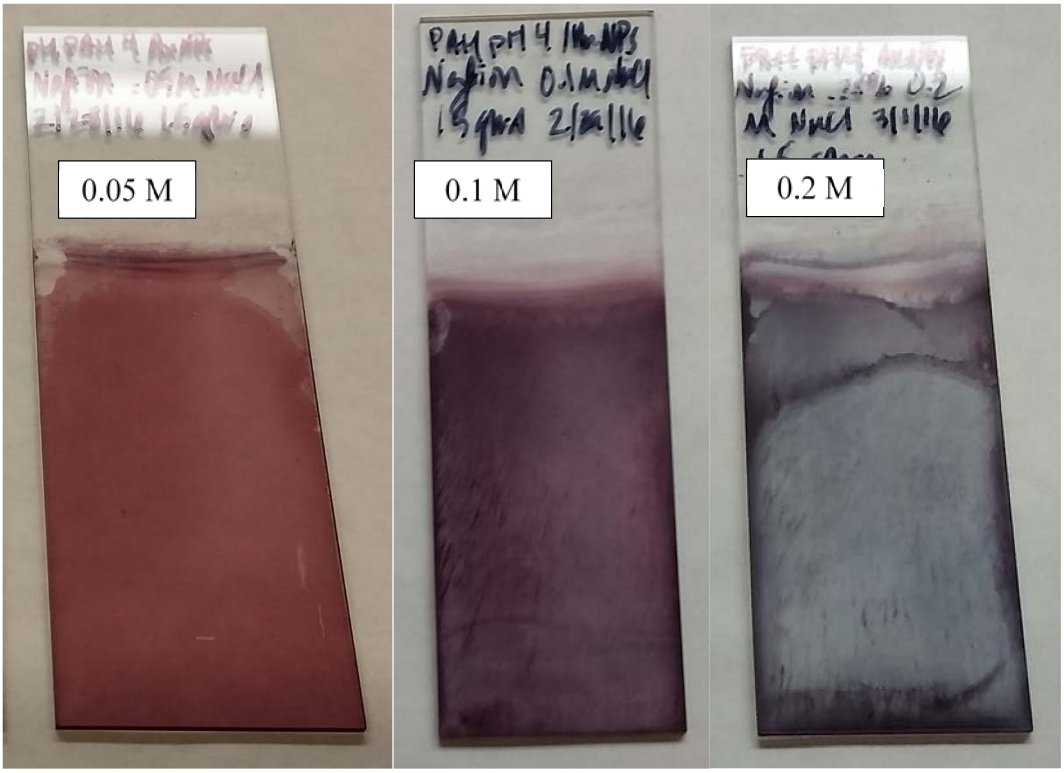

Figure 4.5: Close up of samples fabricated with 0.05, 0.1, and 0.2 M NaCl in Nafion. The sample containing 0.05 M NaCl in Nafion is visibly much smoother and more uniform than the right two samples. The 0.1 and 0.2 M NaCl in Nafion caused agglomerations or streaky features on the film.

The roughness occurring in the 0.1 and 0.2 M NaCl samples arise because the NaCl in higher concentrations greatly reduced the solubility, as mentioned previously. Agglomerations formed after immediate addition of the NaCl to the Nafion solution. DeLongchamp and Hammond[6] noticed a "cloudiness" in their Nafion solutions containing 0.4 M NaCl and higher, and precipitates at 1.0 M NaCl. Their solutions were 2 mM Nafion in water with 4.4% alcohol, which was very similar to solution concentrations used in the CNC films here.[6] The same agglomeration did not occur in the methanol/water mixture Nafion solutions. Since the methanol/water solution was the original plan, solutions of all salt concentrations were prepared before the initial deposition. The images below in Figure 4.6 show the aqueous Nafion solutions after multilayer film fabrication. The images were taken after hours left unstirring following deposition. The materials in the solution separated. In the 0.1 M and 0.2 M beakers of Nafion solution, there are two layers. The bottom layer appears to be a complex containing gold nanoparticles, as the color is the same as the AuNP colloid. All other chemicals used were

transparent. This indicates that some of the multilayer was washed off in the Nafion solution, perhaps because the deposition time for the Nafion solution was so long, and the NaCl present caused reduced deposition and poorer dissolution of the Nafion/NaCl. The beakers containing lower NaCl concentrations resembled the 0.05 M NaCl solution. No layer was visible at the bottom.

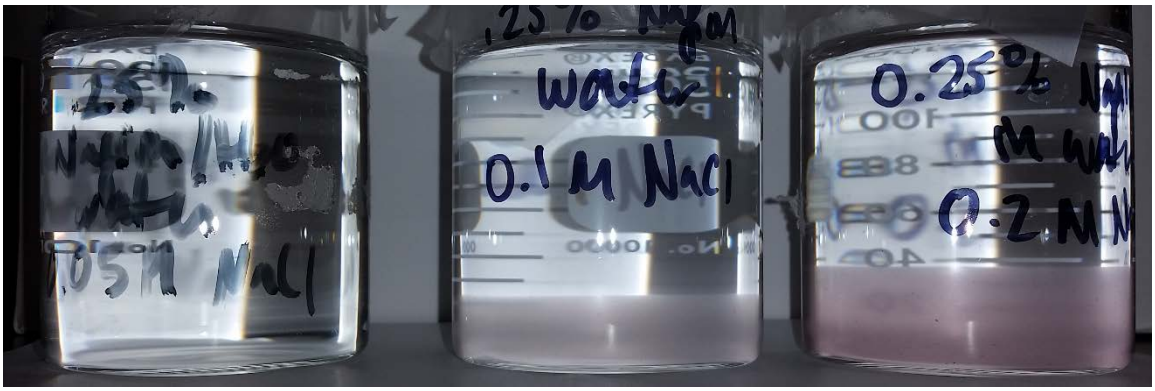

Figure 4.6: Nafion solutions after film fabrication. Notice the different layers of material in the right two samples, which contained the most NaCl.

4.5.3 Ionic liquid soaking

After fabricating the actuator samples, a sample of each run was submerged in EMI-Tf ionic liquid at 40 °C for 30 minutes to determine how amenable the CNC was to the ionic liquid. A low temperature was used to prevent CNC damage, which occurred in the PAMPS-containing CNCs at high temperatures. The equal time length and temperature soak also helped narrow down a time length for soaking when trying to fabricate samples to test their actuation. Ionic liquid is a strong factor in bending measurements, so getting samples with similar weight percent uptakes is important for directly comparing the quality of the CNC in terms of producing a bending actuator. Figure 4.7 below shows the uptake for each sample when exposed to EMI-Tf at 40 °C for 30 minutes. A low temperature was used to start in order to prevent degradation of the CNC at elevated temperatures.

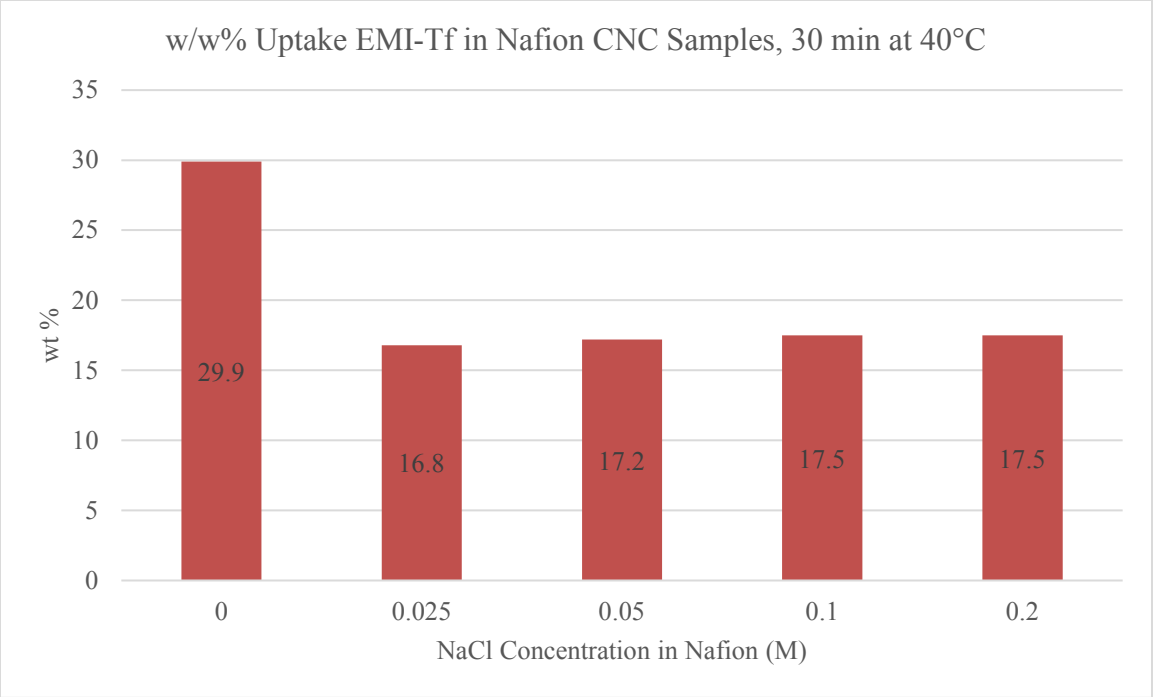

Figure 4.7: Weight percent uptake of EMI-Tf by each sample after soaking at 40 °C for 30 minutes.

Surprisingly, nearly all the samples had very similar weight percent uptakes under equal soaking conditions. PAMPS-containing CNCs had much more variation. The similarity indicates that for all samples, ionic liquid uptake was unrestricted by the CNC. These weight percent uptake values for short soaking times at low temperatures seemed more promising for obtaining a higher weight percent uptake for all samples for actuator testing. Since control samples had already been tested at 45 wt% uptake, 45 ±3 wt % was set as the goal for Nafion CNC actuators.

In order to obtain 45 wt%, the soaking temperature was increased to 80 °C—the soaking temperature used for the standard PAH/AuNPs only samples. Samples with lower salt concentrations in the Nafion layer achieved the 45 wt% uptake goal within 40-45 minutes, without visible damage. The CNC for 0.2 M NaCl sample however, easily came off when drying the excess ionic liquid after 30 minutes, and achieved only 42 wt% uptake EMI-Tf.

Figure 4.8: Before and after soaking at 80 °C for the 0.2 M NaCl in Nafion sample. The CNC degraded significantly, and wiped off, as shown above.

This led to the conclusion that a 45 wt% goal was unrealistic, but 35 wt% might be more obtainable at a lower temperature, since 80 °C caused some films to become unstable. Soaking temperature was reduced to 40 °C to preserve the integrity of the CNC films, but samples then required very long soaking times to reach 35 wt%. The temperature was increased to 50 °C, and film stability was evaluated during drying excess ionic liquid. CNC films were stable at 50 °C, but 35 ±3 wt% uptake seemed impossible for all samples. Instead, 32 ± 3 wt% was more realistic. A table of the soaking times, temperatures, and weight percent uptakes is shown below in Table 10. One sample of each NaCl concentration within this weight uptake range was fabricated for accurate comparisons on the actuator function.

Ionic Liquid Soaking Trials – Nafion-Containing Samples				
pH PAH	**Temperature (°C)**	**Time (min)**	**[NaCl] (M) in Nafion Solution**	**wt% EMI-Tf**
4	40	30	0	29.9
4	40	30	0.025	16.8
4	40	30	0.05	17.2
4	40	30	0.1	17.5
4	40	30	0.2	17.5
4	40	22	0	20.2
4	40	19	0	18.2
4	40/80	22/30	0	41.7
4	40/80	22/40	0	42.5
4	80	45	0.05	48.5-CNC came off
4	80	41	0.1	48.2
4	80	30	0.2	41.8-CNC wiped off easily.
Decided 35 wt% goal, ended with 32 wt% goal.				
4	40	60	0.2	9.4
4	40	120	0.2	34.6
4	50	30	0	29.2
4	50	36	0	31.3
4	50	56	0	30.4
4	50	40	0.1	23
4	50	80	0.1	34.3
4	50	60	0	30.2
4	50	100	0	33.5
4	50	60	0.05	30.2
4	50	60	0.025	33.1
4	50	75	0.1	31.1

Table 10: Ionic liquid soaking temperatures and times for all Nafion/NaCl samples. The final goal weight percent was 32.0±3.0 wt%. One sample of each NaCl concentration was fabricated within this ionic liquid uptake range for testing.

4.5.4 Actuator bending

After ionic liquid soaking, actuator samples were fabricated by hot pressing gold electrodes on the outside. Three samples of each different NaCl concentration run were tested to measure bending curvature and speed. As in the samples made using PAMPS in the CNC, there was significant variation in the largest positive bending curvatures in both directions. Again they are plotted showing the samples with the largest positive curvature sample and the largest negative curvature. Results from these measurements are shown below. Variation between the positive and negative bending curvatures and times occurred between different samples of the same sample run. Most notably, the 0.025 M NaCl samples and the control samples with a CNC composed of only PAH and AuNPs showed the greatest variation. The plots in Figure 4.9 show

that the Nafion-containing CNC samples had comparable and sometimes have greater bending curvatures than the control samples. The largest positive and negative bending curvature points for each sample are highlighted and labeled.

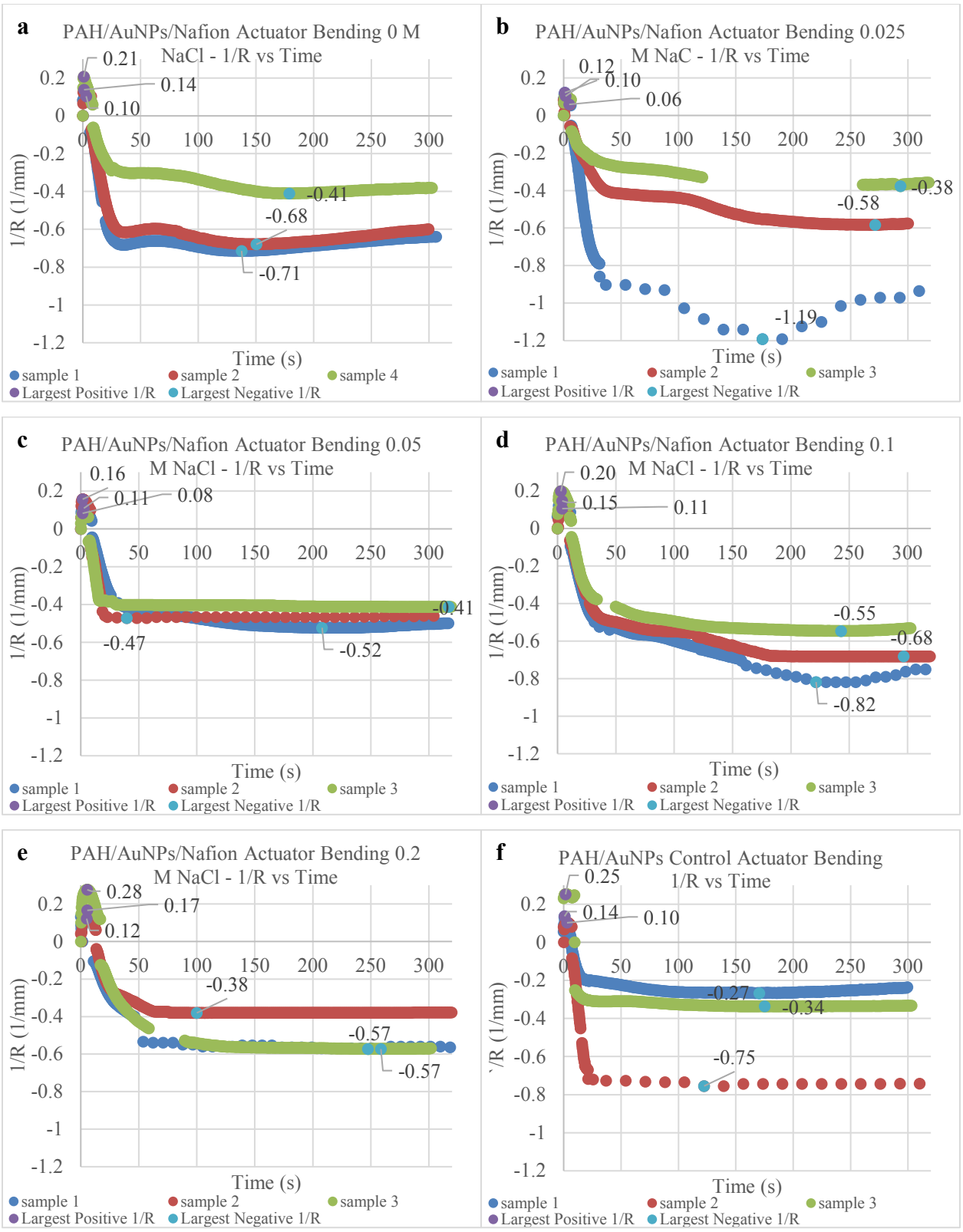

Figure 4.9: Plots showing bending curvature as a function of time for varying NaCl concentration in Nafion solution during LbL film growth. All samples are approximately 32 wt% EMI-Tf.

For samples containing 32 wt% EMI-Tf, the most negative bending was shown by the 0.025 M NaCl sample, which has a thin CNC. The next largest negative bending occurred in 0.1 M NaCl sample followed by the control, then the salt free sample. Increasing the NaCl content slowed bending down, since the thickness increased, increasing the distance ions were required to travel and as a result, increasing the bending time. The largest positive bending occurred in the 0.2 M NaCl sample, though it was also the slowest. Speed versus bending curvature observations are consistent with those observed in the PAMPS-containing CNC samples.

In Figure 4.10a, samples with the largest positive (cationic) bending curvature are shown. 0.2 M NaCl caused the largest but slowest bending. The control sample had a similar bending curvature but was several seconds faster. Increasing salt concentration increased the time it took to reach the maximum curvature, with only minor enhancements in bending curvature. Again, this is consistent with Liu *et al*'s[1] observation on CNC thickness versus bending speed and curvature.

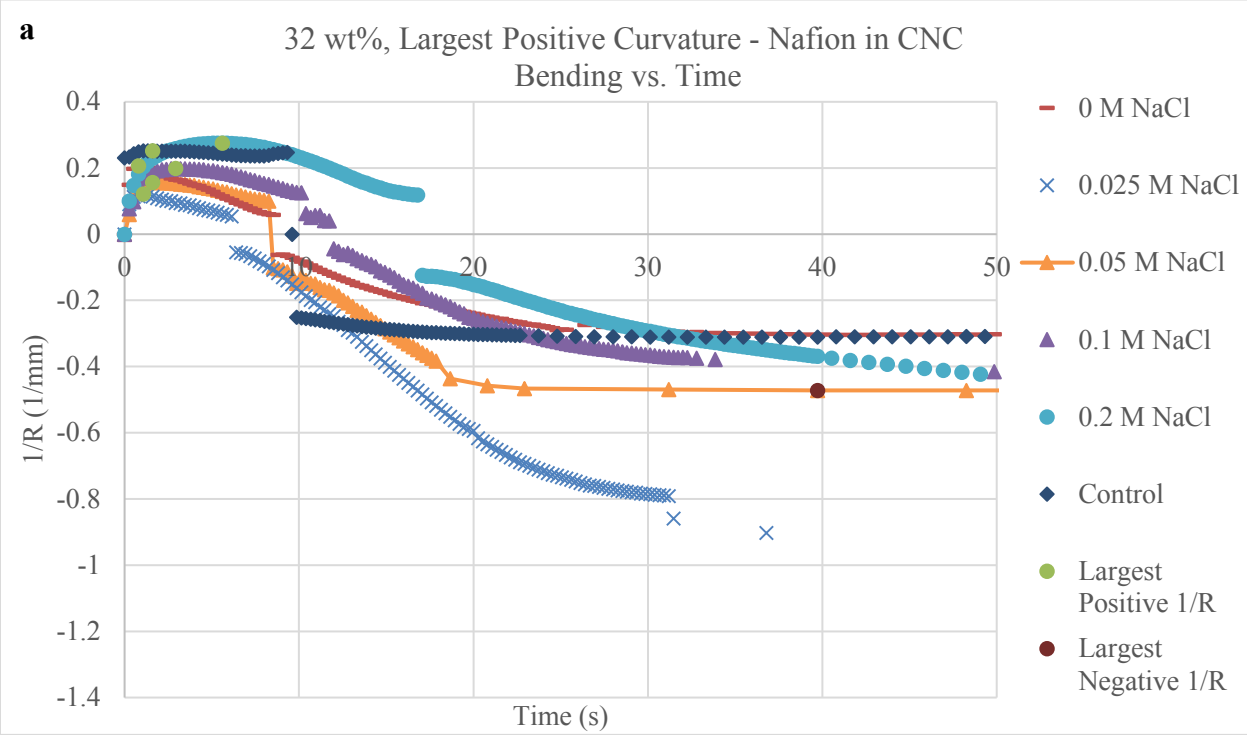

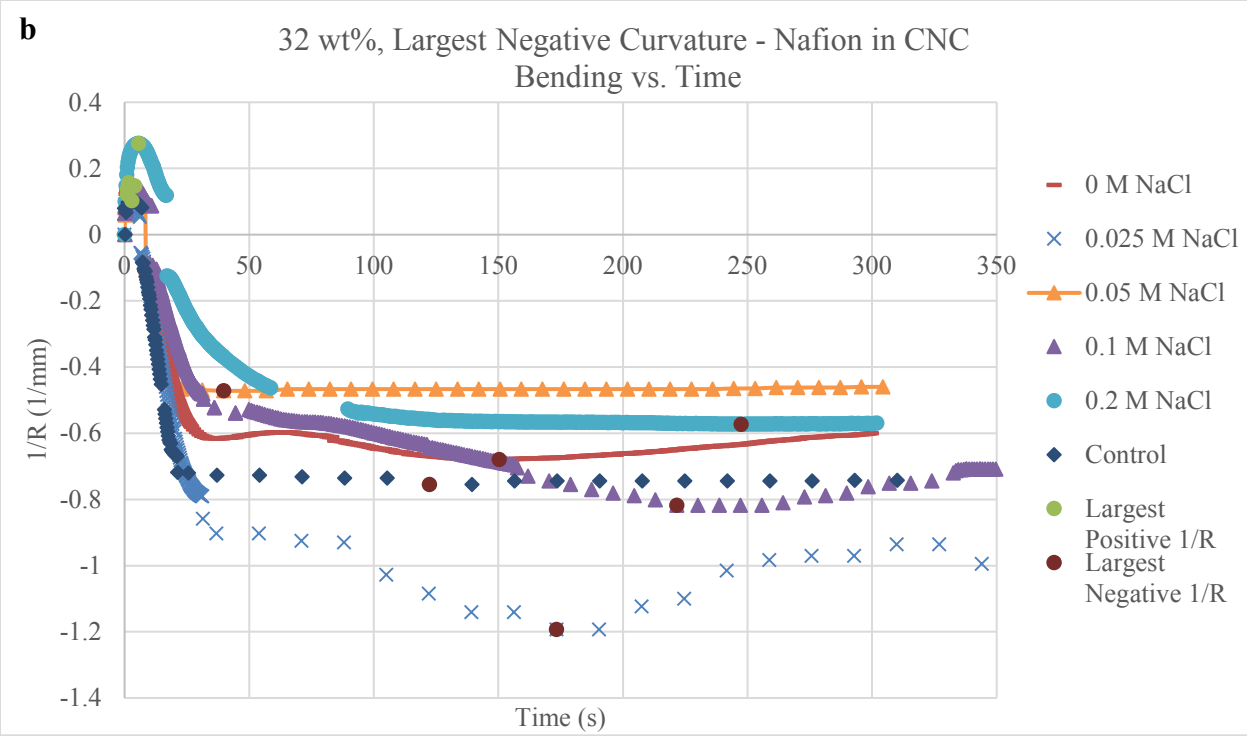

Figure 4.10: Samples with the largest bending curvature in both directions for samples with varying NaCl content in Nafion. Some of the same samples had both the largest positive and negative bending curvatures, which is ideal. These are 0.025, 0.05, and 0.2 M samples.

The bending results indicate that by replacing half the CNC's AuNPs layers with Nafion, improved bending curvature in both directions can be achieved over PAH/AuNP CNC actuators. In the 0.025 M NaCl/Nafion sample, an even larger negative bending curvature than the control was obtained. The 0.1 M NaCl/Nafion sample had a greater positive bending curvature than the control. Bending timescales were similar for all samples during cationic bending, while the anionic bending times showed more variation. The control samples and the lower NaCl concentration samples showed faster bending overall in both directions, as a result of the thickness variation. A table of all the largest positive and negative curvature values with their corresponding times is shown below in Table 11.

Nafion-Containing CNC Bending Curvature Measurements 32 wt%					
M NaCl	**sample #**	**Largest Positive 1/R time**	**Largest Positive 1/R**	**Largest Negative 1/R time**	**Largest Negative 1/R**
0	1	2.93	0.10	138	-0.71
0	2	1.07	0.14	150	-0.68
0	4	0.80	0.21	179	-0.41
0.025	1	1.07	0.12	173	**-1.19**
0.025	2	4.80	0.06	271	-0.58
0.025	3	1.60	0.10	294	-0.38
0.05	1	2.67	0.11	208	-0.52
0.05	2	1.60	0.16	40	-0.47
0.05	3	1.60	0.08	317	-0.41
0.1	1	4.00	0.15	222	-0.82
0.1	2	4.00	0.11	297	-0.68
0.1	3	2.93	0.20	243	-0.55
0.2	1	5.07	0.12	259	-0.57
0.2	2	5.60	0.17	100	-0.38
0.2	3	5.60	**0.28**	247	-0.57
Control	1	0.80	0.14	170	-0.27
Control	2	2.93	0.10	122	-0.75
Control	3	1.60	0.25	175	-0.34

Table 11: The largest bending curvature for both directions with corresponding times. The time columns are highlighted from green to red with dark green showing the fastest times and red showing the longest times. The Largest Positive 1/R column shows smaller numbers in red and larger numbers in green, while the reverse is true for the Largest Negative 1/R column. For all columns green indicates more desirable qualities.

Greater NaCl concentrations cause much slower cationic bending, but greater curvatures, which is caused by the increased thickness. Anionic bending speeds vary widely even between samples with the same NaCl concentration, but lower NaCl concentrations caused larger bending. Some improvements over the control were made, but largely in terms of anionic (negative) bending curvatures.

The samples with approximately 17 wt% ionic liquid were also tested for bending since the initial ionic liquid soaking test produced samples with very similar EMI-Tf uptakes. Trends between bending time and cationic curvature as a function of salt concentration were the same as the 32 wt% uptake samples. The table below shows the averages for each NaCl concentration condition. The 17 wt% samples showed more of a trend for the negative bending curvature however. Lower salt concentrations enhanced the negative bending, as was seen in the samples containing PAMPS. Of course, anionic bending curvatures are larger and faster for the 32 wt% samples than they are in the 17 wt% samples, which is because of the larger ion concentration to cause bending. Cationic bending is also faster with more ionic liquid, but strangely the average

largest cationic bending curvature is greater for the lower weight percent samples, at least in these averaged values. Relative bending speeds based on the ion concentration could be a result of the fact that the samples studied had a bending direction preference resulting from hot pressing. More data on the 17 wt% samples is included in Appendix A.

Average Nafion-Containing CNC Bending Curvature Measurements								
17 wt % samples								
M NaCl	**Time**	**Time Std. Dev.**	**Largest Positive 1/R**	**Largest Positive 1/R Std. Dev.**	**Time**	**Time Std. Dev.**	**Largest Negative 1/R**	**Largest Negative 1/R Std. Dev.**
0	3.02	3.16	0.10	0.03	268.00	103.06	-0.43	0.16
0.025	6.58	1.89	0.15	0.05	96.89	12.25	-0.41	0.03
0.05	6.76	1.11	0.23	0.10	255.11	131.29	-0.34	0.14
0.1	9.24	0.41	0.18	0.08	372.53	62.87	-0.28	0.13
0.2	15.73	1.16	0.29	0.07	369.96	121.40	-0.03	0.21
Control	9.33	2.01	0.14	0.06	150.22	16.62	-0.59	0.08
32 wt% samples								
0	1.60	1.16	0.15	0.05	155.64	21.16	-0.60	0.17
0.025	2.49	2.02	0.09	0.03	246.13	64.01	-0.72	0.42
0.05	1.96	0.62	0.12	0.04	188.27	139.72	-0.47	0.06
0.1	3.64	0.62	0.15	0.05	253.78	38.76	-0.68	0.14
0.2	5.42	0.31	0.19	0.08	202.04	88.55	-0.51	0.11
Control	1.78	1.08	0.16	0.08	156.00	29.20	-0.45	0.26

Table 12: Comparison of average values between samples with 17 wt% vs 32 wt% EMI-Tf. Similar trends are seen in both time column, as well as the largest positive radius of curvature.

4.5.5 Comparison between PAMPS- and Nafion-containing CNCs

Comparisons between the samples with the largest cationic and anionic bending curvatures and speeds for both PAMPS and Nafion are shown in Figure 4.11. The PAMPS sample that was chosen for the comparison was not the one with the largest positive bending curvature, but it was very close, and had a faster response time. Both samples containing PAMPS as the ion conducting polyelectrolyte in the CNC outperformed the Nafion-containing samples. The positive bending curvature and time for the maximum bending were very similar, so the PAMPS-containing sample was only slightly better in terms of cationic bending. On the largest negative bending curvature samples, however, the PAMPS sample had significant improvement in bending curvature, and a slight benefit in bending speed.

PAMPS's superior bending results indicate that in the use of ion conducting polyelectrolytes in the CNC, it would be better to focus on PAMPS instead of Nafion. This may be a result of differences such as the equivalent weight of the two polymers, which indicates the molar mass of polymer per charged ionic group in polyelectrolytes. Nafion's equivalent weight is 1100 (g/mol) while PAMPS is about 200 (g/mol). Therefore Nafion has much more material

that doesn't participate in electrostatic bonding that enables film growth. Other causes could be related to the solubility differences between the two polymers, and how their solution conformations translated to chain conformations after adsorption onto the growing film.

Another reason may be simply because LbL film growth structure likely prevents the same phase-separation that promotes ion conduction so strongly in cast films. Zaluski and Xu[30] saw reduced ionic conductivity in Nafion films once they had been deconstructed and recast. DeLongchamp's and Hammond's work comparing LPEI/PAMPS and LPEI/Nafion films showed that the PAMPS-containing film resulted in superior ionic conductivity. The ionic conductivity of the LPEI/Nafion films was slightly less than that of the commercially available solution cast membrane, further indicating that the strongly ion conducting molecular organization in the solution cast film may not be present in the LbL form. The comparison between PAMPS and Nafion LbL films in the IPMC actuator presented here aligns with this theory, since PAMPS outperformed Nafion when included in the ISAM CNC. Table 13 shows a summary of the largest average positive and negative bending curvatures and their respective times.

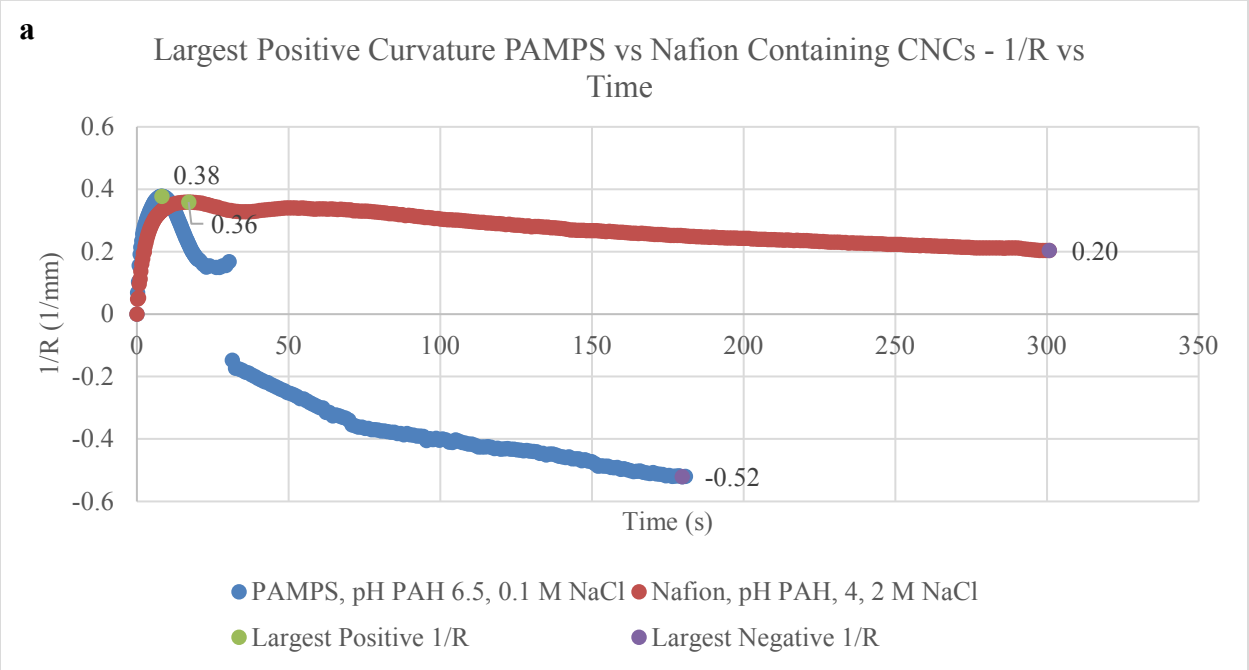

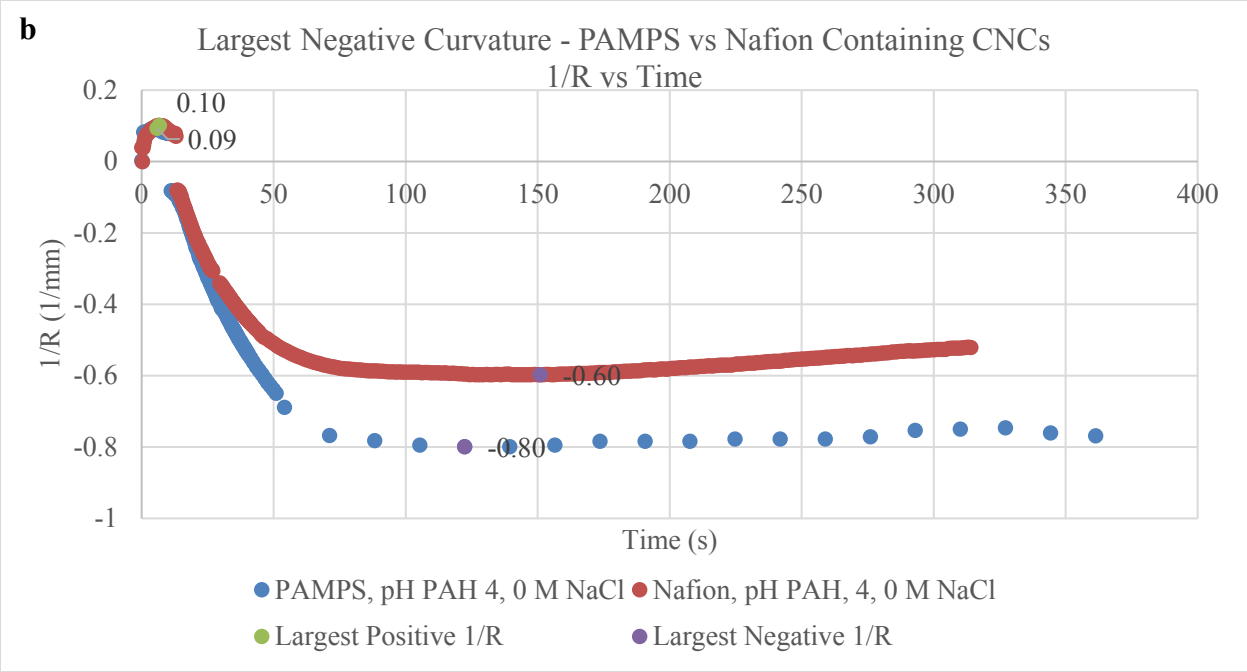

Figure 4.11: Comparisons of the best performing samples of PAMPS and Nafion-containing CNCs. PAMPS samples showed larger bending curvature than the Nafion-containing samples.

Comparison of Largest Avg Positive and Negative PAMPS and Nafion Bending Curvature Measurements

Poly-electrolyte	pH PAH	[NaCl] (M)	Largest Pos. 1/R time	Largest Pos. 1/R Time Std. Dev.	Largest Pos. 1/R	Largest Pos. 1/R Std. Dev.	Largest Neg. 1/R time	Largest Neg.1/R Time Std. Dev.	Largest Neg. 1/R	Largest Neg. 1/R Std. Dev.
PAMPS	6.5	0.1	24.91	37.83	0.31	0.07	156.73	66.09	-0.37	0.21
Nafion	4	0.2	15.73	1.16	0.29	0.07	369.96	121.40	-0.03	0.21
PAMPS	4	0	6.13	0.27	0.14	0.05	111.73	25.72	-0.65	0.15
Nafion	4	0	3.02	3.16	0.10	0.03	268.00	103.06	-0.43	0.16

Table 13: Comparisons between the largest average positive and negative bending curvatures and corresponding times for the Nafion and PAMPS-containing actuators with the greatest bending. PAMPS actuators surpassed the properties of the Nafion-containing actuators.

The large average positive curvature for the pH 6.5 PAH and 0.1 M NaCl in PAMPS samples was caused by one measurement of a sample that did not show negative bending at all, and also resulted in very slow positive bending. The other measurements such as the one shown on the plot in Figure 4.11 above had much shorter positive bending times. Those values are listed in Table 6.

4.6 Conclusion

In conclusion, an IPMC actuator composed of Nafion film with a CNC of 60 total layers in the order of PAH/AuNPs/PAH/Nafion showed improvement in bending curvature from an actuator made from Nafion film with a CNC of 60 total layer of PAH/AuNPs. Lower salt concentrations used to modulate the ionic strength of the aqueous Nafion solution produce smooth films while greater salt concentrations increase film roughness. 0.025 M NaCl in Nafion produced an actuator sample with the largest negative bending curvature, indicating that the ionic conducting polyelectrolyte can improve actuator bending performance over the previous standard, composed of PAH/AuNPs. Improvement over the control samples was less apparent in the Nafion-containing CNCs than the PAMPS-containing CNCs, however. Additionally, actuators containing PAMPS in the CNC outperformed those containing Nafion in the CNC. All the films were capable of absorbing enough ionic liquid to provide strong bending properties at an intermediate humidity level.

4.7 References:

1. S. Liu, R. Montazami, Y. Liu, V. Jain, M. R. Lin, X. Zhou, J. R. Heflin and Q. M. Zhang, Sensor Actuat a-Phys **157** (2), 267-275 (2010).
2. Y. Liu, R. Zhao, M. Ghaffari, J. Lin, S. Liu, H. Cebeci, R. G. de Villoria, R. Montazami, D. Wang, B. L. Wardle, J. R. Heflin and Q. M. Zhang, Sensors and Actuators A: Physical **181**, 70-76 (2012).
3. R. Montazami, S. Liu, Y. Liu, D. Wang, Q. Zhang and J. R. Heflin, Journal of Applied Physics **109** (10), 104301 (2011).
4. M. D. Green, D. Wang, S. T. Hemp, J. H. Choi, K. I. Winey, J. R. Heflin and T. E. Long, Polymer **53** (17), 3677-3686 (2012).
5. R. Montazami, D. Wang and J. R. Heflin, International Journal of Smart and Nano Materials **3** (3), 204-213 (2012).
6. D. M. DeLongchamp and P. T. Hammond, Chem Mater **15** (5), 1165-1173 (2003).
7. C. Heitner-Wirguin, Journal of Membrane Science **120** (1), 1-33 (1996).
8. K. A. Mauritz and R. B. Moore, Chemical Reviews **104** (10), 4535-4586 (2004).
9. M. Shahinpoor, K. J. Kim and D. J. Leo, Polym Composite **24** (1), 24-33 (2003).
10. D. R. Morris and X. Sun, J Appl Polym Sci **50** (8), 1445-1452 (1993).
11. J. N. Ashcraft, A. A. Argun and P. T. Hammond, Journal of Materials Chemistry **20** (30), 6250-6257 (2010).
12. J. P. Randin, Journal of The Electrochemical Society **129** (6), 1215-1220 (1982).
13. B. J. Akle, M. D. Bennett, D. J. Leo, K. B. Wiles and J. E. McGrath, Journal of Materials Science **42** (16), 7031-7041 (2007).

14. S. Liu, R. Montazami, Y. Liu, V. Jain, M. Lin, J. R. Heflin and Q. M. Zhang, Appl Phys Lett **95** (2), 023505 (2009).
15. Y. Daiko, H. Sakamoto, K. Katagiri, H. Muto, M. Sakai and A. Matsuda, Journal of The Electrochemical Society **155** (5), B479-B482 (2008).
16. Y. Daiko, K. Katagiri, T. Yazawa and A. Matsuda, Solid State Ionics **181** (3–4), 197-200 (2010).
17. D. G. Abebe and T. R. Farhat, Soft Matter **6** (6), 1325-1335 (2010).
18. J. Ping, J. Wu, X. Luo and Y. Ying, Ionics **17** (5), 443-449 (2011).
19. J. Hemmerle, V. Roucoules, G. Fleith, M. Nardin, V. Ball, P. Lavalle, P. Marie, J. C. Voegel and P. Schaaf, Langmuir **21** (23), 10328-10331 (2005).
20. Y. Daiko, K. Katagiri and A. Matsuda, Chem Mater **20** (20), 6405-6409 (2008).
21. Y. Daiko, K. Katagiri and A. Matsuda, Journal of Nanoscience and Nanotechnology **9** (1), 404-407 (2009).
22. W. Sun, D. Wang, G. Li, Z. Zhai, R. Zhao and K. Jiao, Electrochim Acta **53** (28), 8217-8221 (2008).
23. O. Sinai and D. Avnir, The Journal of Physical Chemistry B **113** (42), 13901-13909 (2009).
24. R. F. Tarek, in *Amphiphiles: Molecular Assembly and Applications* (American Chemical Society, 2011), Vol. 1070, pp. 105-116.
25. A. Vishnyakov and A. V. Neimark, The Journal of Physical Chemistry B **105** (32), 7830-7834 (2001).
26. D. Rivin, C. E. Kendrick, P. W. Gibson and N. S. Schneider, Polymer **42** (2), 623-635 (2001).
27. J. A. Elliott, S. Hanna, A. M. S. Elliott and G. E. Cooley, Polymer **42** (5), 2251-2253 (2001).
28. S. Sangribsub, P. Tangboriboonrat, T. Pith and G. Decher, Polym Bull **53** (5), 425-434 (2005).
29. E. Poptoshev, B. Schoeler and F. Caruso, Langmuir **20** (3), 829-834 (2004).
30. C. Zaluski and G. Xu, Macromolecules **27** (23), 6750-6754 (1994).
31. T. D. Gierke, G. E. Munn and F. C. Wilson, Journal of Polymer Science: Polymer Physics Edition **19** (11), 1687-1704 (1981).
32. R. B. Moore and C. R. Martin, Macromolecules **22** (9), 3594-3599 (1989).
33. D. Wang, Dissertation/Thesis, Virginia Tech 2015.

Chapter 5: IPCNC Actuators as Humidity Sensors

5.1 Introduction

The humidity dependence of Nafion, LbL, and polymer systems has been documented for several years, including the ionic conductivity's dependence on relative humidity and/or water content in the polymer film. Typically ionic conductivity increases with increasing water content or relative humidity.[1-11] IPMC actuators have also been studied by several groups in terms of humidity dependence on their mechanical and electrical properties, making use of resistive and capacitive changes, or other parameters like impedance.[5, 12-27] Other groups have used different materials in LbL films for humidity sensing,[28, 29] or even other polymeric devices.[10, 30, 31] The relative low cost and flexibility, among other properties make polymer-based sensors highly applicable.[29] For Nafion-based IPMC actuators, relative humidity influences electrical and mechanical properties, as the sulfonic acid groups in the Nafion chains are highly hydrophilic. Nafion readily adsorbs moisture from the environment, and retains it within the structure in the ion-conducting channels even after drying, as discovered by Morris and Sun[32] in the early 1990s.

The last part of this study builds on the work of Dong Wang,[20] who examined the relative humidity dependence of Nafion-based IPMC actuators with a PAH/AuNP CNC, containing EMI-Tf ionic liquid on bending, as well as measured current through the device under varying humidity. His work showed that the performance of the IPMC actuator is significantly affected by relative humidity of the operating environment, and the resulting humidity dependence can be used as a relative humidity sensor. In his dissertation, he presented the discovery that current measured through the actuator begins in a very sharp drop, once a voltage is applied after starting from zero potential. A steady-state current is quickly achieved, which is dependent on %RH and is attributed to water electrolysis of the IPMC actuator's internal adsorbed water, balanced by additional water being adsorbed. The humidity sensor device described in the following chapter makes use of this property. His testing and results, which are described in Section 5.2 showed significant promise for an IPMC-based relative humidity sensor using steady-state current measurements.[20]

While the relative humidity sensitivity of bending and current was discovered on its own for the device presented here, a history of using similar factors for humidity sensors exists in the literature. However, since the combination of an IPMC actuator with an LbL conductive

network composite electrode is unique, the goals in this work were to determine how the addition of the CNC electrode adds to relative humidity sensing functionality, and if it produced better sensing results than a plain Nafion IPMC actuator. Section 5.2 discusses similar devices from the literature. The rest of the chapter discusses further humidity sensitive measurements in the IPMC actuator. The test voltage was optimized, then the effects of CNC properties such as varying the pH of PAH used in making the device, as well as the ionic liquid concentration were examined. Lastly, the relative speed of the response to large changes in relative humidity was compared to a much faster and higher quality commercial hygrometer than had been employed in the previous work.

5.2 Literature Review: Polymer Humidity Sensing Devices

Most humidity sensors involving polymer materials such as LbL films, and IPMC actuators, used electrical changes, such as changes in impedance,[19, 29] capacitance,[10, 22-26, 33] resistance,[21] or current[20] to detect changes in relative humidity. Polymer based humidity sensors largely fall into two categories based on whether they use resistive or capacitive changes to detect relative humidity.[29, 34] Sensors utilizing the material resistance typically use polyelectrolytes or polymer-salt complexes. Hydrophobic polymers are used for capacitive sensors.[29] In other cases, investigators used mechanical responses to detect change,[30] or quartz-crystal microbalance (QCM) frequency changes.[28] Some studies focus on the humidity dependence of various properties on these polymer-based devices, while others examine them with the intent of actually making RH sensors. Techniques have been used to fabricate polymer-based humidity sensitive devices, such as dip coating,[27] screen and ink-jet printing,[35, 36] as well as LbL films.[28, 29, 37-39] Below, some of the important projects studying RH sensor development using IPMC actuators, Nafion, or other polymers are discussed.

Morris's and Sun's[32] Nafion based humidity sensor made use of both electrical conductivity and the water diffusion coefficient, which changed based on the amount of adsorbed water inside the film. To form the sensor, Nafion was applied to a glass substrate, followed by a platinum-black Nafion slurry, then a steel gauze electrode. Current was measured through the device at various water-vapor pressure values. The device gave a quick response, of about 1 minute, and was shown to be stable for a couple of weeks. This was rather early work conducted in 1993.[32]

Another example by Mahadeva, Yun, and Kim[10] showed a functioning temperature and humidity sensor based on a cellulose-polypyrrole nanocomposite. In this case, pyrrole was polymerized onto a cellulose surface, and the polymerization time, and subsequent amount of polypyrrole was varied in order to determine the best time length for humidity sensing applications. Capacitance of the nanocomposite was used in order to determine relative humidity, since it increases with increasing adsorbed water. Response time of their device was about 418 s for either increasing or decreasing RH by approximately 65%, or 7 s per 1%RH. The reversibility of their device was good, showing that polymer-based materials have applications for making effective humidity sensors.

A more unique humidity sensor was fabricated by Islam and Serpe[30] out of a poly(N-isopropylacrylamide) microgel actuator, and made use of mechanical, rather than chemical or electrical changes to determine relative humidly. While this seems less practical for commercial production or use, the ideas involved are interesting. The actuator bends under varying relative humidity, as a result of a poly(diallyldimethyl ammonium chloride) layer on top of the microgel, which shrinks as it dries. Thereby, the electrostatically attached substrate bends in response. A chain of paper clips were used as weights, and were suspended over a balance. Differences in bending caused the number of paper clips resting on the balance to change, therefore registering a change in relative humidity.[30]

Must *et al.*[19] used a very similar type of actuator to the IPMC based device studied in this thesis. They fabricated a Nafion based actuator containing an ionic liquid, with a high surface area composite electrode of titanium carbide-derived carbon (TiC-CDC) within a Nafion matrix, sandwiched between two outer conductive gold electrodes. The TiC-CDC particle matrix is indeed a CNC, although it was not called that. However, it was produced using the direct assembly process method introduced by Akle *et al.*[40] They made use of the changes in impedance with varying relative humidity in order to fabricate a sensor. They also discussed the fact that both humidity and temperature affect the viscosity of the ionic liquid, as well as ionic conductivity, which in turn govern the impedance in the system. However, differentiation between impedance changes as a result of temperature and humidity is difficult.[19]

In another publication Must *et al.*[41] used the same type of ionic liquid containing Nafion-based IPMC actuator with a titanium carbide-derived carbon electrode to detect humidity gradients and harvest energy based on the same principle. The two electrodes of the actuator are

exposed to different relative humidity and over time, a diffusion gradient of water begins through the actuator, which causes the ionic liquid to move and form an electric double layer boundary, and a current flows. The ionic liquid motion also causes a volume imbalance which leads to bending. In addition to humidity gradient detection, the current can be collected and used to supply electrical energy.

Su and Cheng[28] successfully detected humidity with an LbL film of carboxyl-modified mica particles with PAH on a QCM. They were able to create a calibration curve for the frequency change of the QCM based on the amount of water adsorbed in the film. They found good sensitivity even at low humidity conditions, a linear relationship between frequency and adsorbed water, fast response time, and reversible water adsorption.[28] They tried combinations of films with pH 3 and pH 7, and with and without salt in the mica solution. The best results occurred at pH 7.0 and using solutions containing salt. The difference in frequencies was greater with salt containing PEs and pH 7.0 allowed for higher frequency changes across the range of humidity studied. This was attributed to thicker layers occurring as a result of more COOH groups at the higher pH, thereby providing a greater charge density, and greater interaction with adsorbed water. Salt-containing solutions helped because the salt rendered the LbL film more hydrophilic, allowing a greater interaction with adsorbed water.[28]

In a later study, Su *et al*.[29] developed a transparent and flexible humidity sensor that functions by measuring impedance with an LbL film of polyelectrolyte multilayers. The transparent humidity sensor was built by forming LbL multilayers of several polymers including PAMPS doped with two salts, poly(diallyldimethylammonium chloride), poly(styrenesulfonic acid) sodium salt, and sodium dodecyl sulfate, on a PET substrate with aluminum-doped zinc oxide electrodes. Humidity sensing was optimized by studying the effects and improvements caused by the number of deposited layers, the polyelectrolyte concentration, the doping salt concentration, temperature effects, response and recovery time, and stability.[29]

For Su *et al*'s[29] sensor, intermediate PAMPS concentration (10 mM) allowed for the greatest ion conducting properties, and impedance increased with increasing layer number, since ion conduction occurs largely on the outskirts of the film. Then PAMPS was doped with two different salts to increase the RH sensitivity at values lower than 60%. Sodium chloride was used for lower humidity, because it dissociates at low humidity. They also added K_2CO_3, which dissociates at higher RH values, and improved the sensitivity at higher RH. The addition of both

salts improved the performance and widened the range of detection capability to 20-90%RH. Their RH sensor had fast response (about 1 min) and recovery (70s) with consistent performance for at least 50 measurements.[29]

Dong Wang[20] studied the humidity dependent aspects of IPMC actuators with an LbL CNC, such as the control actuators tested in previous chapters. He characterized IPMC actuator performance under different relative humidity. It was determined that actuation in terms of speed and curvature increases with increasing relative humidity until very high %RH values, where water easily condenses on the outer gold electrode. The condensation then decreases actuator bending and speed, as a result of adsorbed water on the outer surface of the electrode.

As Wang[20] discussed in his dissertation, the current measurement under a constant applied voltage through the actuator has a characteristic shape. When an ionic liquid containing IPMC actuator is placed under a constant low applied voltage at constant relative humidity, there is an initial sharp drop in current in the first few seconds. As the measurement continues, the current through the actuator decreases more slowly, and reaches a steady-state within a couple of minutes. The steady-state current varies strongly with relative humidity of the measuring environment. Water electrolysis within the actuator was used to explain this phenomenon. Adsorbed water inside the device is electrolyzed under applied voltages greater than ~1.3 V, and as water is lost to electrolysis, more water vapor from the environment adsorbs, so that electrolysis and the steady-state current can continue. Larger %RH result in faster electrolysis and adsorption, and therefore an increase in the steady-state current.[20]

His work also included studying the effects of applied voltage on the resulting current in actuators with a CNC and plain Nafion IPMC actuators. At low voltages (~2.0-3.0 V), the output currents are equal, but they diverge slightly with increasing voltage, with the CNC containing actuator producing a larger current than the CNC-free actuator. Steady-state current output was determined to be approximately proportional to the surface area of the sample being tested. One further promising test showed that the IPMC actuator's response to large changes in humidity is about 20 times faster than a slow commercial hygrometer. The Fluke 971 fast hygrometer used to determine relative humidity in this thesis is expensive ($300) and the hope is that a device made with these actuator materials would be cheaper.[20]

A wide variety of polymer based humidity sensitive and sensor devices have been described in the literature, making use of many different polymers and varying properties. After

the promise showed by the Nafion-based IPMC actuator containing ionic liquid, Wang[20] discussed that further exploration and development of the device was necessary in order to determine the feasibility of a true humidity sensor. His work is expanded upon in the following sections.

5.3 Materials and Methods

5.3.1 Materials

Actuator samples used in the relative humidity sensing tests were all made with CNCs composed only of LbL-assembled PAH and AuNPs, or bare Nafion without a multilayer film. The Nafion, PAH, AuNPs, gold electrodes, and ionic liquid EMI-Tf used were all the same materials discussed in the introduction and general methods. Multilayer film fabrication, ionic liquid soaking, and hot pressing of the gold electrode procedures were also all the same.

As in previous experiments, tests were conducted in a controlled environment. Humidity was increased in the chamber by using an ultrasonic humidifier and decreased by adding N_2 to the chamber. Voltage, time length, and current measurements were controlled through a μAutolabIII/FRA2 impedance analyzer. Relative humidity was determined using a Fluke 971 humidity/temperature meter. During the response speed comparison test, the hygrometer reading was recorded with a Sony HDR-AS100V video camera.

5.3.2 Methods

Initial tests included confirming the current output though an IPMC actuator observed by Dong Wang.[20] Early work also focused on determining optimal sample and test parameters including experiments on operating voltage, sample size, and the relative humidity sensitivity limits and range. Other initial measurements included experimenting with different sample materials (with or without CNC). The first tests were made using Nafion 111 actuator samples with 30 bilayer CNCs at pH 4.0 PAH and AuNPs, in 1x10 mm^2 strips containing approximately 33 wt% EMI-Tf. Measurements were taken under 2.5 V, starting at low RH, then increased in 5% increments. Upper range RH 70%RH and greater values frequently caused current overloads in the impedance spectrometer, which has a maximum current range of 10 mA. No trends or commonalities other than the high humidity were apparent. Measurements were repeated in order to obtain a sample that was capable of measuring RH values greater than 50-70%. Voltage was decreased to 1.5 V in an effort to lower the current enough to prevent current overload in the impedance spectrometer.

Current overloading was problematic because samples that underwent a current overload seemed to either short, or they would be more susceptible to current overloading again, at lower RH values. Current overloaded samples were unreliable and could not be used for further testing. Further indications of damaged samples, especially after current overload, were found in the residual voltage. Residual voltage is the potential that is left over after the external electric field is turned off. Since ions migrate to the oppositely charged electrodes while under the external potential, they redistribute from Coulombic repulsion once no external force keeps them in place. This usually takes several minutes to decrease, though it takes much longer at lower RH values, since the additional water enhances conductivity and is a plasticizer. Damaged samples show a much faster decrease in this residual voltage; sometimes it is nearly instantaneous.

Further improvements were attempted through making smaller samples, as the current is proportional to the sample's area.[20] Tests on samples made from Nafion 111 film with no CNC were conducted, and tested under the same conditions, 1.5 V, 2x2 mm^2 sample size, with 25 wt% EMI-Tf, at various RH levels. Observations of a faster residual voltage decrease at RH values greater than about 50-60% were made. Some samples that were tested at high RH showed normal measurements for the first part, but then had a current overload after a couple of minutes under applied voltage. Extended measurement times at high RH levels may add to the likelihood of a current overload. Eventually, some success was reached and it was observed that the current scaled with RH over a large RH range. Then the same process was done in 1%RH increments, to determine the sensitivity to small RH differences.

The next step in obtaining samples with reliable and repeatable measurements, from which a current versus humidity calibration curve could be made, was to fabricate fresh samples. Loss of functionality in IPMC actuators with time has been observed, so fresh samples had the potential to increase reliability and decrease current overloading. After fabricating new samples with fresh CNC layers, and fresh ionic liquid, the operating voltage was optimized by taking measurements at varying voltages in the range of 1.5 V to 4 V. This voltage range was chosen based on the requirements for electrolysis to occur, which depends on thermodynamic variables like temperature and pressure. Electrolysis is known to occur in perfluorosulfonated ionomers like Nafion under applied voltage that meets the requirements.[42-45] 1.23 V is the minimum voltage required to decompose water at 25 °C at 1 atm of pressure, also called the reversible

voltage. But in these conditions, additional heat is necessary for a continued reaction. Under adiabatic conditions, 1.48 V is necessary for electrolysis, which is also called the thermoneutral potential. This additional potential requirement greater than 1.23 V is called overvoltage, and incorporates the nonideality and losses in the system.[46, 47] Measurements at different voltages above the thermoneutral potential along with a range of relative humidity values were obtained. This allowed for determining the optimal device operating voltage over a wide range of humidity. Early measurements with older samples caused the impedance spectrometer to be overloaded with current at high relative humidity values. These voltage optimization tests were performed in order to ensure that the chosen voltage would not cause any current overload problems even at high relative humidity values.

At each voltage tested, measurements at 20, 50, and 80% RH were taken, to determine if there were any differences in the actuator's current behavior, as well as to ensure that current overloading of the system did not occur. This was especially a risk at high voltages (within the range tested) and high relative humidity. All subsequent samples measured were 1x5 mm^2 in order to prevent current overload from the sample area being too large, and were fabricated with CNCs grown at PAH pH 4.0, with approximately 30 wt% EMI-Tf. Current was measured for 5 minutes under a constant voltage, using the Autolab software interface, called Nova. This time length ensured that the steady state current was reached, and was within the time range before the relative humidity decreased out of the ±1.5%RH range through air leakage from the chamber.

In determining the effect that ionic liquid concentration, as well as any effect that the pH of the PAH during CNC growth has on the system, samples with varying ionic liquid contents were tested, using the same 5 minute measurement, at 2.5 V. Samples with pH 4.0 and 7.0 for PAH, as well as a CNC-free sample (bare Nafion) were tested, each with 0 wt %, approximately 17 wt%, and approximately 35 wt% ionic liquid. Each sample was tested at 20, 50, and 80%RH, to determine how the ionic liquid content and pH affect the current measurement at different water contents from differing relative humidity values.

Dong Wang discovered the device's fast response to changes in relative humidity as compared to a standard laboratory humidity meter, which has a lower detection limit of 25%RH, and found it was much faster. This study compared the response to the higher quality fast hygrometer. First, samples were cut to 1x5 mm^2 strips, and then conditioned at 4V, by turning on the applied voltage and switching the direction several times, allowing the ions to build paths

through the actuator for easier movement. The residual voltage was allowed to decrease. Following conditioning, the humidity in the chamber was increased to approximately 40%RH above the rest of the laboratory's humidity. This varied from day to day, depending on the weather, and the temperature outside. Once the humidity level in the chamber had equilibrated, the measurement program was started. 2.5 V was applied across the actuator for 5 minutes, while the current was measured, allowing time for the initial ion motion, and for the steady-state current to be reached. Then the doors to the chamber were quickly opened, and a timer and video recording were started, while the 2.5 V potential across the device was maintained. The video camera recorded the response of the digital hygrometer with time, as the previously elevated chamber humidity equilibrated with the lower external humidity value. Measurements were recorded for 20 minutes. Initially, a longer period was used, but 20 minute measurements allowed for plenty of time for the samples to reach a new steady state current based on the new humidity, and for the digital hygrometer to reach a stable reading.

The digital hygrometer reading was obtained as a function of time with the same image extraction technique used for obtaining actuator bending data with time. Frame numbers and rates from the image extraction were used to calculate the corresponding time for a particular image, and the timer value in the same image was used to confirm that the frame-based time matched. Once both the hygrometer-reported %RH versus time and current versus time were obtained, they were plotted and compared.

Relative response speeds for both the hygrometer reading and actuator's current were calculated using a method similar to determining the rise or fall time for electronics. In this case, it corresponds to the fall time. It was calculated using the time difference between the points where it falls below 0.9 and 0.1 times the total difference between the initial and final values.[48, 49] The final value was set to the time at 20 minutes for the relative response speed comparison between the actuator's current and digital hygrometer as in section 5.4.4, and 5 minutes for measurements with a constant relative humidity, as in section 5.4.3. In some cases, the change fell below 10% of the total difference, but rose above 10% later, and in some of the less stable samples, this was seen several times. The point chosen was one where the change dropped below 10%, and was stable. This was difficult to determine in samples that never underwent a steady state current as a result of damage. The speed comparisons for those cases are not reliable.

5.4 Results and Discussion

5.4.1 Testing the detectable humidity range

As explained above, it was very difficult to acquire a sample that could operate under a wide range of humidity conditions, since many of the samples were not freshly made. Much trial and error in testing voltage was completed in order to find the relative humidity range that could be detected through this technique. As a result of current overloading, samples were frequently damaged which prevented further use. After many tests with many samples, a sample was used in the range of 10-80%RH, in intervals of 10%RH. The steady-state current is certainly distinguishable in 10%RH intervals, and also scales with increasing humidity.

Figure 5.1 shows the current measurements of a single sample, fabricated with a CNC at pH 4.0 PAH, with 33.6 wt% EMI-Tf, and is approximately 1x9 mm^2. Measurements were made in order of increasing relative humidity. Samples behaved normally as they displayed the initial current drop as the ionic liquid ions suddenly move, then are slowed to the steady state current that followed. At 70%RH, there was a jump in the steady-state towards the end of the measurement, indicating something was interfering with the steady-state current, making it unreliable. At 80%RH, the steady-state did not last for the entire measurement. The fact that the two largest relative humidity curves initially matched the expected output indicates that the longer the sample is subjected to the elevated relative humidity, while also under an applied potential, there can be degradation and unreliability. Later, stability improvements were made by using fresher samples. 80%RH measurements were easily attainable with the fresh samples.

The wide detection range shown here alludes to the possibility of making a functioning humidity sensor based on current through the IPMC actuator. Other researchers have had greater limitations on the detection range of their humidity sensors that use similar methods of detection, and not were capable of detecting below 20%RH.[29]

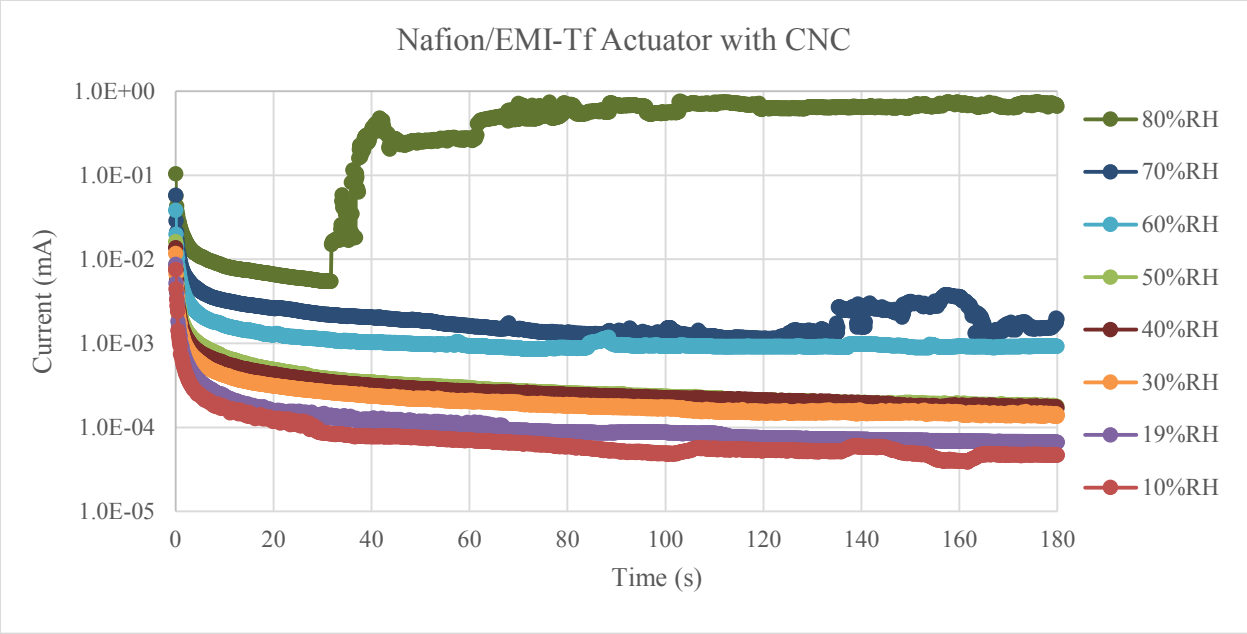

Figure 5.1: A sample of a Nafion-based actuator with CNC and ionic liquid and its current output as a function of time under an applied voltage of 1.5 V at varying RH levels.

Figure 5.2 shows the steady state section of the measurements from 10-50%RH in Figure 5.1, along with their average values for each measurement. The 40% and 50% lines are very close but not indistinguishable. The steady-state currents are very stable even at this highly zoomed in range, but do have a slight decrease, particularly at larger %RH. This is a result of a slow decrease in the chamber's relative humidity, since it is not airtight. In all measurements taken at a relative humidity above that of the outside room, the digital hygrometer showed a slow, but steady decrease in relative humidity inside the chamber. With better control of the chamber's relative humidity, this current decrease would likely be eliminated, and a true steady-state current would be observed.

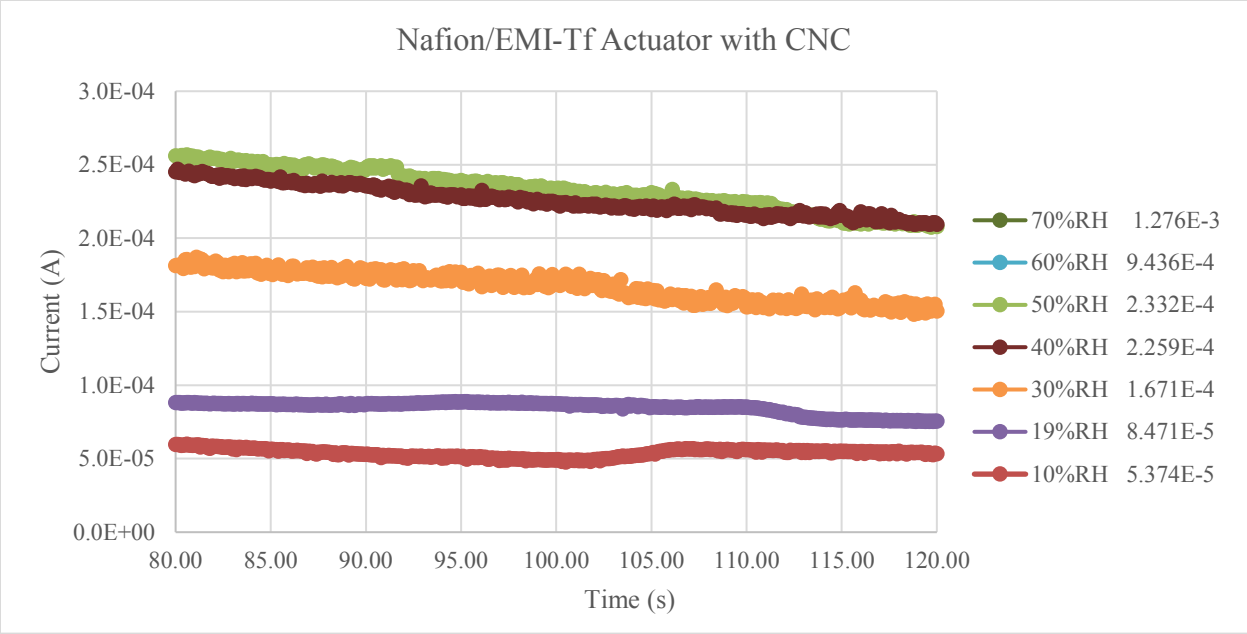

Figure 5.2: Steady state current averages for 10-70%RH measurements in a single actuator sample.

An additional test was done in 1%RH increments to determine if the steady-state current was distinguishable for very small RH differences. Results indicated the currents are different, which can be seen when zoomed in very closely. Again, a slow decrease in current is shown during the measurement from the decrease in chamber relative humidity. Also, the current values did not all increase with increasing %RH. This could be a result from the fact that the actuator's current sensitivity is several times faster than the fast hygrometer used to determine the %RH, which will be discussed further in section 5.4.4. Additionally, the hygrometer's tolerance is ±2.5 %RH between 10-90%RH, so it could be that the hygrometer's reading may be not exact, and it cannot distinguish between the two different humidity values that are only 1.0%RH apart. This very small %RH interval experiment would be improved by measurement in a system where the relative humidity is more controlled, homogeneous, and stable, as well as determined by a hygrometer with a smaller tolerance.

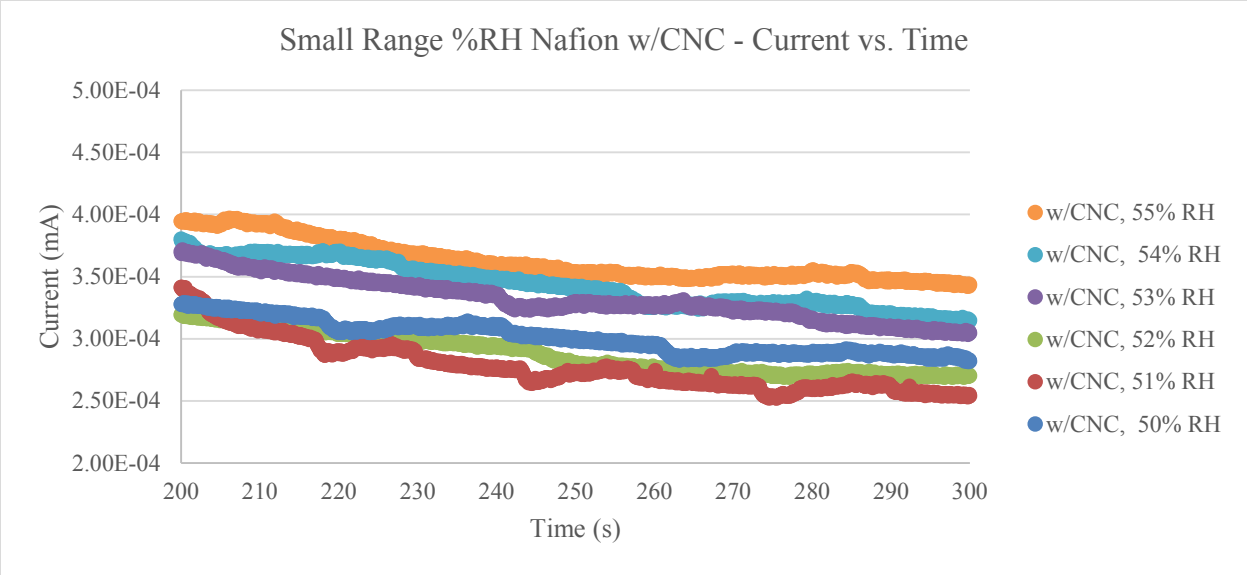

Figure 5.3: A much narrower %RH range is shown, indicating that small %RH differences are distinguishable.

Other measurements were completed at approximately 5%RH intervals, where steady state current was found to continue to increase with increasing %RH. Two samples were required to test throughout the whole range, as the first sample did not work after leaving it compressed between the electrodes overnight. The second sample appears to have become damaged after testing at 55%RH. Additionally, the current at 50% and 55% RH are separate, but close enough that they are difficult to tell apart on the scale of the second plot.

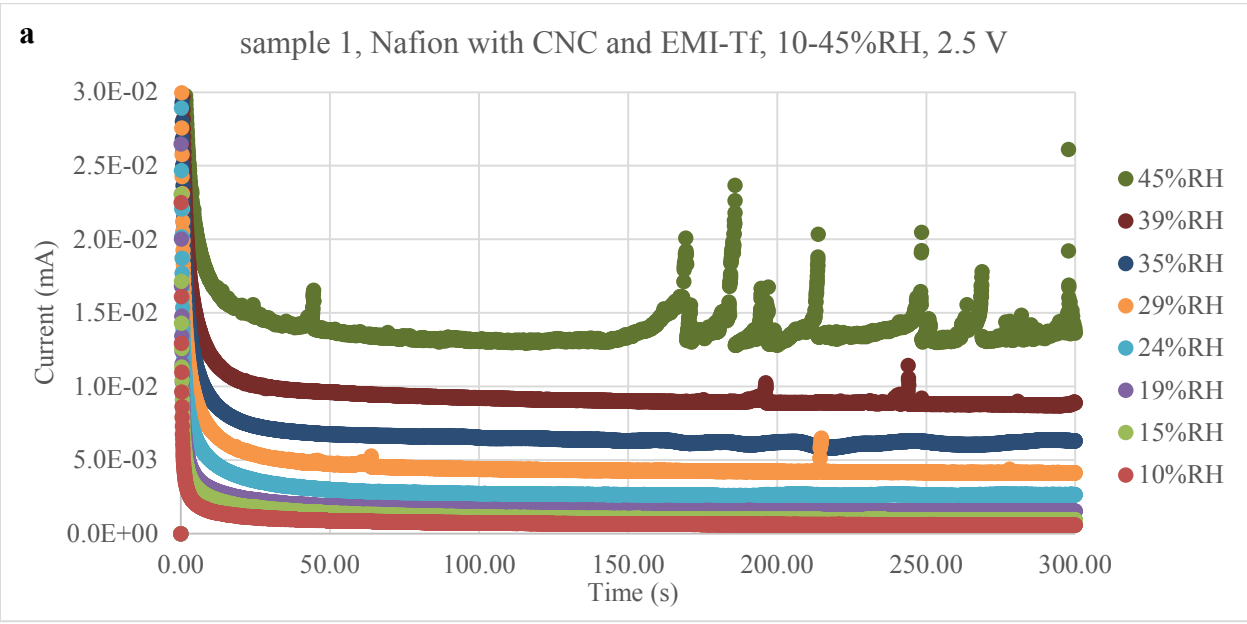

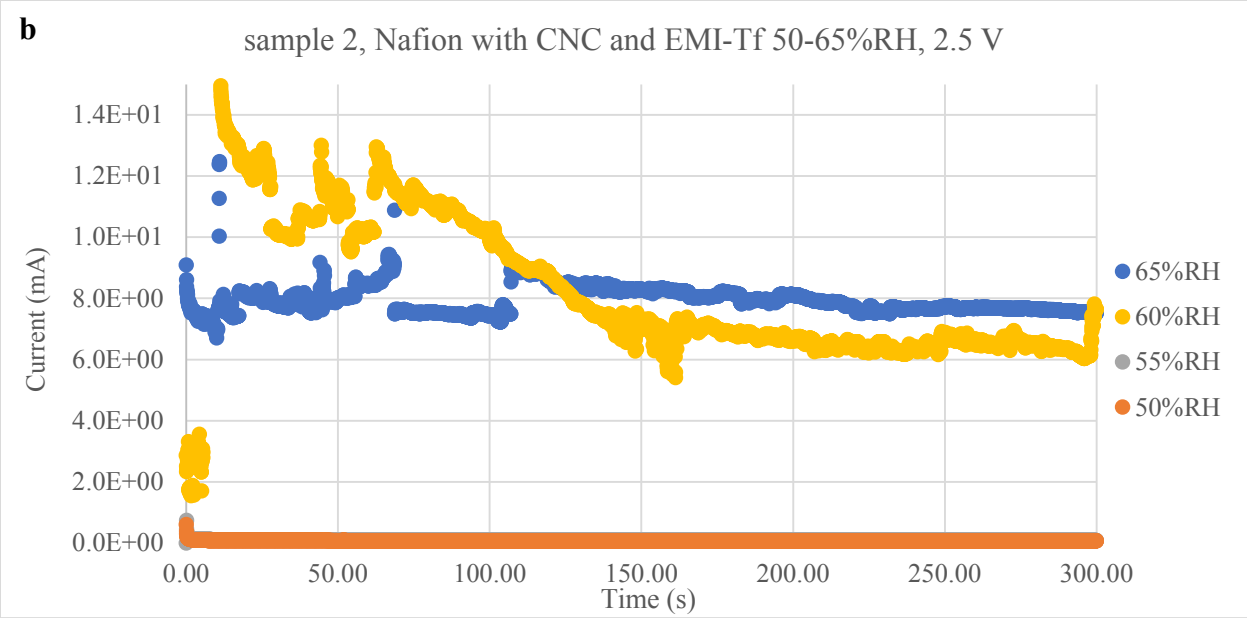

Figure 5.4: Current measurements of two separate samples at approximately 5%RH intervals.

This testing at various humidity levels indicates that samples can be used for multiple measurements and current at intervals of 5-10%RH (and likely smaller) are distinguishable from one another. The detection range is at least 10-70%RH, with indication that the upper limit can possibly be further extended. Test improvements could be made by ensuring that the correct relative humidity in the measuring chamber is shown by the digital hygrometer. A smaller tolerance is necessary for coming up with a calibration curve, in order to distinguish between smaller %RH differences.

5.4.2 Effects of test voltage on measured current at different %RH

After the problems that occurred with reliability and current overload with older samples, test voltage was examined to find one that worked even at high %RH. As the minimum voltage required for water electrolysis under 1 atm and at 25°C is 1.48 V, samples were measured at 1.5, 2.0, 2.5, 3.25, and 4.0 V, all at 20, 50, and 80%RH. Measurements were taken in order of increasing expected current, from low to high voltage, starting at the lowest RH and working upward. This was to prevent ruining a sample by current overload, and preventing other measurements from being taken on the same sample. As expected, undamaged samples saw increasing current with increasing applied voltage at the same RH. The same was true for increasing relative humidity at equal applied voltage.

In the three plots in Figure 5.5, measurements at 20% RH and 50% RH, behaved normally at all voltages tested. However, at 4 V and 20%RH, and at 3.25 V and above at 50%RH, the measured current has the typical initial quick drop in the first few seconds, but instead of leveling out to a constant current value, the current slowly rises for the rest of the measurement. The cause of this current increase is unknown, but it is undesirable for a humidity sensor based on the measured current reaching a steady state value. This phenomenon was also observed in the other sample tested at 50%RH, and also at 80% RH at 3.25 V. In the 80%RH measurement for sample 2 shown below, the sample was damaged during the first low voltage measurements, and behaved unexpectedly for all subsequent measurements.

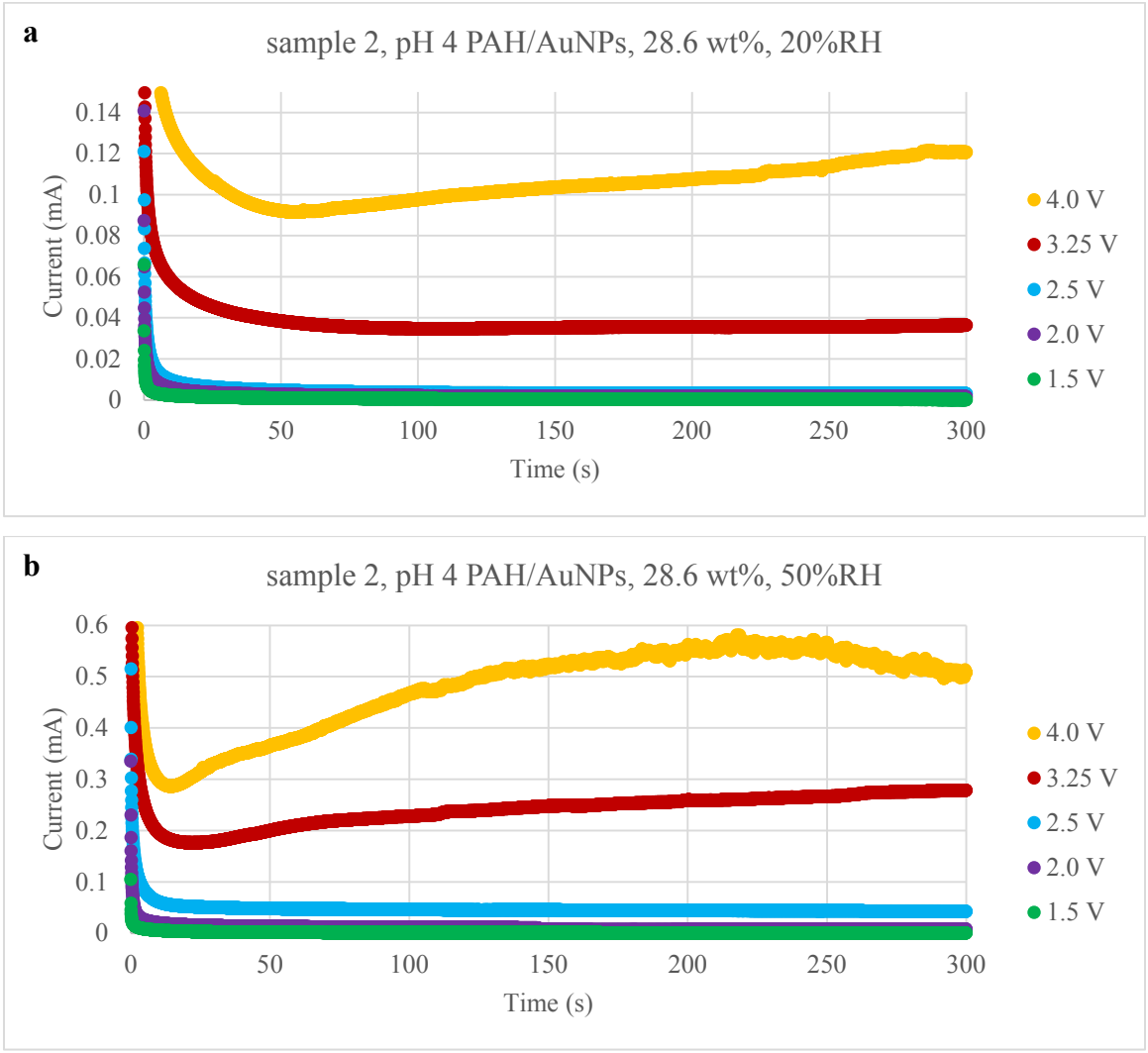

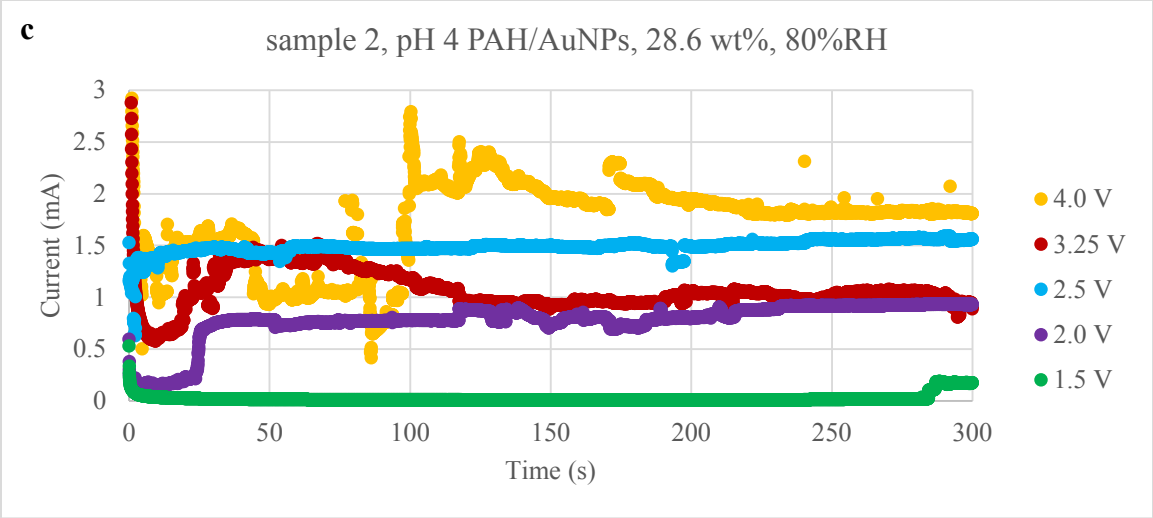

Figure 5.5: Current measurements for a single sample at various %RH and applied voltage values, to determine future test voltage to use based on sample stability.

A third sample was tested only at 80%RH, since problems occurred with the previous samples being damaged at the high relative humidity and voltage. Current overload was not much of a problem, but samples were still damaged under these high humidity and voltage conditions. More stable measurements were obtained, but they did not follow all of the trends of previous samples measured at 80%RH. Most notably, current did not increase with increasing voltage over the entire voltage range tested. This could again be because of a damaged sample. Continual current rises were not seen at 3.25 V and above, as in other samples, as shown in Figure 5.6.

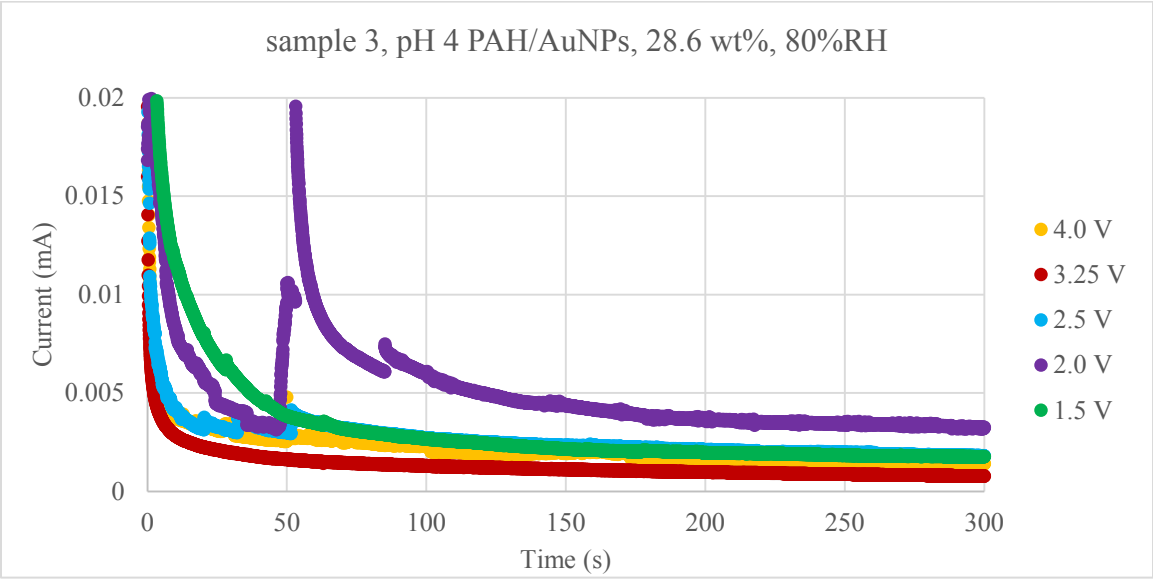

Figure 5.6: A third sample was measured at each applied voltage at 80%RH.

After observing that the combination of large voltage and high RH easily causes sample damage and unreliable measurements, 3.25 V and above were ruled out for use in future tests. 1.5 V is very close to the minimum necessary voltage for water electrolysis in these laboratory conditions, and typically registers very small current values, which could be too small to differentiate between small RH changes. Therefore, 2.5 V was used for all further testing.

5.4.3 Effects of ionic liquid content and different pH values in PAH

Once the best voltage for further experiments was determined, the effects of the amount of ionic liquid in the actuator, pH of the PAH during assembly, and the CNC's presence was examined at a wide range of relative humidity. The relative humidity was varied in order to make sure that a particular type of sample was not more susceptible to current overload, and therefore damage. These factors helped in determining the optimum parameters for fabricating a humidity sensor out of an IPMC actuator.

Two samples of each pH of PAH in the CNC (or no CNC) and ionic liquid weight percent were tested at 20%, 50%, and 80%RH. The first samples were tested in order of increasing relative humidity so that samples would not be damaged by current overloading, and then require testing at another RH. Once it was determined that current overload was not a problem with these fresh samples, the second sample set was tested in a random %RH order. This three-variable test yielded many plots, only some of which are shown within this section, 5.4.3. Different plots were made in order to compare each of the variables. Current versus time measurements for samples with the same ionic liquid uptake at each relative humidity tested are shown in Figure 5.7 - Figure 5.9. Plots comparing all samples with the same weight percent ionic liquid are shown in Appendix D along with plots comparing all measurements at a single relative humidity. But putting all measurements that are comparable on a single plot makes it uninterpretable due to the large amount of data. The results show that most samples performed as expected, with few errors reported by the system for measurement of the current and no current overloads. These tests showed that this device is much more reliable with samples with freshly fabricated CNC layers and freshly soaked in ionic liquid, compared to the earliest tests on samples that were several months old.

Figure 5.7: Samples 1 and 2 at 20%RH for each ionic liquid wt%. Labels with no pH value mean there is no CNC.

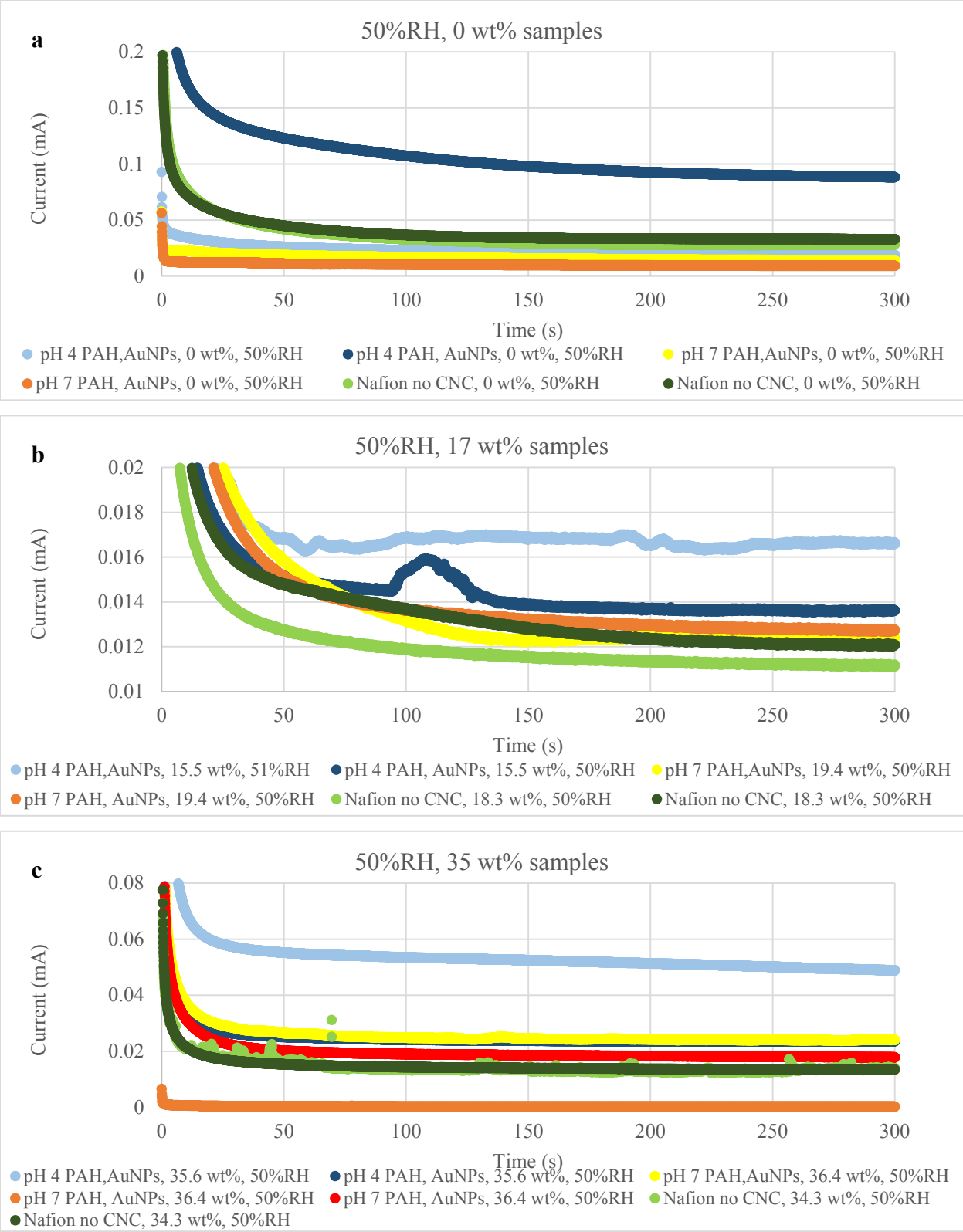

Figure 5.8: Samples 1 and 2 at 50%RH for each ionic liquid wt%. Labels with no pH value mean there is no CNC.

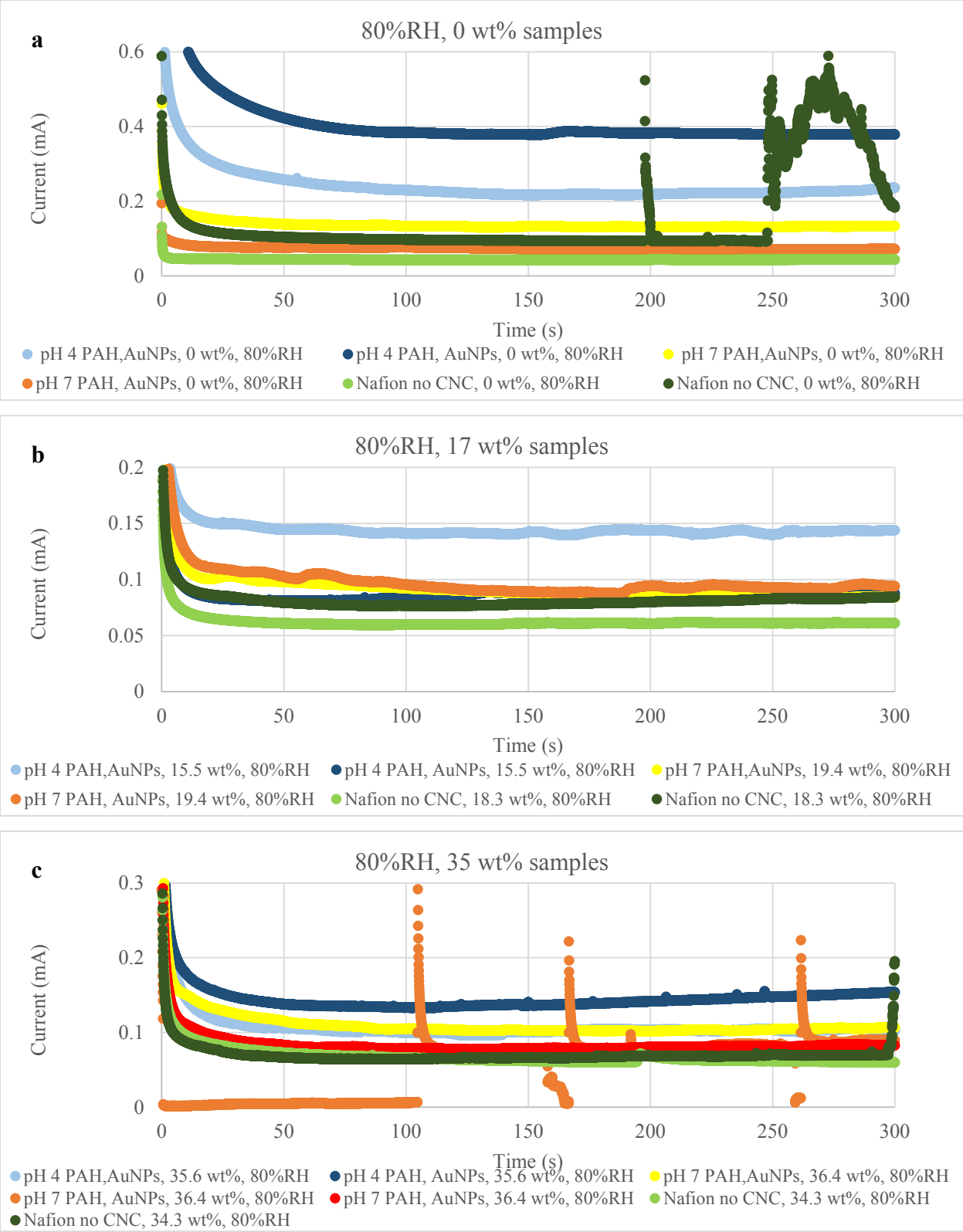

Figure 5.9: Samples 1 and 2 at 80%RH for each ionic liquid wt%. Labels with no pH value mean there is no CNC.

In all samples, the current increased with relative humidity. There was less visible separation between the current curves for the different sample types at 20%RH. 50%RH showed greater variation between samples, and at 80%RH, different sample types had widely varying steady-state currents. In some cases at 80%RH, a longer period of time was needed before reaching the steady-state current.

At 80%RH, the 17 wt% samples in particular showed some variation in the steady-state current. This could be a result of turning the humidifier on and off during 80%RH measurements. At very high humidity, the chamber's elevated humidity leaked more quickly, which required humidity modulation during the measurement, in order to keep the value within the ±1.5%RH range. In some cases, there was less current fluctuation in samples with no ionic liquid. But the fluctuations that do exist are not large enough to be problematic. Also, at 80% RH, there are a few samples that show significant noise and spikes in the steady-state current that would cause a problem in device operation. This occurred more often in the second set of samples tested, meaning that measurements were taken longer after sample fabrication. However, only about a week passed between the two sets of measurements. Further comparisons of the same data can be found in Appendix D.

Table 14 shows the average steady-state current and standard deviation of each measurement, from each sample tested at 3 RH values. The current average was taken between 100-300 seconds, which is usually enough time to reach the steady-state current. This is a simpler way to show any trends that occur in all the data, since there were three variables in the samples. The left side of the table shows all the first samples that were tested, while the right side contains the second set of samples. The table is to aid in comparing trends that exist for all samples. Colors indicate smaller to larger current, from red to blue. Both sets of columns are arranged in the same order.

Steady-State Current Average for Each Sample Type									
Sample 1					Sample 2				
pH PAH	wt% EMI-Tf	%RH	Avg Current (mA) (100-300 s)	Std. Dev.	pH PAH	wt% EMI-Tf	%RH	Avg Current (mA) (100-300 s)	Std. Dev.
4	0	20	7.40E-04	3.90E-08	4	0	20	3.34E-03	2.44E-07
4	0	50	2.06E-02	1.16E-06	4	0	50	9.41E-02	4.57E-06
4	0	80	2.23E-01	4.44E-06	4	0	50	9.43E-02	5.28E-06
4	15.5	20	1.77E-03	2.53E-07	4	0	80	3.81E-01	2.23E-06
4	15.5	51	1.67E-02	1.78E-07	4	15.5	20	1.43E-03	2.38E-07
4	15.5	80	1.42E-01	1.35E-06	4	15.5	50	1.40E-02	6.09E-07
4	35.6	20	5.50E-03	2.04E-07	4	15.5	80	8.78E-02	1.66E-06
4	35.6	50	5.13E-02	1.36E-06	4	35.6	20	2.52E-03	7.86E-08
4	35.6	80	1.02E-01	2.36E-06	4	35.6	50	2.37E-02	1.61E-07
7	0	20	5.70E-05	9.16E-09	4	35.6	80	1.42E-01	6.11E-06
7	0	50	1.51E-02	8.04E-07	7	0	20	4.86E-05	1.15E-08
7	0	80	1.50E-01	2.39E-06	7	0	50	9.55E-03	3.55E-07
7	0	80	1.32E-01	8.15E-07	7	0	80	7.23E-02	1.58E-06
7	19.4	20	1.07E-03	1.46E-07	7	19.4	20	8.43E-04	1.75E-07
7	19.4	50	8.34E-03	7.74E-08	7	19.4	50	1.30E-02	2.61E-07
7	19.4	50	1.24E-02	1.63E-07	7	19.4	80	9.21E-02	2.36E-06
7	19.4	80	8.68E-02	2.23E-06	7	36.4	20	2.53E-03	2.12E-07
7	36.4	20	2.13E-03	1.54E-07	7	36.4	50	1.83E-02	1.82E-06
7	36.4	50	2.43E-02	3.04E-07	7	36.4	80	8.03E-02	3.33E-07
7	36.4	80	1.04E-01	1.34E-06	No CNC	0	20	3.91E-03	1.09E-07
No CNC	0	20	1.81E-03	9.26E-08	No CNC	0	50	3.37E-02	8.80E-07
No CNC	0	50	2.89E-02	1.36E-06	No CNC	0	80	1.72E-01	1.37E-04
No CNC	0	80	4.35E-02	2.22E-07	No CNC	0	80	5.70E-01	3.58E-04
No CNC	18.3	20	9.46E-04	5.00E-08	No CNC	18.3	20	1.22E-03	1.10E-07
No CNC	18.3	50	1.14E-02	2.03E-07	No CNC	18.3	50	1.25E-02	4.62E-07
No CNC	18.3	80	6.10E-02	5.59E-07	No CNC	18.3	80	8.02E-02	2.44E-06
No CNC	34.3	20	1.41E-03	2.28E-07	No CNC	34.3	20	1.90E-03	6.00E-08
No CNC	34.3	50	1.33E-02	5.80E-07	No CNC	34.3	50	1.38E-02	2.50E-07
No CNC	34.3	80	6.25E-02	2.17E-06	No CNC	34.3	80	6.84E-02	6.61E-06

Table 14: Table of sample properties and their corresponding average steady-state current values. Some measurements were repeated, especially those at larger %RH, if a stable measurement was not obtained the first time. This caused the lines in the table to not always directly match.

As expected, the darkest red highlighted averages, indicating the lowest values are consistently at 20%RH, and occur in all sample types. In all cases, the current increased monotonically with increased humidity. Notice the two Nafion with no CNC at 0 wt% EMI-Tf samples in column 2. The standard deviations are highlighted, as they are orders of magnitude larger than for any other sample. The first of the two measurements is shown in the first plot in Figure 5.9. The large current from this sample is misleading since, it deviated from the steady-state, which negatively impacted the average and standard deviation. The data presented in Table 14 is also shown below in graphical form grouped by relative humidity in Figure 5.10 and by ionic liquid weight percent in Figure 5.11.

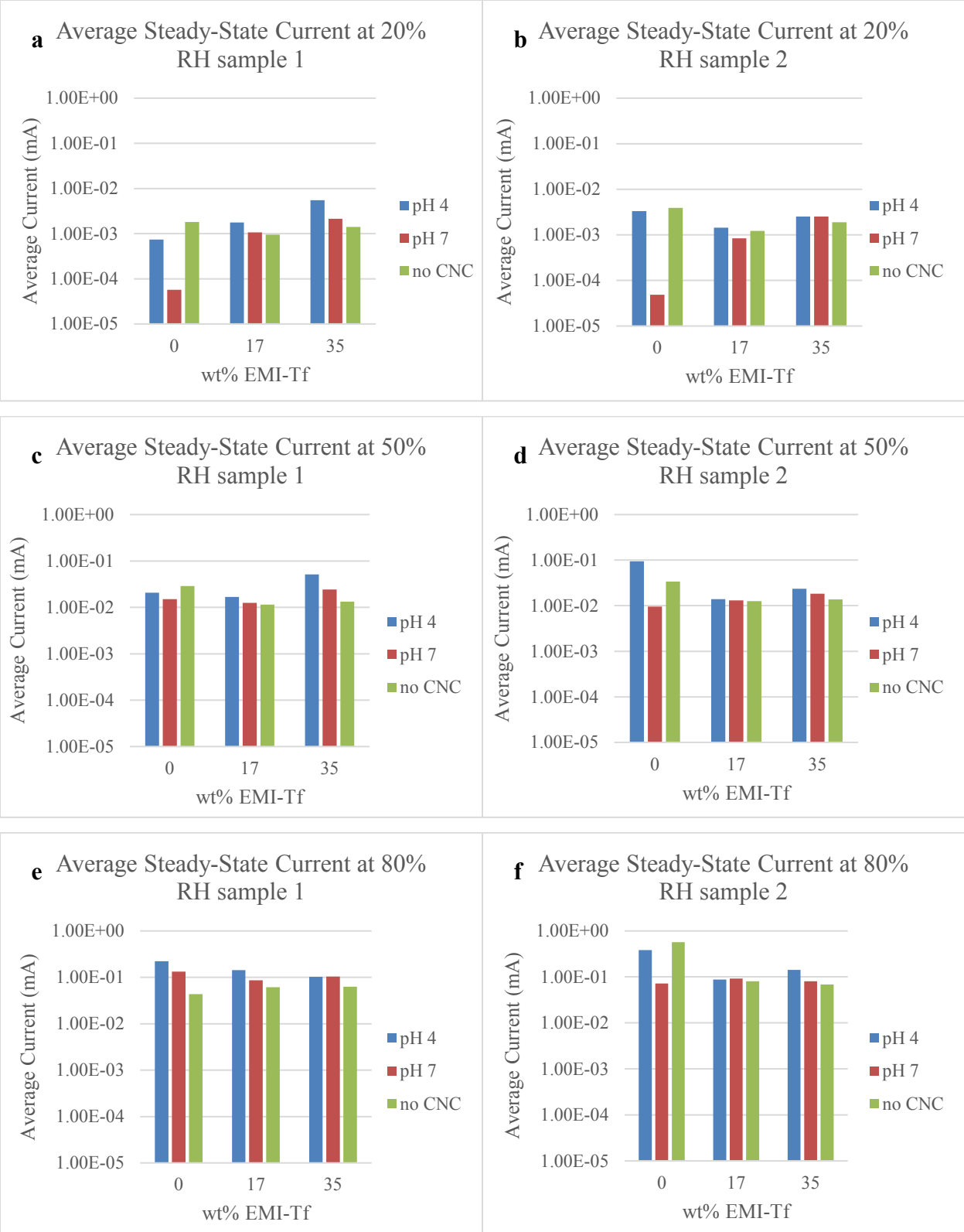

Figure 5.10: The average steady-state current values for each measurement grouped at each relative humidity grouped by sample characteristics. Values are also shown in Table 14.

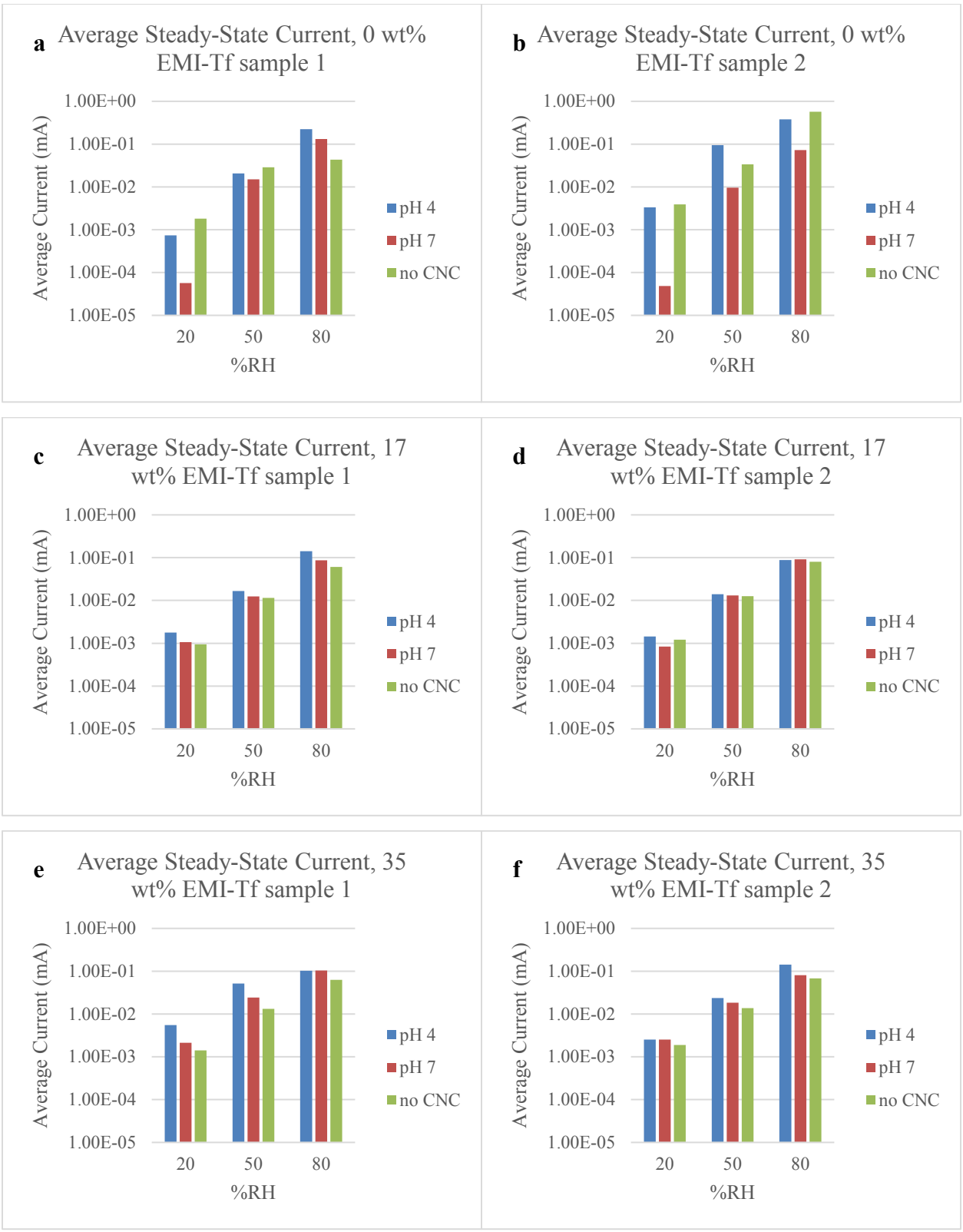

Figure 5.11: The average steady-state current values for each measurement grouped at each ionic liquid uptake grouped by relative humidity and CNC characteristics. Values are also shown in Table 14.

As shown in Figure 5.10, the 0 wt% ionic liquid samples show the largest current variation between samples with different CNC characteristics. Some 0 wt% samples' average steady-state currents are orders of magnitude different from each other at 20% RH, while this is less true at 50% and 80% RH. Also for samples with the same PAH pH in the CNC, or no CNC, 0 wt% ionic liquid samples had more widely varying steady-state current values between samples with different pH or CNC at each relative humidity. The 17 wt% ionic liquid samples had the closest steady-state current values for samples with different CNC characteristics.

Figure 5.10 also reaffirms that the 0 wt% ionic liquid samples have the largest average steady-state current at 80%RH. pH 4.0 samples also have large steady-state currents at 80%RH, as discussed above. The one case where the second 0 wt% ionic liquid/no CNC sample is significantly larger has a large standard deviation, which is highlighted in Table 14.

The same information is shown in Figure 5.11, but is grouped and plotted differently. This shows more clearly that no ionic liquid allows for the largest dynamic range between low and high relative humidity, but both 17 wt% and 35 wt% ionic liquid also show a significant range of more than an order of magnitude. The average current at a given relative humidity is less varied between different types of CNCs (or no CNC) when ionic liquid is included.

Another way to represent this steady-state current data is shown in Figure 5.12. Each CNC type (or no CNC) is plotted separately by average steady-state current versus relative humidity.

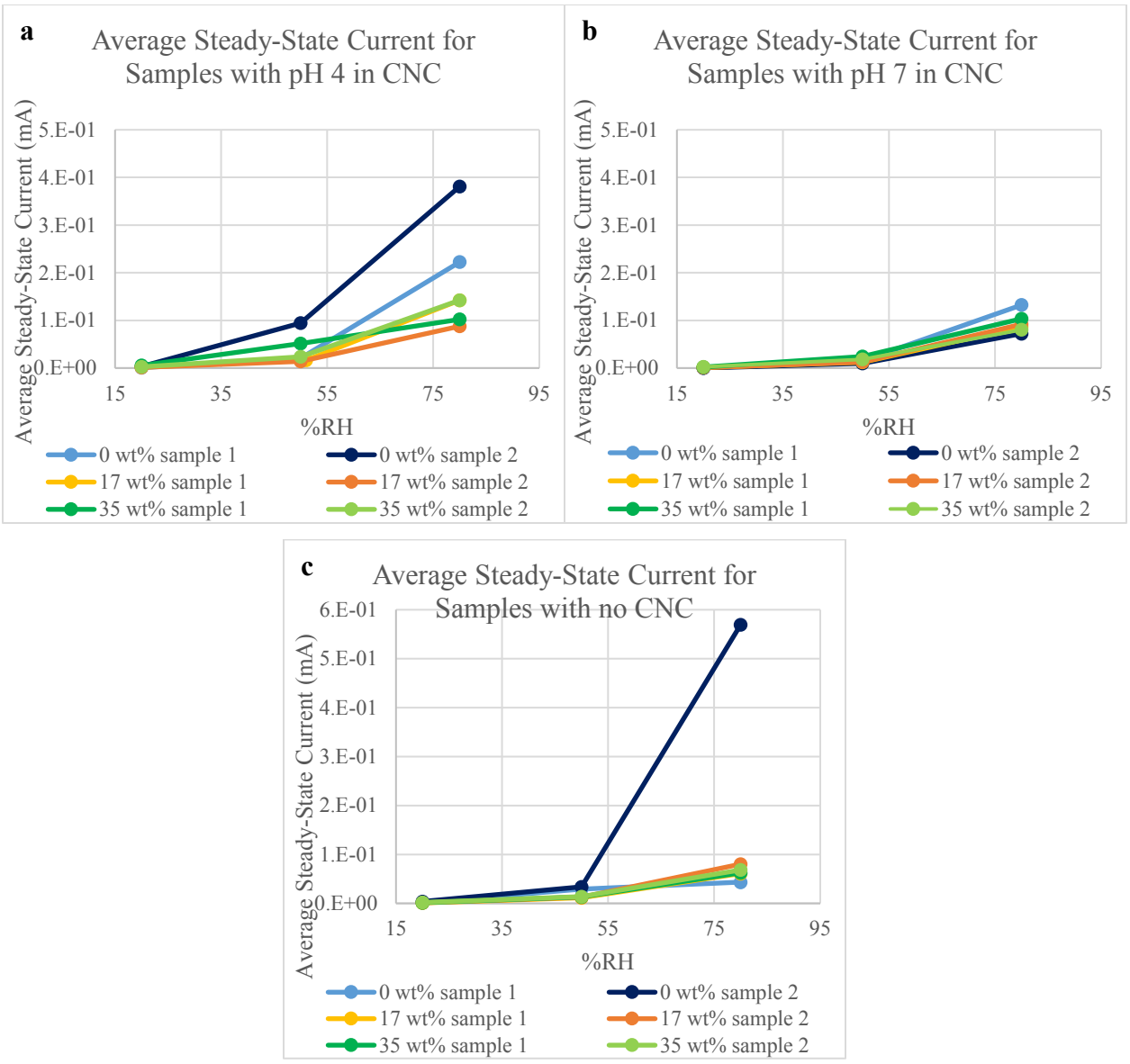

Figure 5.12: Average steady-state current versus relative humidity for each sample measured. Values are also shown in Table 14.

This further confirms the information gathered from the other representations of this same data. While the 0 wt% sample 2 line in the "no CNC" plot looks like it has the largest separation between low and high relative humidity, this is the same data point that had a very large standard deviation resulting from the measurement deviating from the steady state, and is not an accurate representation of the current at steady-state. In light of this fact, the pH 4.0, 0 wt% samples show a larger current separation between low and high relative humidity. However, the other samples at pH 4.0 still have about an order of magnitude current difference

between 20% and 80% RH, which is significant, and is enough for a humidity sensing device. There is still some variation between the two different samples at pH 4.0 0 wt %. pH 7.0 samples had much less variation with different ionic liquid content. This was also true for samples with no CNC except for the 0 wt% sample 2 measurement at 80%RH.

The average steady-state current separation, or dynamic range, between the steady-state current at 20% and 80% RH is shown directly in Table 15 for each sample. In general, a wider difference between the steady state current at two separate %RH values would make composing a calibration curve easier, as there would be better distinction between the current values at each humidity.

Average Steady-State Current Difference Between 20 and 80%RH for Each Sample		
pH PAH	**wt% EMI-Tf**	**Avg Current Difference (80-20%RH)**
4	0	2.22E-01
4	0	3.78E-01
4	15.5	1.41E-01
4	15.5	8.64E-02
4	35.6	9.67E-02
4	35.6	1.40E-01
7	0	1.50E-01
7	0	7.22E-02
7	19.4	8.57E-02
7	19.4	9.13E-02
7	36.4	1.02E-01
7	36.4	7.78E-02
Nafion no CNC	0	4.16E-02
Nafion no CNC	0	5.66E-01
Nafion no CNC	18.3	6.01E-02
Nafion no CNC	18.3	7.90E-02
Nafion no CNC	34.3	6.11E-02
Nafion no CNC	34.3	6.64E-02

Table 15: Average steady-state current separation between 80% and 20% RH for each sample tested based on the calculated average steady-state current values in Table 14.

The largest difference is from the sample that failed during the measurement, shown in the first plot of Figure 5.9, so this value is not an accurate representation of the steady-state current difference. However, the pH 4, 0 wt % samples have the next largest difference consistently, meaning that these parameters would be beneficial from the device perspective. It would allow for a current to relative humidity calibration curve with a wider tolerance. Also, samples with pH 4.0 of PAH usually had the largest current, indicating that it would be a good choice for use in an IPMC humidity sensor. Several samples (difference highlighted white in Table 15) still have at least an order of magnitude between the current at low and high relative

humidity. These likely provide a large enough range for a device, and needed to be evaluated further since the current separation is not the only important characteristic.

The fall time for each measurement was calculated, as discussed in section 5.3.2, and are shown below in Figure 5.13 grouped by the weight percent uptake of the measured sample.

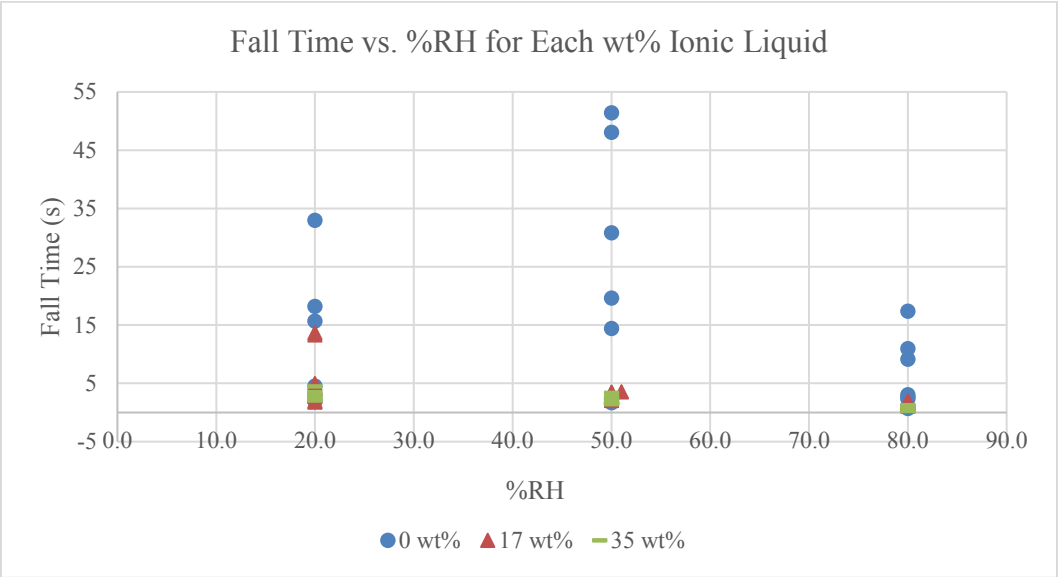

Figure 5.13: Time required for each measurement to reach a current value within 10% of the final value.

There was much larger variation between the time required to reach the steady-state value at 0 wt% than in samples containing ionic liquid. Further, adding ionic liquid significantly reduced the response time necessary to reach the steady-state. This makes sense as the ionic liquid acts as a solvent for the Nafion and CNC internal structure, thereby promoting ionic conduction.[50-52] Since samples with approximately 35 wt% ionic liquid show significantly faster equilibration times, but samples with no ionic liquid shown a larger dynamic range, there is a choice to be made on which characteristic is more beneficial to device function. Adding ionic liquid to the system increases performance in terms of detection speed, while maintaining a reasonable current difference between different humidity values. This combination of benefits from adding ionic liquid suggests that it may be advantageous from a device perspective to include on the order of 35 wt% ionic liquid. Samples with a thin CNC, (fabricated from PAH at pH 4) show the most promising results for fabricating a humidity sensing device. More details supporting these choices are shown in the next section on the relative response speed to changes in humidity.

5.4.4 Relative response speed

Dong Wang compared the relative speed of our actuator device for detecting changes in relative humidity to a lower grade standard laboratory humidity sensor that has a fairly slow response time of approximately 30 minutes.[20] He discovered the actuator-based system to be 20 times faster through the same experimental setup used in this project. Because of such success in the relative response speed compared to a standard hygrometer, in this thesis we compared response speed with the fast and expensive Fluke 971 hygrometer. The procedure for determining the relative response speed here was much the same as used previously.[20]

First the relative humidity of the environmentally controlled chamber was elevated and allowed to equilibrate. Equilibration was ensured by increasing the relative humidity of the chamber with the humidifier to approximately 5 %RH above the planned starting relative humidity. The chamber is large and it takes several minutes for the moist air coming from the humidifier in the right corner to diffuse evenly throughout the entire chamber. After the humidifier was switched off, the measured humidity would then fall slowly, as the chamber is not airtight, and come to equilibrium. After this initial chamber equilibration, once the chamber humidity fell to 1.0 %RH greater than the starting RH value, a 5 minute current versus time measurement was taken. The measurement used the same procedure as the prior experiments studying current at varying RH levels. This 5 minute stabilization measurement allows for the ions to migrate to the oppositely charged electrodes and reach a steady-state current at the initial humidity level. The chamber's internal relative humidity fell slightly from during the stabilization measurement, usually approximately 2.0 %RH. This allowed the current measurement to stay within ±1.0% RH during the stabilization measurement.

Typical measurements obtained during this step are like the ones shown previously in this chapter, with varying current values based on the humidity during testing and the sample. These consist of an initial maximum current, followed by a steep drop off, and then a steady state current, which is humidity dependent, and has been attributed to water electrolysis occurring in the internal space in the actuator, perhaps at the surface of the gold nanoparticles.[20]

The high quality Fluke hygrometer was positioned close to the actuator sample, so that they would experience the same relative humidity at the same time. After the initial 5 minute measurement, a camera was positioned so that the measured relative humidity on the hygrometer could be recorded over time. The doors were opened and a timer was started quickly to ensure

the time matched during image extraction, and accurate plots could be made. Both the current through the actuator and the relative humidity values on the hygrometer were recorded for 20 minutes to ensure adequate time for humidity equilibration.

Samples with pH values of 4.0 and 7.0 of the PAH in the CNC as well as samples with no CNC, with different ionic liquid concentrations, were tested in order to determine if these factors have an effect on the speed or sensitivity of the device to relative humidity. Some samples did not behave as expected, and never obtained stable currents after RH equilibration. Results from the more consistent measurements comparing the relative humidity shown by the hygrometer as well as the actuator current are shown below in Figure 5.14. Samples that worked well after an initial measurement were used in a second trial, to be sure that the behavior was reproducible.

The relative speed of detection can be determined qualitatively by looking at the slopes of the curves. In all of the cases shown in Figure 5.14 through Figure 5.16, the current responds faster than the Fluke hygrometer, as the current curve decreases faster. Additionally, for most of these samples, the current response was a smoother change than the one observed by the digital hygrometer. In many measurements, the Fluke hygrometer showed values that increased in humidity for a short period of time, then fell again, despite the fact that the chamber's humidity level was equilibrating with the lower humidity outside. While all of these plots only show the first several minutes of measurement, values were measured for 20 minutes or longer. However, for samples that respond as expected, plots past 5 minutes or so just show more steady state values. The final value used in quantifying the relative speeds was taken at 20 minutes after the start of the experiment.

Actuator samples with CNCs fabricated with PAH at pH 4.0 were tested with a high ionic liquid concentration as well as without any ionic liquid to determine the effects of ionic liquid on the current response.

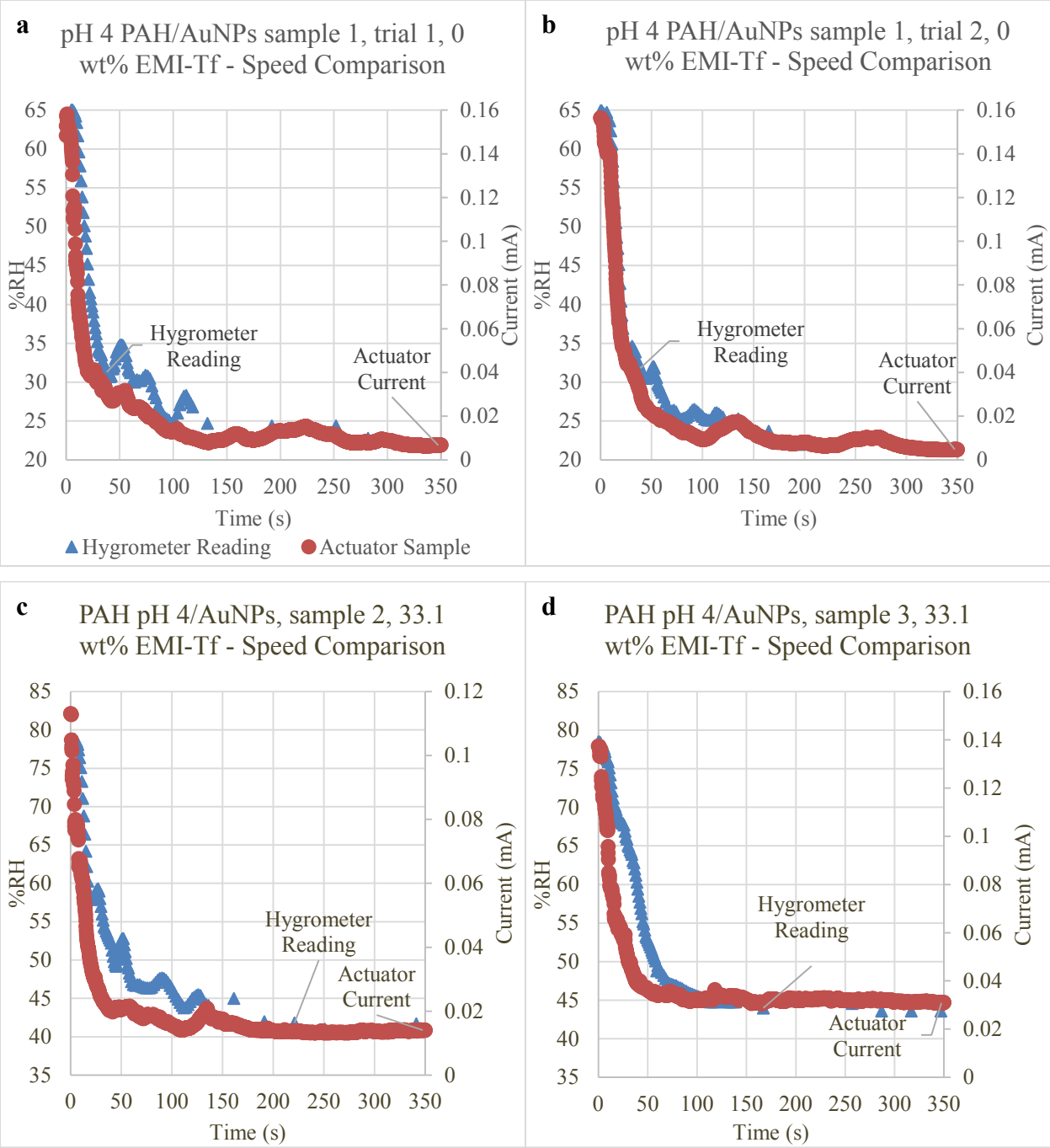

Figure 5.14: Relative speeds of actuator samples with pH 4.0 for PAH compared to the digital hygrometer's response to a large change in relative humidity. Samples with no ionic liquid were tested in comparison to samples with 33.1 wt% ionic liquid. Samples with ionic liquid showed faster response and less variation in current at earlier time periods. The legend in plot (a) applies to plots (a)-(d).

A similar study was completed using pH 7.0 PAH samples, but the results from the sample without ionic liquid were not good. One pH 7.0 PAH/0 wt% EMI-Tf sample was tested twice. During the first measurement, a steady state current was reached, but the drop from the initial current to the steady-state current was nearly instantaneous, indicating a problem. A second trial was done with the same sample and steady state current was never reached. An ionic liquid containing sample was also tested twice, without any damage from the extended period at an applied external voltage. These results are shown in Figure 5.15 and demonstrate fast and smooth response to the rapidly decreasing humidity.

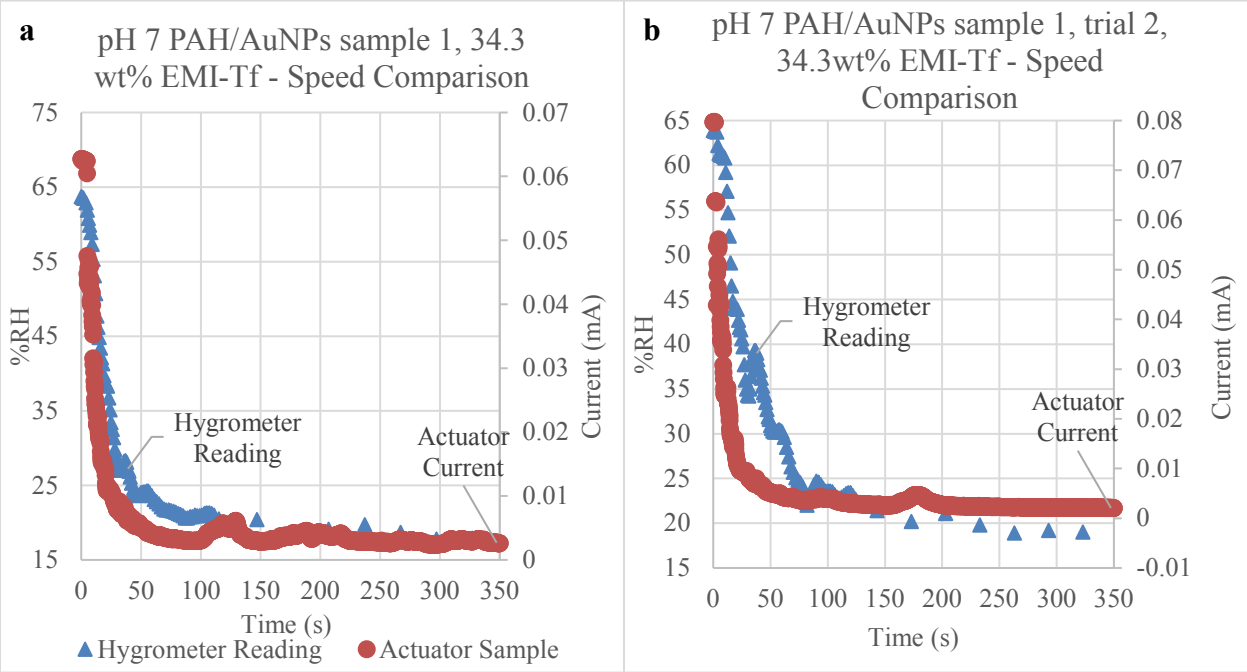

Figure 5.15: One sample of pH 7.0 PAH, at 34.3 wt% ionic liquid, tested twice. The legend in plot (a) applies to (b). Steady-state current was reached both times indicating that the lifetime of a sample is enough for multiple measurements, even after being left under an applied voltage for an extended period of time.

Comparisons were also made for samples with no CNC, which are thus composed of just Nafion with a gold electrode. From the plots in Figure 5.16, the sample with ionic liquid appears to respond faster to the humidity change, than the sample without any ionic liquid based on the separation between the curve for the actuator current measurement and the hygrometer's reading. However, samples both with and without ionic liquid were successful in detecting a relative humidity change.

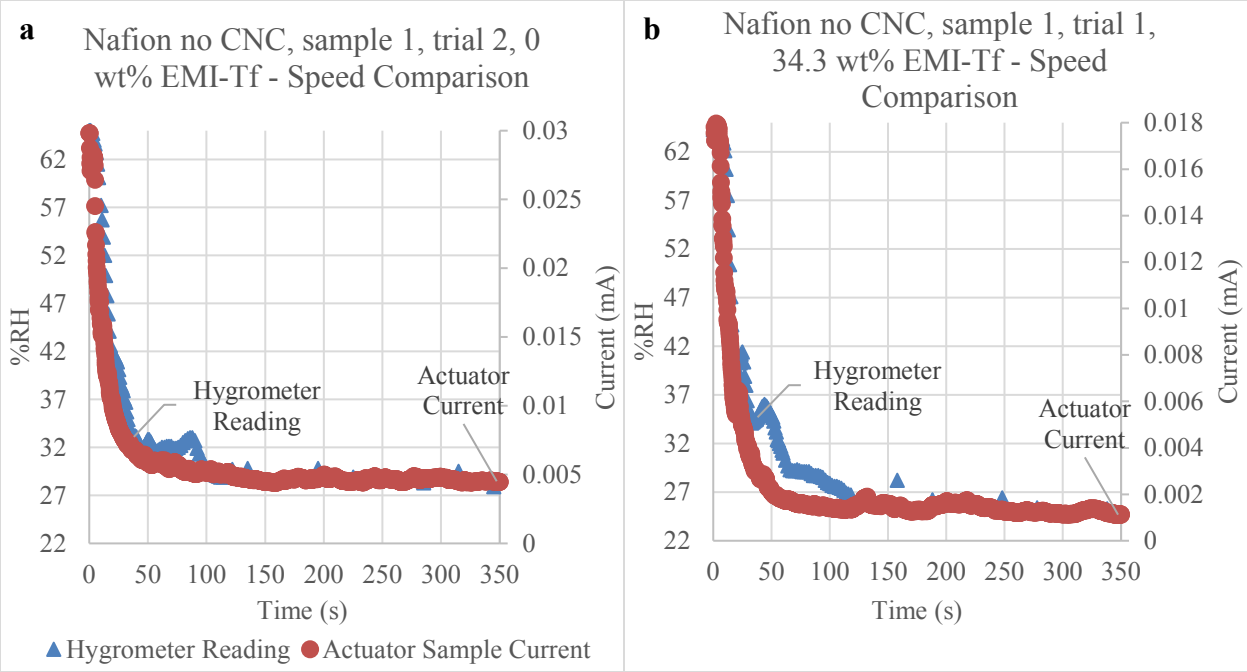

Figure 5.16: Comparisons of Nafion samples with no PAH/AuNPs CNC with and without ionic liquid. The legend in plot (a) applies to both plots.

Table 16 contains the time differences and speed comparisons between the current response in the actuator and the response from the Fluke 971 digital hygrometer to relative humidity change. The Δt values give the time difference between when the change goes from 90% to 10% of the total drop, for both current and %RH measured by the hygrometer. This is a standard way of characterizing the response time in electronic circuits, for example. The total drop was defined as the first point of the measurement to the value after 20 minutes of measurement, which is plenty of time for the steady state to be reached.

The table is sorted from largest to smallest for the ratio of the time difference between the hygrometer's response and the current response in the actuator. The middle block of measurements contains the samples that worked well, reached a steady state current, and behaved normally. The "5 minute stabilization normal?" column indicates how the current responded during the initial 5 minute equilibration period for the steady state current at the initial constant humidity value. Any anomalies in typical behavior during the stabilization period corresponded with unreliable current response to the humidity change, which is noted in the last column.

Relative Humidity Change Detection Speed Comparison								
Δt Hygro-meter (s)	**Δt Actuator Current (s)**	**Δt Hygrometer/ Δt Actuator Current**	**pH PAH**	**wt % EMI-Tf**	**Sample #**	**Trial #**	**5 Min Stabilization Normal?**	**Current stabilizes when humidity equilibrates?**
54	0.2	270.00	7	0	1	1	Small bump, mostly steady	Strangely fast, perhaps damaged
132	20	6.60	7	34.3	1	2	Yes	Yes
180	29.2	6.16	4	33.1	2	1	Yes	Yes
177	41.8	4.23	no CNC	34.3	1	1	Yes	Yes
103	31.4	3.28	7	34.3	1	1	Yes	Yes
88	30.6	2.88	no CNC	0	2	2	Yes	Yes
153	55.4	2.76	4	0	1	2	Yes	Yes
79	32.8	2.41	no CNC	0	2	1	Yes	Yes
71	35.4	2.01	4	33.1	3	1	Yes	Yes
120	75.8	1.58	4	0	1	1	Yes	Yes
388	965.4	0.40	7	0	1	2	Yes	Not stable but mostly in 10% range at end
98	267.4	0.37	4	36.4	1	1	Atypical, discontinuity in steady state, otherwise normal	Jumpy initially but eventually stable
54	302.4	0.18	no CNC	0	1	1	Not very stable	Not stable but mostly in 10% range at end
111	904.2	0.12	4	33.1	1	1	Plateau, otherwise stable	Stable but has a strange plateau

Table 16: Results for the relative speeds between current response in the actuator and the digital hygrometer. Additionally, notes on the quality of the current measurements are listed.

For samples that performed well, the average relative speed ratio between the current and digital hygrometer was 3.6 (standard deviation 1.8). For samples that contained approximately 35 wt% ionic liquid, responses were typically faster—4.5 times the speed of the digital hygrometer's response (standard deviation 1.9). Samples containing no ionic liquid had a slower average response time of 2.4 times faster (standard deviation 0.6). These results show that the addition of a CNC and ionic liquid boosts the response speed of the current to a large change in relative humidity. The response is several times faster than a high quality hygrometer, but even samples with no ionic liquid were more than twice as fast as the high end digital humidity sensing device.

Regarding additional observations among the different parameters of actuator fabrication, it should be noted that there also were some samples at both pH 4.0 and pH 7.0 as well as without a CNC that did not show fast responses. This is also true for samples with and without ionic liquid. So there are some details in the fabrication process that need to be identified to make a fully reliable set of devices. However, there was a large fraction of devices that performed better than the Fluke hygrometer.

One thing to notice from Table 16 above is that the second trial measurements are faster than the first. For the samples with normal behavior that were tested twice, the second trial measurement is always faster than the first. This shows that the relative speed of detection increases with further use, even when the samples were conditioned by switching voltage directions several times at 4 V before any measurements were taken.

Whether or not a CNC is present seems to have some impact on the speed of humidity detection, but pH has less influence. A CNC appears to increase the speed, but not enough samples were tested to make reliable conclusions on this aspect. Of the samples listed in the table that behaved as expected (middle section), the first two samples listed indicate thicker CNC samples stabilize faster than thinner ones, or samples with no CNC. Again, more study is necessary to be conclusive on whether those factors have an effect. If these trends are borne out by more extensive data, a possible explanation is that the more material present, as in samples with a CNC and/or larger pH of PAH, the more water can be adsorbed from the environment and subsequently desorbed upon an RH change. This could cause a greater sensitivity to ambient humidity, and a quicker response. The gain in detection speed by adding ionic liquid indicates is beneficial for humidity sensing applications.

The data from measurements studying the effects of ionic liquid and the pH of PAH in section 5.4.3, as well as the relative response speed measurements in section 5.4.4 showed that samples with a CNC display better characteristics for humidity sensing applications. However, no ionic liquid was better in terms of the dynamic current range, but 35 wt% ionic liquid had a faster response time. The advantages gained in the detection speed by adding ionic liquid outweigh those obtained in ionic liquid-free samples, since the dynamic range is still large in ionic liquid-containing samples. This indicates that including on the order of 35 wt% ionic liquid is a better choice from a device perspective. The CNC also adds functionality, but thinner

layers, such as those obtained through fabrication at pH 4.0 for PAH yield better current differentiation results than thicker CNC layers.

5.5 Conclusion

This chapter described results that significantly extend the study of the potential for using the steady-state current of an IPMC actuator with a CNC as a humidity sensor. The results look promising for future applications for this device, as it was observed that the actuator current responds to a rapid change in humidity with a faster and smoother response than a high-end Fluke 971 hygrometer. The work here builds on Dong Wang's earlier study of actuator current as a function of humidity, and response speed characterization. From the research presented here, the detection range was further expanded to at least 10-80%RH, and likely could be extended further without significant additional sample modification. Samples that were several months old were also capable of detecting humidity but may have a smaller detection range, with upper RH values particularly difficult to measure. Damage to the device under applied potential at high RH values is also more likely in older samples than in fresh ones. Experiments on how the current responds at different applied voltages were also completed, with the determination that 2.5 V provides a good balance between preventing sample damage at large currents while being above the minimum voltage necessary for water electrolysis. Additionally this shows that the same sample could be used successfully in a number of measurements at this voltage level.

The effects of the presence of a CNC, as well as the relative thickness, determined by the pH of PAH were also studied. The CNC did show larger current differentiation at different %RH under 2.5 V of applied potential, though samples with pH 4.0 PAH (thinner CNC) outperformed those fabricated at pH 7. These variables were additionally tested with varying amounts of ionic liquid as an electrolyte and ion source, including 0 wt%, 17 wt%, and 35 wt% EMI-Tf. Samples with no ionic liquid had notably different characteristics than measurements with samples that included ionic liquid. Samples without ionic liquid, showed a greater difference in steady state current between high and low %RH, but slower equilibration times. However, samples with approximately 35 wt% ionic liquid also showed a significant difference (about an order of magnitude) in average steady-state current between 20% and 80%RH which should be ample dynamic range in a device application. The benefits gained from detection speed in samples with high ionic liquid content outweigh the slightly larger dynamic range in ionic liquid-free samples.

Additional tests were conducted to directly compare the response speed of the actuator current and the fast Fluke 971 hygrometer to a large %RH change. Again, samples without a CNC, as well as ones with a CNC fabricated with different pH values of PAH were tested. For each of these, samples with 35 wt% ionic liquid and without any were also tested to directly compare ionic liquid content effects on the relative response speed. Samples containing ionic liquid were consistently faster than ionic liquid-free samples. There was some evidence that thicker CNCs allow for a faster relative response compared to the hygrometer, but this needs further study. Despite the pH 7.0 sample with ionic liquid having the fastest response overall compared to the hygrometer, other aspects of measurement indicate that pH 4.0 PAH in the CNC is better suited for making a relative humidity sensing device. Finally, response speed was increased when the measurement was repeated on a given sample.

5.6 References

1. M. Cappadonia, J. W. Erning, S. M. S. Niaki and U. Stimming, Solid State Ionics **77**, 65-69 (1995).
2. M. C. Wintersgill and J. J. Fontanella, Electrochim Acta **43** (10–11), 1533-1538 (1998).
3. D. M. DeLongchamp and P. T. Hammond, Chem Mater **15** (5), 1165-1173 (2003).
4. Y. Akgöl, C. Cramer, C. Hofmann, Y. Karatas, H.-D. Wiemhöfer and M. Schönhoff, Macromolecules **43** (17), 7282-7287 (2010).
5. B. C. Lavu, M. P. Schoen and A. Mahajan, Smart Mater Struct **14** (4), 466-474 (2005).
6. A. Ostendorf, C. Cramer, G. Decher and M. Schönhoff, J Phys Chem C **119** (17), 9543-9549 (2015).
7. E. Kharlampieva, V. Kozlovskaya and S. A. Sukhishvili, Adv Mater **21** (30), 3053-3065 (2009).
8. S. Yang, Y. Zhang, Y. Guan, S. Tan, J. Xu, S. Cheng and X. Zhang, Soft Matter **2** (8), 699-704 (2006).
9. R. Steitz, V. Leiner, R. Siebrecht and R. v. Klitzing, Colloid Surface A **163** (1), 63-70 (2000).
10. S. K. Mahadeva, S. Yun and J. Kim, Sensors and Actuators A: Physical **165** (2), 194-199 (2011).
11. S. De, C. Cramer and M. Schönhoff, Macromolecules **44** (22), 8936-8943 (2011).
12. P. Brunetto, L. Fortuna, P. Giannone, S. Graziani and S. Strazzeri, IEEE Transactions on Instrumentation and Measurement **60** (8), 2951-2959 (2011).
13. E. Shoji and D. Hirayama, The Journal of Physical Chemistry B **111** (41), 11915-11920 (2007).
14. C. Lim, H. Lei and X. Tan, 2013 (unpublished).

15. H. L. Lei, Wen; Zhu, Guoming; Tan, Xiaobo, presented at the ASME Smart Materials, Adaptive Structures and Intelligent Systems, Stone Mountain, Georgia, USA, 2012 (unpublished).
16. E. Shoji and D. Hirayama, Polym Advan Technol **18** (5), 346-352 (2007).
17. J. Yip, F. Ding, K.-L. Yick, C.-W. M. Yuen, T.-T. Lee and W.-H. Choy, Sensor Actuat B-Chem **162** (1), 76-81 (2012).
18. I. Must, V. Vunder, F. Kaasik, I. Põldsalu, U. Johanson, A. Punning and A. Aabloo, Sensor Actuat B-Chem **202**, 114-122 (2014).
19. I. Must, U. Johanson, F. Kaasik, I. Poldsalu, A. Punning and A. Aabloo, presented at the Advanced Intelligent Mechatronics (AIM), 2013 IEEE/ASME International Conference on, 2013 (unpublished).
20. D. Wang, Dissertation/Thesis, Virginia Tech 2015.
21. G. Liu, J. Zhao, Q. Sun and G. Zhang, The Journal of Physical Chemistry B **112** (11), 3333-3338 (2008).
22. P.-G. Su and C.-P. Wang, Sensor Actuat B-Chem **129** (2), 538-543 (2008).
23. C. P. L. Rubinger, C. R. Martins, M. A. De Paoli and R. M. Rubinger, Sensor Actuat B-Chem **123** (1), 42-49 (2007).
24. P.-G. Su and S.-C. Huang, Sensor Actuat B-Chem **113** (1), 142-149 (2006).
25. T. Kuroiwa, T. Hayashi, A. Ito, M. Matsuguchi, Y. Sadaoka and Y. Sakai, Sensor Actuat B-Chem **13** (1), 89-91 (1993).
26. H. Grange, C. Bieth, H. Boucher and G. Delapiere, Sensors and Actuators **12** (3), 291-296 (1987).
27. N. Yamazoe and Y. Shimizu, Sensors and Actuators **10** (3), 379-398 (1986).
28. P.-G. Su and K.-H. Cheng, Sensor Actuat B-Chem **137** (2), 555-560 (2009).
29. P.-G. Su, W.-C. Li, J.-Y. Tseng and C.-J. Ho, Sensor Actuat B-Chem **153** (1), 29-36 (2011).
30. M. R. Islam and M. J. Serpe, Rsc Adv **4** (60), 31937-31940 (2014).
31. E. C. Venancio, L. H. C. Mattoso, P. S. d. P. Herrmann Júnior and A. G. MacDiarmid, Sensor Actuat B-Chem **130** (2), 723-729 (2008).
32. D. R. Morris and X. Sun, J Appl Polym Sci **50** (8), 1445-1452 (1993).
33. Y. Li, Y. Chen, C. Zhang, T. Xue and M. Yang, Sensors and Actuators B: Chemical **125** (1), 131-137 (2007).
34. Y. Sakai, Y. Sadaoka and M. Matsuguchi, Sensors and Actuators B: Chemical **35** (1–3), 85-90 (1996).
35. P. G. Su, I. C. Chen and R.-J. Wu, Analytica Chimica Acta **449** (1–2), 103-109 (2001).
36. C.-W. Lee, D.-H. Nam, Y.-S. Han, K.-C. Chung and M.-S. Gong, Sensors and Actuators B: Chemical **109** (2), 334-340 (2005).
37. D. Li, Y. Jiang, Y. Li, X. Yang, L. Lu and X. Wang, Materials Science and Engineering: C **11** (2), 117-119 (2000).
38. R. Nohria, R. K. Khillan, Y. Su, R. Dikshit, Y. Lvov and K. Varahramyan, Sensors and Actuators B: Chemical **114** (1), 218-222 (2006).
39. H. Yu, T. Cao, L. Zhou, E. Gu, D. Yu and D. Jiang, Sensors and Actuators B: Chemical **119** (2), 512-515 (2006).
40. B. J. Akle, M. D. Bennett, D. J. Leo, K. B. Wiles and J. E. McGrath, Journal of Materials Science **42** (16), 7031-7041 (2007).

41. I. Must, U. Johanson, F. Kaasik, I. Poldsalu, A. Punning and A. Aabloo, Physical chemistry chemical physics : PCCP **15** (24), 9605-9614 (2013).
42. P. W. T. Lu and S. Srinivasan, J Appl Electrochem **9** (3), 269-283 (1979).
43. M. Carmo, D. L. Fritz, J. Mergel and D. Stolten, Int J Hydrogen Energ **38** (12), 4901-4934 (2013).
44. E. Rasten, G. Hagen and R. Tunold, Electrochim Acta **48** (25–26), 3945-3952 (2003).
45. P. H. Choi, D. G. Bessarabov and R. Datta, Solid State Ionics **175** (1-4), 535-539 (2004).
46. I. Pilatowsky, R. J. Romero, C. A. Isaza, S. A. Gamboa, P. J. Sebastian and W. Rivera, in *Cogeneration Fuel Cell-Sorption Air Conditioning Systems* (Springer London, London, 2011), pp. 25-36.
47. O. V. Roussak and H. D. Gesser, in *Applied Chemistry: A Textbook for Engineers and Technologists* (Springer US, Boston, MA, 2013), pp. 85-103.
48. H. E. Kallmann, R. E. Spencer and C. P. Singer, P Ire **33** (3), 169-195 (1945).
49. W. C. Elmore, Journal of Applied Physics **19** (1), 55-63 (1948).
50. M. D. Green, D. Wang, S. T. Hemp, J. H. Choi, K. I. Winey, J. R. Heflin and T. E. Long, Polymer **53** (17), 3677-3686 (2012).
51. S. Liu, R. Montazami, Y. Liu, V. Jain, M. R. Lin, X. Zhou, J. R. Heflin and Q. M. Zhang, Sensor Actuat a-Phys **157** (2), 267-275 (2010).
52. M. D. Bennett and D. J. Leo, Sensors and Actuators A: Physical **115** (1), 79-90 (2004).

Chapter 6: Summary and Future Work

6.1 Summary of Results and Conclusions

This thesis describes work to incorporate ion conducting polyelectrolytes, such as PAMPS, and Nafion into the CNC of a Nafion-membrane based IPMC actuator using the ISAM film deposition process. A second major focus on this work was to test the humidity sensing properties of an IPMC actuator with ISAM CNC and EMI-Tf ionic liquid. The incorporation of PAMPS in the CNC showed some improvement in the IPMC actuator's bending amplitude and speed, while incorporation of Nafion did not yield significant changes in actuator performance. In the second part, the properties of an IPMC humidity sensor were thoroughly studied as a function of applied voltage, humidity range, inclusion of a CNC with PAH at pH 4.0 or 7, and ionic liquid content. Further, it was shown that the current of such an actuator responded to a rapid decrease in humidity with a faster (by ~4 times) and smoother response than a high quality commercial hygrometer device.

The inclusion of the ion-conducting polyelectrolyte PAMPS into a quadlayer CNC composed of PAH, AuNPs, PAH, and PAMPS of an actuator with EMI-Tf ionic liquid in a Nafion membrane demonstrated some increases in the bending speed and curvature compared to the previously studied CNC of just PAH and AuNPs. The ISAM film was optimized for CNC function by varying the pH of PAH, as well as the NaCl concentration in PAMPS solution, which allowed for adjusting the ionic screening and therefore the thickness and internal structure of the ISAM film. Thinner CNC films produced the most enhanced bending characteristics overall, with pH 4.0 and low salt concentrations improving bending speeds for both the cationic and anionic directions as well as increasing anionic bending curvature. Thicker films, using larger pH values and higher salt concentrations, increased the magnitude of the cationic bending curvature but slowed it down significantly.

For quadlayer CNC films containing Nafion in the CNC, there were more modest changes in the actuation speed and magnitude and none of the conditions for CNCs with Nafion showed clear improvements in multiple properties compared to a CNC without Nafion. Although the pH of PAH in the Nafion-containing films was kept at 4.0 for all samples, the thickness of the CNC from salt concentration affects the bending behavior in a similar general manner to what was found in the PAMPS study. The same overall trends in thickness versus

actuator performance based on the salt content were observed in the Nafion-containing samples as well. Thin CNCs produced some improved actuation over the control samples, in terms of bending speed in both directions and bending curvature on the negative side for the samples tested with 32 wt% EMI-Tf. The 17 wt% EMI-Tf samples only showed improvement in the cationic bending speed. Thicker CNCs produce large positive curvature but slow bending.

Comparatively, PAMPS enhanced bending in both directions more than Nafion. Cationic bending curvatures were similar but PAMPS clearly outperformed Nafion on the anionic bending side in both curvature and speed. This could be related to the fact that Nafion loses its highly ion conducting phase-separated structure when formed into LbL films, or the fact that water is not a good solvent for Nafion, which is then deposited in a highly aggregated form. Additional possibilities for the reduced performance include the higher concentration of sulfonic acid ion conducting groups in PAMPS compared to the amount of polymer chain that does not contribute to ion conduction.

Adding ion conducting polyelectrolytes can lead to some improvement in bending speed and curvature over the previous standard ISAM CNC that included only PAH and AuNPs. It seems the thickness of the CNC is more important than the resulting molecular structure for ion conduction for all CNC materials studied thus far. Further studies of possible enhancements to the CNC should be focused on including the PAMPS-containing quadlayer structure in the CNC.

The humidity-sensitive current through the IPMC actuator shows great potential for application in a polymer humidity sensor. The current measured through the device scales over a wide range of relative humidity (at least 10-80%RH), and can differentiate between at least 5%RH increments, and likely 1%RH. A proper test voltage in the range of 2.5 V was identified in order to minimize sample damage from current overload at high relative humidity but provide enough electrical potential to induce water electrolysis, which is the basis for humidity sensing.

A variety of sample types were tested, making use of the CNC with different thicknesses caused by changes in pH of PAH and varying ionic liquid contents. All variations of the sample worked, but samples with high ionic liquid contents responded the fastest and pH 4.0 samples showed greater current differentiation between different relative humidity values over samples with no CNC. No ionic liquid produced slightly larger dynamic current range, but the increase in response speed by including ionic liquid is more beneficial. Those results show that the CNC enhances relative humidity sensitivity and the ionic liquid increases detection speed, which are

both key components in our IPMC actuator device. Even more promising results showed that all variations of the sample respond faster to relative humidity changes than a high quality commercial Fluke 971 digital hygrometer. Samples with a CNC and high ionic liquid contents enhance the relative detection speed further, and future endeavors to fabricate IPMC actuator humidity sensors should make use of those elements.

6.2 Future work

6.2.1 Ion Conduction Polyelectrolytes in the CNC

Based on the improved performance of PAMPS-containing CNCs, future work on incorporating ion conducting polyelectrolytes should primarily focus on PAMPS rather than Nafion. However, further improvement over Nafion-containing CNCs' current state of bending could possibly be obtained through returning to an alcohol/water solvent mixture, since water is a poor solvent for Nafion/NaCl complexes. Optimizing ISAM film growth in an alcohol/water solution could reduce roughness and improve homogeneity and film deposition, which could lead to increased actuator bending and speed. It could additionally change the film structure since the solvent affects how the Nafion polymer chains deposit. Working with an alcohol/water solution however, would require a new mounting technique that could be easily rinsed in a single step to prevent solution contamination, but would not be affected by the alcohol.

Now that the optimal solution parameters for the CNC have been determined for PAMPS-containing CNCs, a test with a greater ionic liquid uptake could be performed, since the pH 4.0 samples were capable of absorbing more ionic liquid. Bending performance will be enhanced through increasing the ionic liquid content. Future tests could also study the thermal stability of the PAMPS-containing CNC through differential scanning calorimetry (DSC) or thermogravimetric analysis (TGA). It appeared that the PAMPS-containing samples were not stable in ionic liquid at temperatures greater than 40 °C, but this could vary based on the pH of PAH and salt concentration in PAMPS used. A thermal stability test such as DSC or TGA would provide a better characterization than the brief ionic liquid soaking test at increasing temperatures. Another suggestion for future work is to fabricate samples in larger pieces, so that the curling of the sample during the peeling process is minimized. Better bending overall may be achieved this way, since bending direction preference would be reduced.

Another interesting study could examine PAMPS and Nafion-containing actuators at varying relative humidity, and compare the bending to an actuator with a standard PAH/AuNP

CNC. As both PAMPS and Nafion are hydrophilic, their response may improve with increasing %RH at a different rate than PAH/AuNP CNC actuator samples. The addition of extra Nafion within the CNC may cause different water content at different RH values than the standard actuator without Nafion in the CNC.

Since incorporating an ion conducting polyelectrolyte in the CNC added to actuator functionality, despite replacing half of the gold nanoparticle layers, further actuation improvements may occur through incorporating ion conducting polyelectrolytes in the CNC without substituting gold nanoparticle layers. This would require a polycationic ion conducting polymer. Further, the polymer would need to be water-soluble, based on the ISAM film requirements and difficulties found in our film mounting technique when incorporating additional solvents such as methanol.

6.2.2 Humidity Sensing Applications

Future tests involving the prospects of IPMC actuators as humidity sensors should use thin CNCs, such as those obtained when pH 4.0 is used for PAH, and should contain approximately 35 wt% ionic liquid. Perhaps even greater ionic liquid content could be more beneficial. 45 wt% is closer to the uptake limit for this type of sample, so measurements on samples with these parameters may yield even faster relative response to humidity change.

Overall, this device seems promising for a future humidity sensor, though further study should be completed in order to fully understand the mechanisms and optimize the device for this purpose. A smaller chamber would make equilibration times faster and humidity content within more homogeneous. A more precise method of setting relative humidity is also necessary. Saturated salt solutions can be used to very accurately produce a precise relative humidity. Tests using the salt solution as the relative humidity standard should be conducted in order to calibrate a current curve corresponding to relative humidity.

Additionally, the stability of the device at different temperatures and steady-state current dependence on temperature could be examined. The lifetime of a device composed of one sample should be studied under various %RH conditions. Determination of the hysteresis between current measurements at the same %RH is also an important factor in the applicability of the IPMC actuator as a humidity sensor. Ideally, steady-state current would directly overlap at the same %RH conditions. The tolerance and resolution should also be examined. While

there are many aspects of the device left to test, measurements so far indicate promise for fabricating IPMC actuators into relative humidity sensing devices.

Appendix A: PAMPS-containing Sample and Control Sample Data

Run #	pH PAH	[NaCl] in PAMPS	# quadlayers	Average Thickness (nm)	Avg Thickness St. Dev. (nm)	Average Rq (nm)	Rq Std. Dev. (nm)
11	4	0	15	29.35	3.37	7.42	2.63
10	4	0.04	15	40.64	3.23	9.01	1.32
2	4	0.1	15	32.72	2.96	18.27	5.43
15	4	0.4	15	24.95	2.07	6.52	1.77
13	4	2	15	13.74	0.42	12.38	14.30
14	6.5	0	15	109.59	4.58	27.77	3.87
9	6.5	0.04	15	113.78	7.83	34.65	8.14
1	6.5	0.1	15	88.66	1.60	51.76	41.93
5	6.5	0.4	15	62.29	4.14	15.83	5.34
7	6.5	2	15	35.59	1.70	8.92	0.94
12	7	0	15	337.72	5.17	96.00	21.84
4	7.5	0.04	15	275.38	10.09	70.08	9.32
3	7.5	0.1	15	255.71	11.36	81.55	40.45
8	7.5	0.4	15	118.18	4.33	31.79	4.79
6	7.5	2	15	72.93	1.60	18.75	3.74

Table 17: Average thickness and RMS roughness measurements with corresponding standard deviations. Corresponds with data from section 3.5.2.

Control samples, bending curvature PAH/AuNPs only.

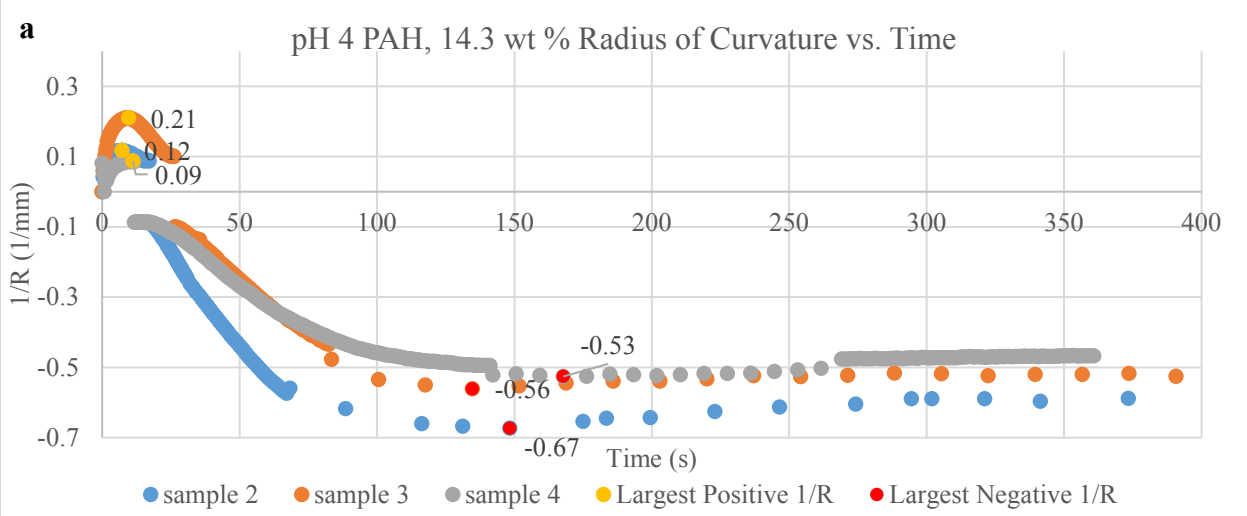

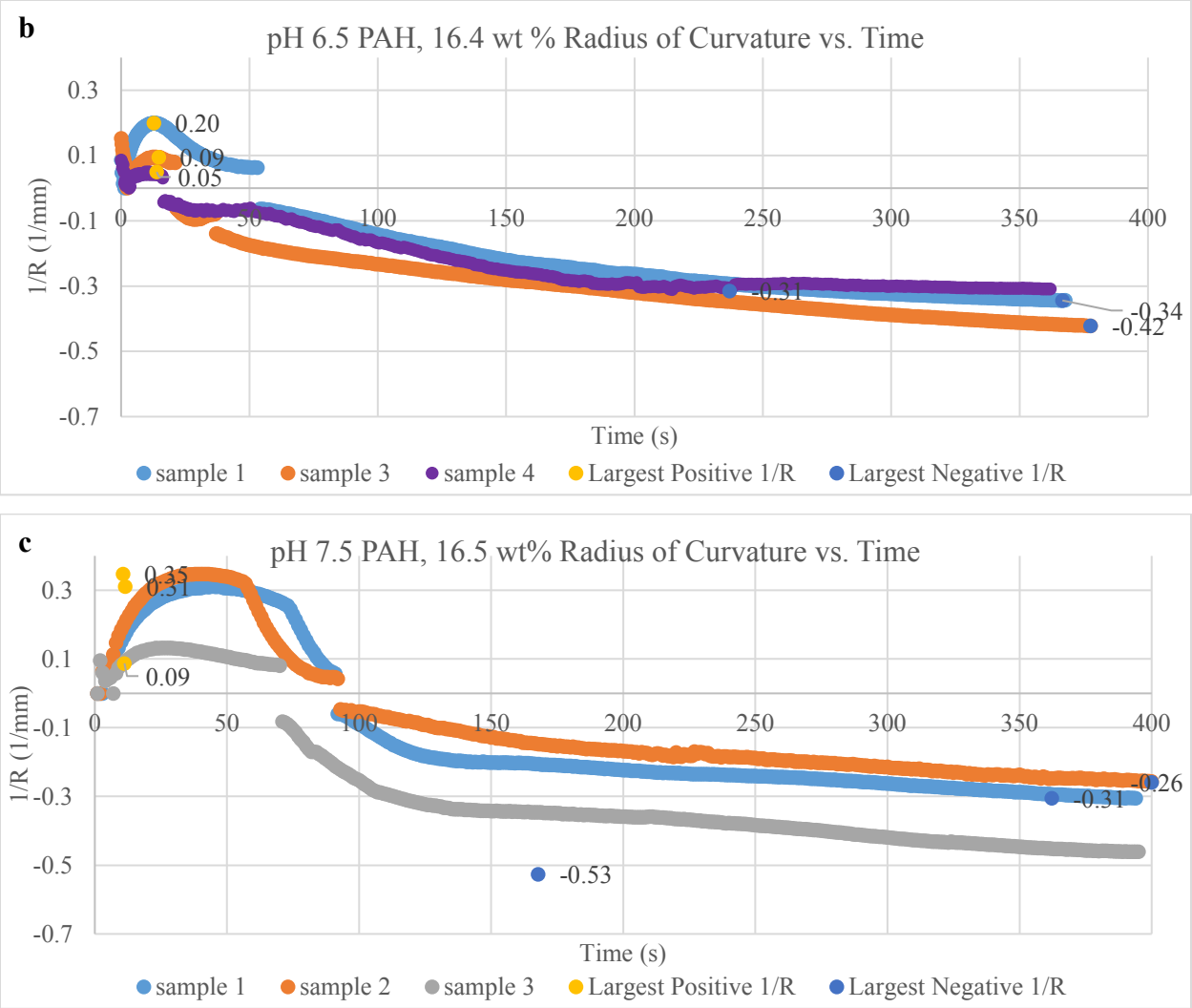

Figure A.1: Control actuator samples with PAH/AuNP CNCs and approximately 17 wt% EMI-Tf. Even the control samples display the same trends with thicker CNCs (larger pH) having greater cationic bending, and thinner CNCs (lower pH) having larger anionic bending.

Below are the averages of the maximum bending and minimum bending for each sample, as well as their corresponding average times.

Average PAH/AuNP Actuator Sample Bending Curvatures 17 wt%								
pH PAH	Largest Positive 1/R Time	Largest Positive 1/R Time St. Dev.	Largest Positive 1/R	Largest Positive 1/R St. Dev.	Largest Negative 1/R Time	Largest Negative 1/R Time St. Dev.	Largest Negative 1/R	Largest Negative 1/R St. Dev.
4	9.33	2.01	0.14	0.06	150.22	16.62	-0.59	0.08
6.5	13.78	0.94	0.11	0.08	327.11	78.17	-0.36	0.06
7.5	9.69	2.42	0.26	0.11	376.27	20.68	-0.34	0.11
no CNC	8.53	1.07	0.23	0.08	237.07	132.63	-0.47	0.24

Table 18: Average bending characteristics for each type of control sample with PAH/AuNPs only. Samples without a CNC at all yielded good results, while adding a CNC was able to improve either the maximum or minimum bending curvature.

PAH/AuNP Actuator Sample Bending Curvatures 17 wt%					
pH PAH	sample #	Time	Largest Positive 1/R	Time	Largest Negative 1/R
Nafion no CNC	sample 1	9.60	0.14	204.53	-0.72
Nafion no CNC	sample 2	8.53	0.27	382.93	-0.24
Nafion no CNC	sample 3	7.47	0.28	123.73	-0.46
pH 4	sample 2	7.20	0.12	148.27	-0.67
pH 4	sample 3	9.60	0.21	134.67	-0.56
pH 4	sample 4	11.20	0.09	167.73	-0.53
pH 6.5	sample 1	12.80	0.20	366.67	-0.34
pH 6.5	sample 3	14.67	0.09	377.60	-0.42
pH 6.5	sample 4	13.87	0.05	237.07	-0.31
pH 7.5	sample 4	11.47	0.31	362.13	-0.31
pH 7.5	sample 1	10.67	0.35	400.00	-0.26
pH 7.5	sample 2	6.93	0.13	366.67	-0.46

Table 19: Bending characteristics for all control samples.

Appendix B: Nafion-containing Sample Data

Thickness and RMS Roughness Measurements for Nafion-containing CNCs							
Nafion Concentration (wt %)	**pH PAH**	**[NaCl] in Nafion**	**# quadlayers**	**Average thickness (nm)**	**Avg Thickness St. Dev. (nm)**	**Average Rq (nm)**	**Avg Rq St. Dev. (nm)**
0.25	7	0	5	26.66	15.11	15.95	12.91
0.25	7	0	10	72.61	5.51	20.09	4.73
0.25	7	0	15	137.90	5.60	164.27	148.84
0.5	7	0	5	30.87	1.97	113.07	200.05
0.5	7	0	10	97.87	3.53	177.90	308.32
0.5	7	0	15	157.49	4.51	138.27	240.42
0.25	4	0	5	10.48	0.74	8.77	8.16
0.25	4	0	10	23.26	0.82	6.33	1.85
0.25	4	0	15	43.41	1.56	15.40	3.29
0.25	4	0.025	5	23.02	2.13	6.14	1.61
0.25	4	0.025	10	81.23	3.73	29.24	6.57
0.25	4	0.025	15	176.99	4.71	44.23	5.58
0.25	4	0.05	5	38.89	2.76	8.35	1.32
0.25	4	0.05	10	142.61	4.26	36.85	9.06
0.25	4	0.05	15	283.54	11.22	131.00	136.17
0.25	4	0.1	5	113.60	8.29	213.52	204.33
0.25	4	0.1	10	195.13	16.51	249.74	111.30
0.25	4	0.1	15	177.14	39.83	310.28	261.20
0.25	4	0.2	5	164.31	80.64	233.01	108.78
0.25	4	0.2	10	100.16	44.77	255.23	97.91
0.25	4	0.2	15	108.53	81.41	290.82	180.71

Table 20: Average thickness and RMS roughness measurements with corresponding standard deviations. Corresponds with data from section 4.5.2.

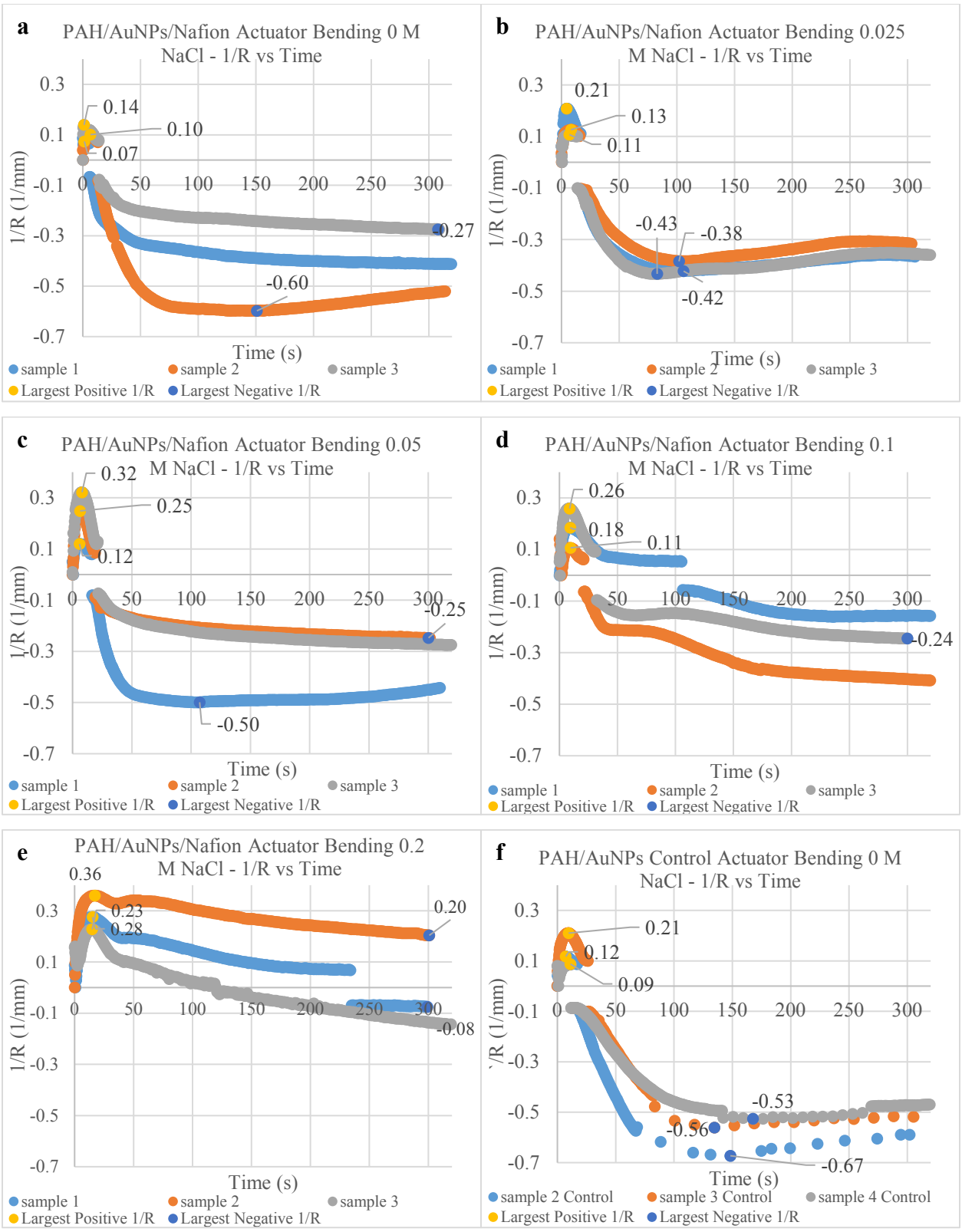

Figure B.1: Bending measurements for PAH/AuNPs/PAH/Nafion CNC samples with 17 wt% EMI-Tf.

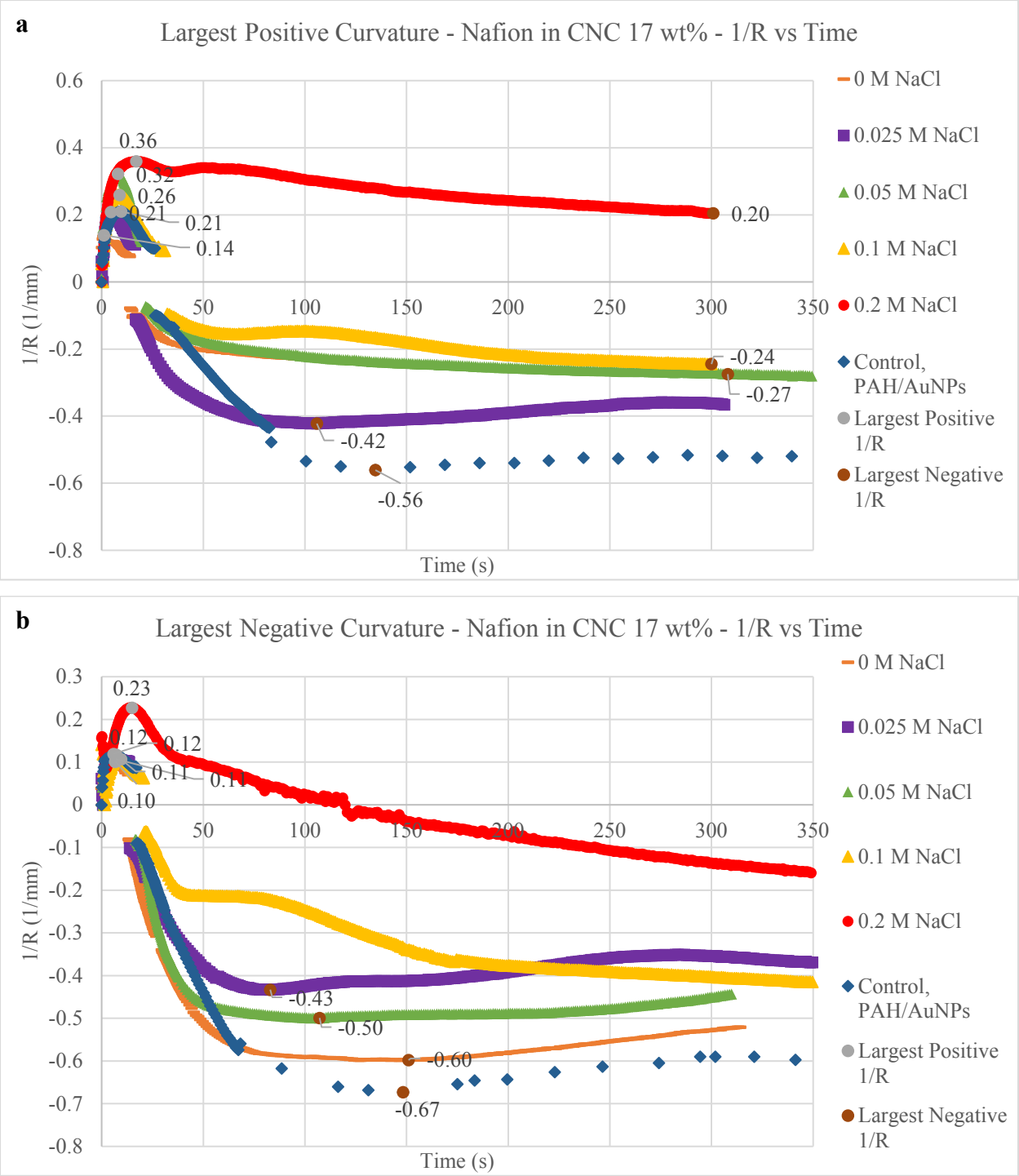

Figure B.2: The samples with the best maximum and minimum curvatures were plotted here. As in the 32 wt% samples, larger salt concentrations increased the cationic bending but slowed the speed. For anionic bending, the control had the greatest bending deformation, but the samples with lower salt content were faster. Some relaxation followed by further bending is observed in the anionic bending section.

Nafion-Containing CNC Bending Curvature Measurements 17 wt%					
M NaCl	**sample #**	**Time**	**Largest Positive 1/R**	**Time**	**Largest Negative 1/R**
0	1	1.33	0.07	345	-0.41
0	2	6.67	0.10	151	-0.60
0	4	1.07	0.14	308	-0.27
0.025	1	4.53	0.21	106	-0.42
0.025	2	8.27	0.13	102	-0.38
0.025	3	6.93	0.11	83	-0.43
0.05	1	5.87	0.12	107	-0.50
0.05	2	6.40	0.25	300	-0.25
0.05	3	8.00	0.32	358	-0.28
0.1	1	9.33	0.18	411	-0.17
0.1	2	9.60	0.11	406	-0.42
0.1	3	8.80	0.26	300	-0.24
0.2	1	15.20	0.28	299	-0.08
0.2	2	17.07	0.36	301	0.20
0.2	3	14.93	0.23	510	-0.21
Control	2	7.20	0.12	148	-0.67
Control	3	9.60	0.21	135	-0.56
Control	4	11.20	0.09	168	-0.53

Table 21: Bending maxima and minima along with their corresponding time points. The control has very good anionic bending, followed by the salt-free sample. The 0.025 M NaCl sample had the fastest anionic bending. The salt free sample had the fastest cationic bending, but the least amount of curvature, while the samples with the most salt had the most cationic bending but the slowest bending time. This is the same as the observation in the 32 wt% samples, but with less bending and slower speeds overall. Only the salt free sample was faster.

Appendix C: Effects of Test Voltage on Measured Current at Different %RH

Additional plots of measurements from testing a second set of samples at different voltages are shown below. Testing of sample 1 started at 50%RH, followed by 80%RH. After those two measurement sets, each voltage at 20%RH was investigated, but damage must have occurred in previous measurements at 80%RH, since the measured current was highly variable. Average current did however increase with increasing voltage even after being damaged.

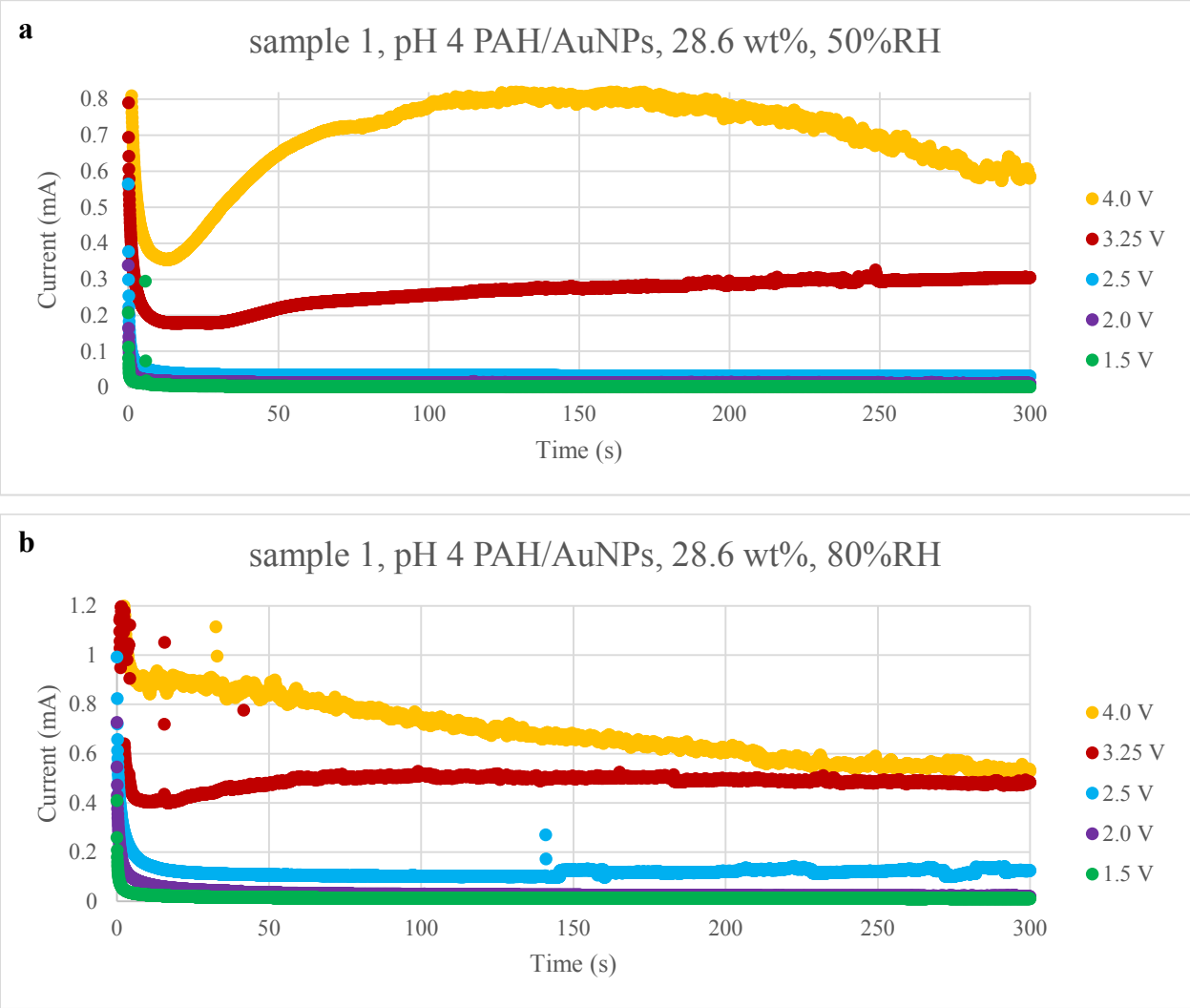

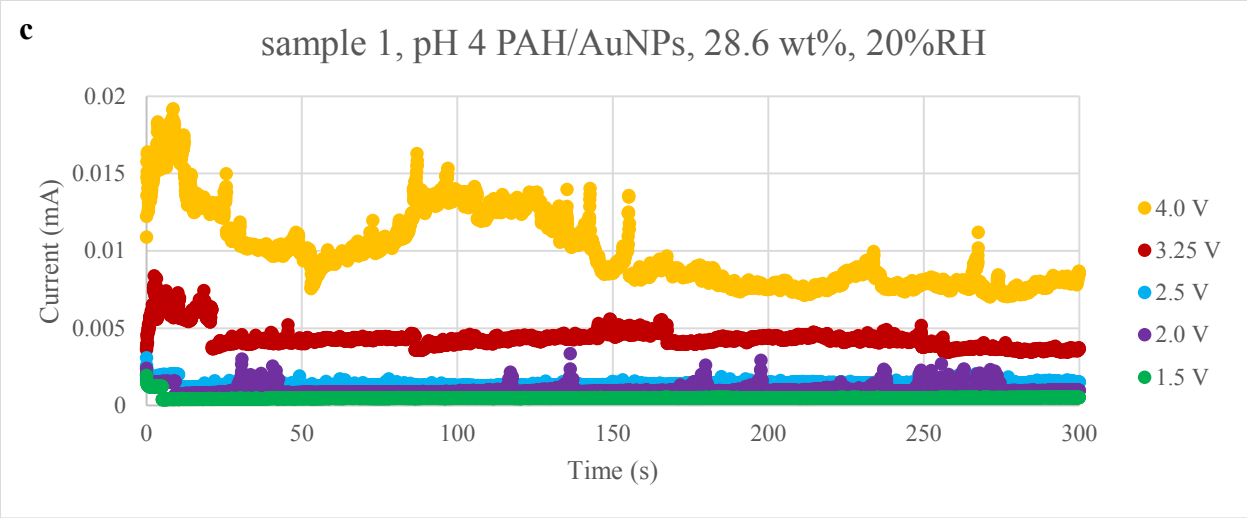

Figure C.1: Current measurements for a single sample at various %RH and applied voltage values, to determine future test voltage to use based on sample stability.

Appendix D: Effects of Ionic Liquid Content and Different pH Values in PAH

In the legends on the plots below, samples that do not indicate a pH value mean that there is no CNC.

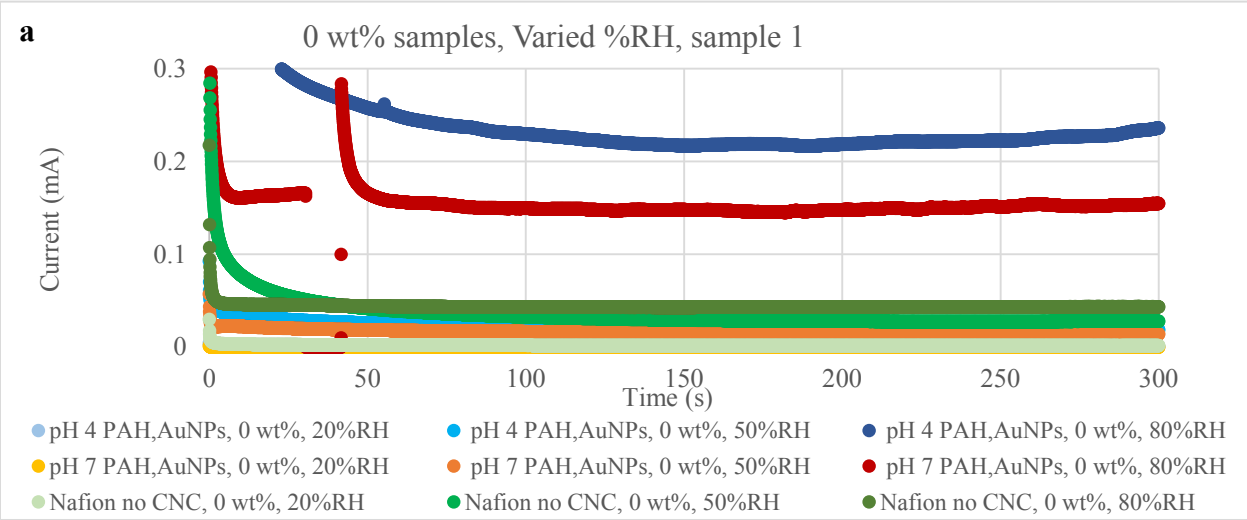

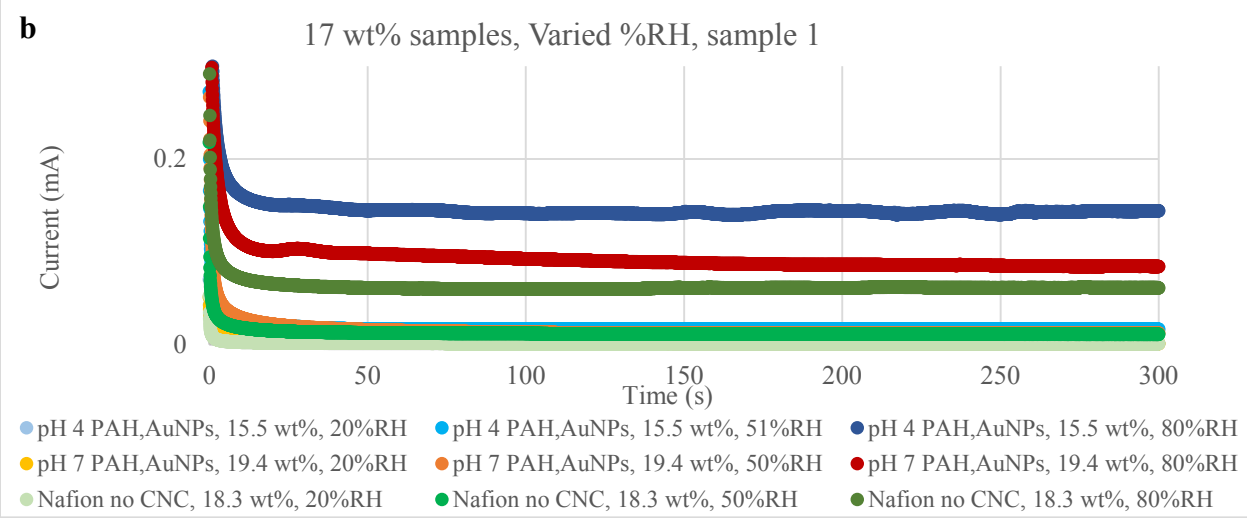

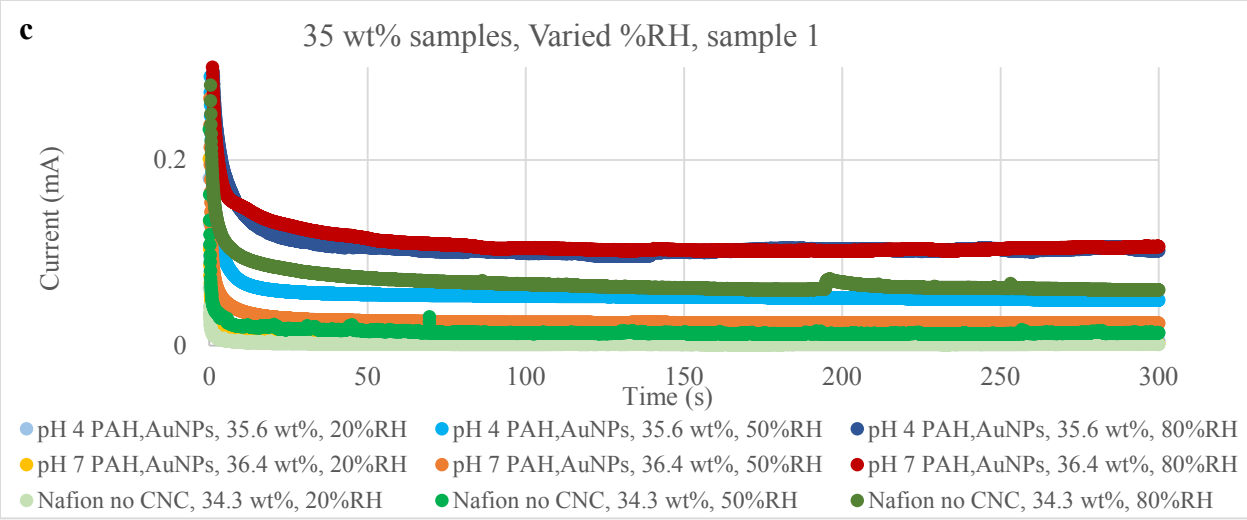

Figure D.1: Measurements grouped by ionic liquid weight percent for sample 1 of each type of sample at varying %RH. Ionic liquid free samples have a slightly steadier current. Samples with pH 4.0 have the largest separation between the 20 and 80%RH measurements.

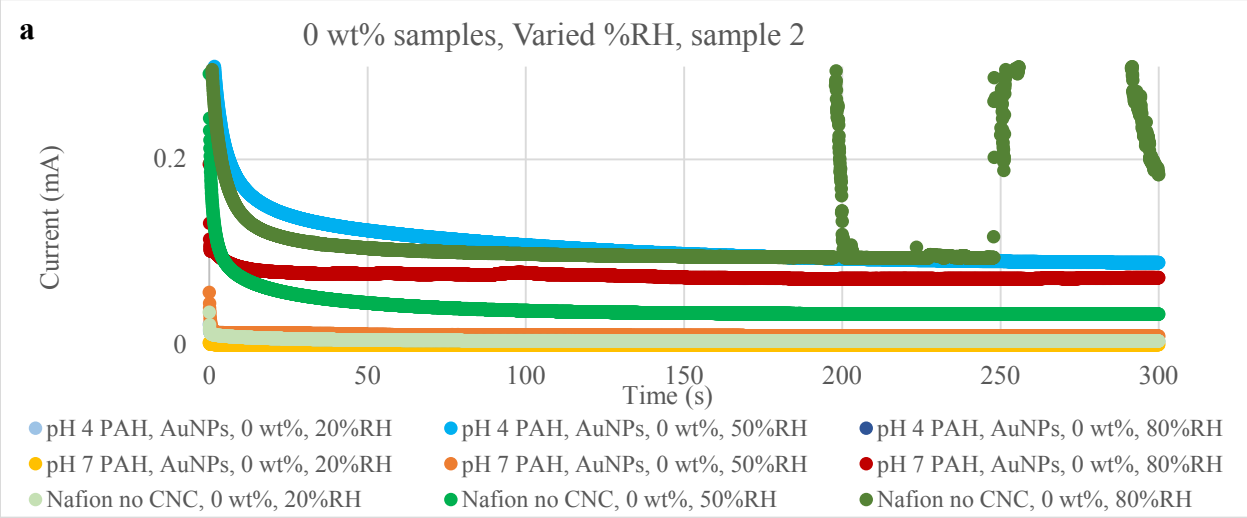

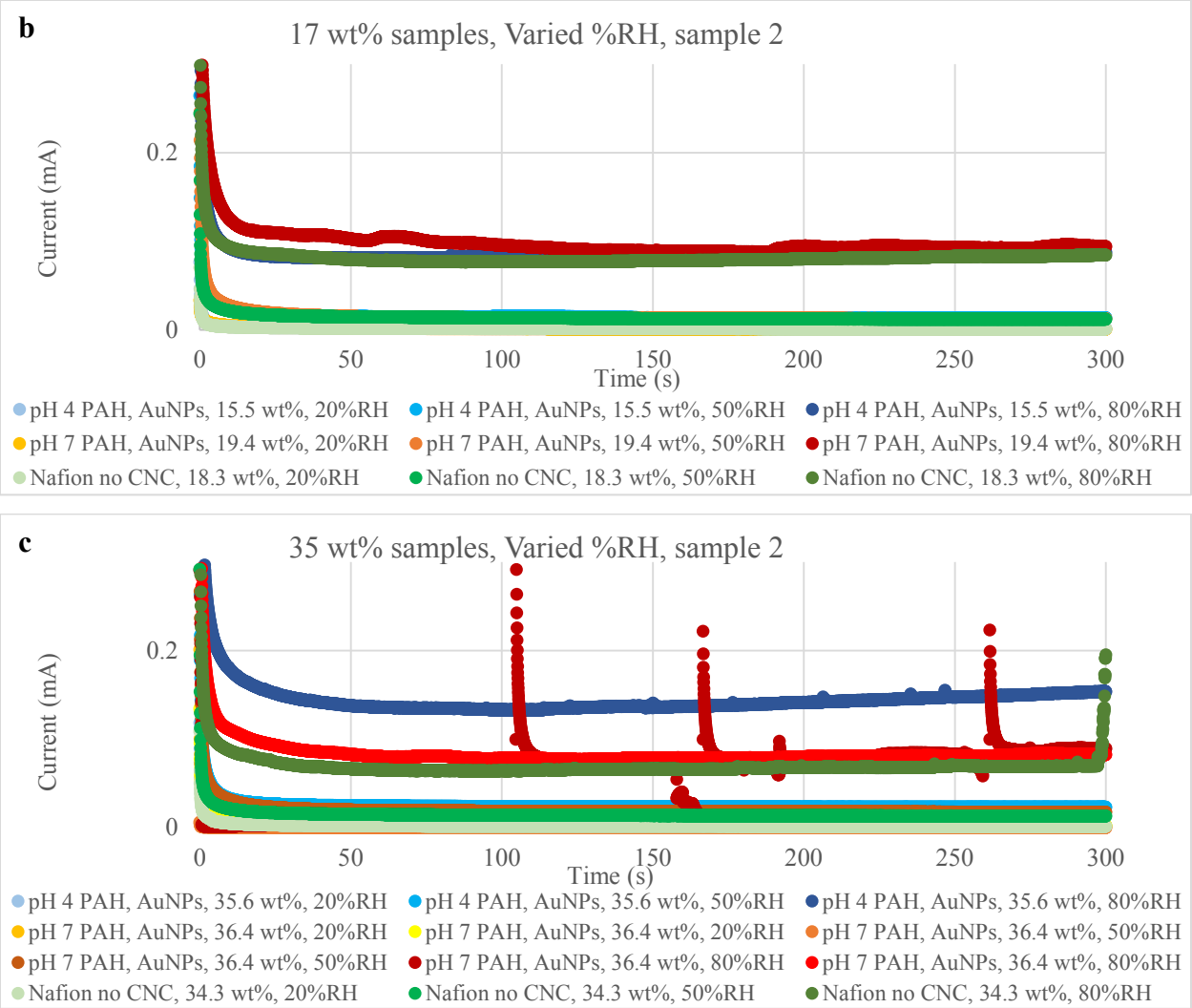

Figure D.2: Measurements grouped by ionic liquid weight percent for sample 2-3 of each type of sample at varying %RH. Ionic liquid free samples have a slightly steadier current. Samples with pH 4.0 have the largest separation between the 20 and 80%RH measurements.

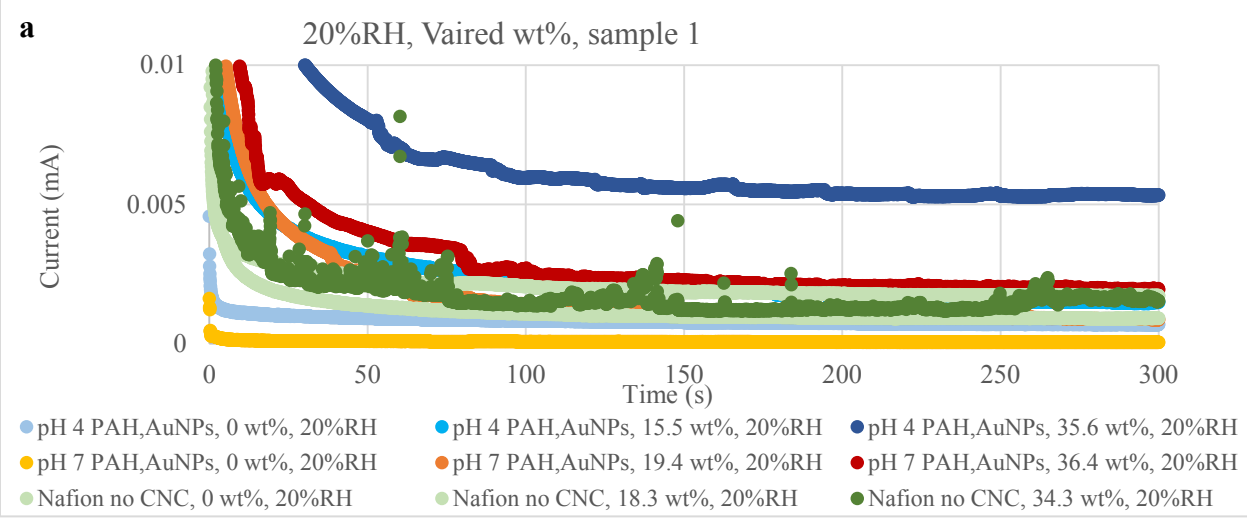
a
20%RH, Vaired wt%, sample 1
Current (mA)
0.01
0.005
0
0
50
100
150
200
250
300
Time (s)
pH 4 PAH,AuNPs, 0 wt%, 20%RH
pH 4 PAH,AuNPs, 15.5 wt%, 20%RH
pH 4 PAH,AuNPs, 35.6 wt%, 20%RH
pH 7 PAH,AuNPs, 0 wt%, 20%RH
pH 7 PAH,AuNPs, 19.4 wt%, 20%RH
pH 7 PAH,AuNPs, 36.4 wt%, 20%RH
Nafion no CNC, 0 wt%, 20%RH
Nafion no CNC, 18.3 wt%, 20%RH
Nafion no CNC, 34.3 wt%, 20%RH

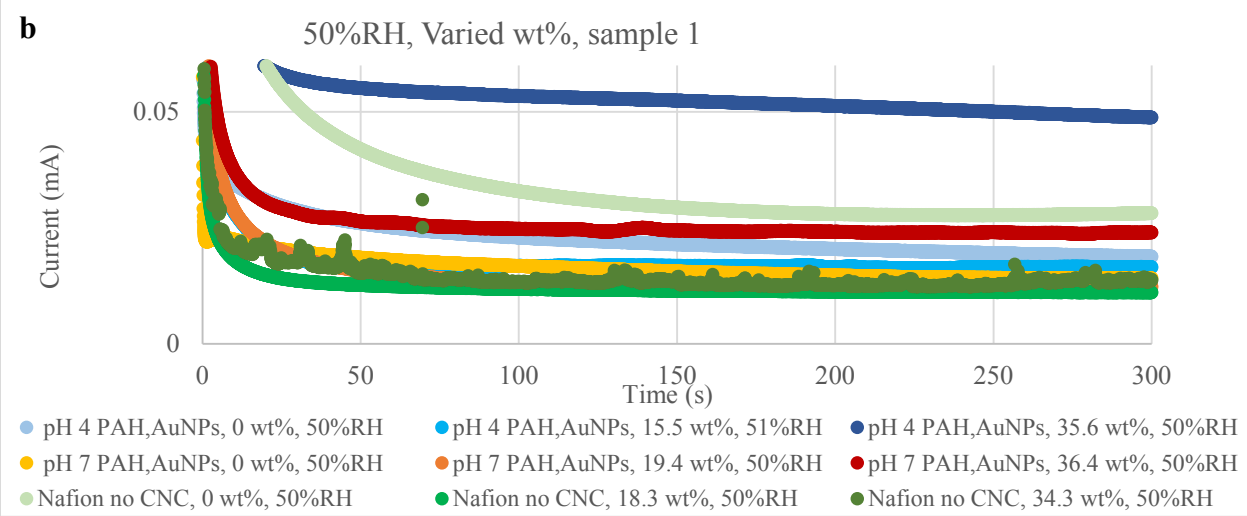
b
50%RH, Varied wt%, sample 1
Current (mA)
0.05
0
0
50
100
150
200
250
300
Time (s)
pH 4 PAH,AuNPs, 0 wt%, 50%RH
pH 4 PAH,AuNPs, 15.5 wt%, 51%RH
pH 4 PAH,AuNPs, 35.6 wt%, 50%RH
pH 7 PAH,AuNPs, 0 wt%, 50%RH
pH 7 PAH,AuNPs, 19.4 wt%, 50%RH
pH 7 PAH,AuNPs, 36.4 wt%, 50%RH
Nafion no CNC, 0 wt%, 50%RH
Nafion no CNC, 18.3 wt%, 50%RH
Nafion no CNC, 34.3 wt%, 50%RH

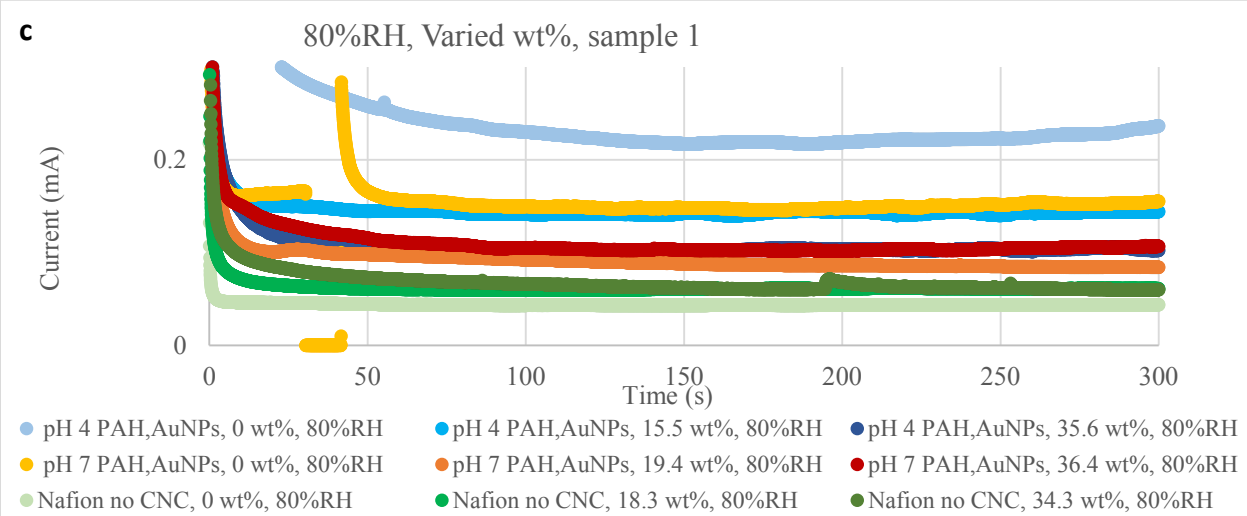
c
80%RH, Varied wt%, sample 1
Current (mA)
0.2
0
0
50
100
150
200
250
300
Time (s)
pH 4 PAH,AuNPs, 0 wt%, 80%RH
pH 4 PAH,AuNPs, 15.5 wt%, 80%RH
pH 4 PAH,AuNPs, 35.6 wt%, 80%RH
pH 7 PAH,AuNPs, 0 wt%, 80%RH
pH 7 PAH,AuNPs, 19.4 wt%, 80%RH
pH 7 PAH,AuNPs, 36.4 wt%, 80%RH
Nafion no CNC, 0 wt%, 80%RH
Nafion no CNC, 18.3 wt%, 80%RH
Nafion no CNC, 34.3 wt%, 80%RH

Figure D.3: Measurements grouped by %RH for sample 1 of each type of sample at varying %RH. Ionic liquid free samples have a slightly steadier current. Samples with either the most ionic liquid or none have the largest average steady state current.

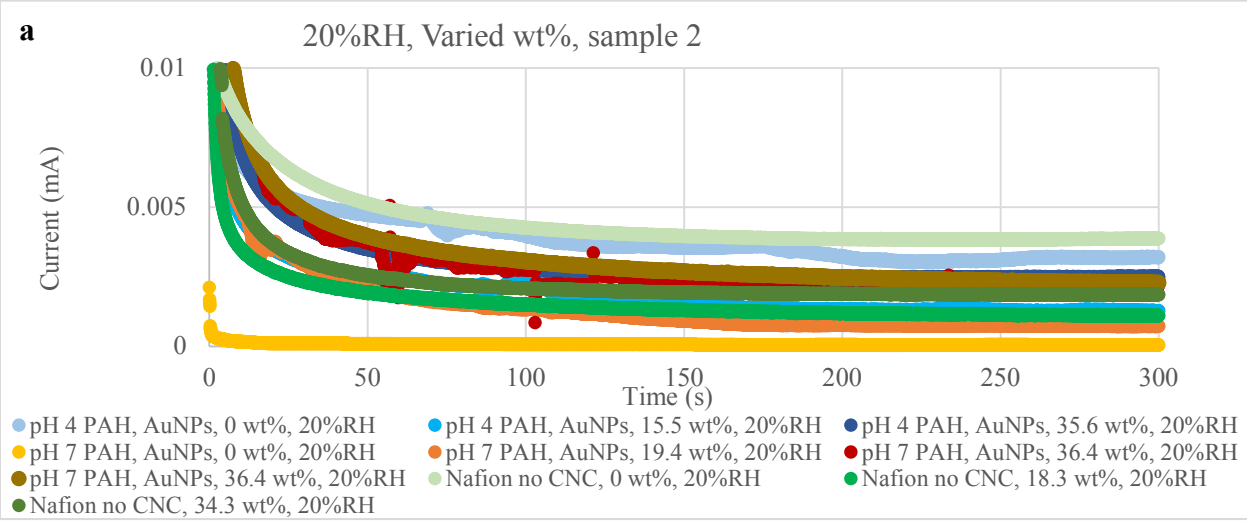

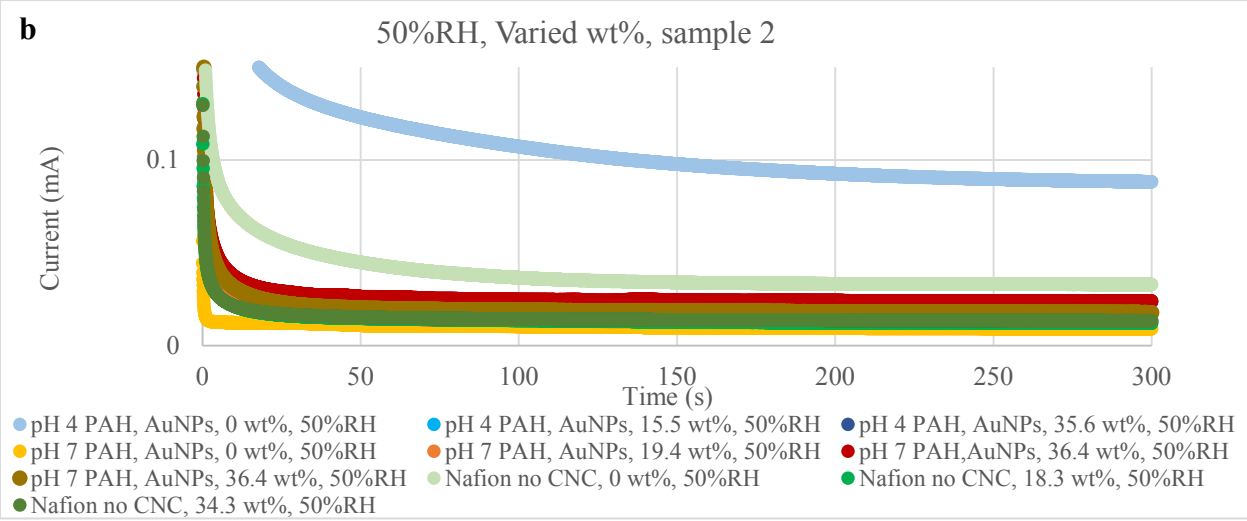

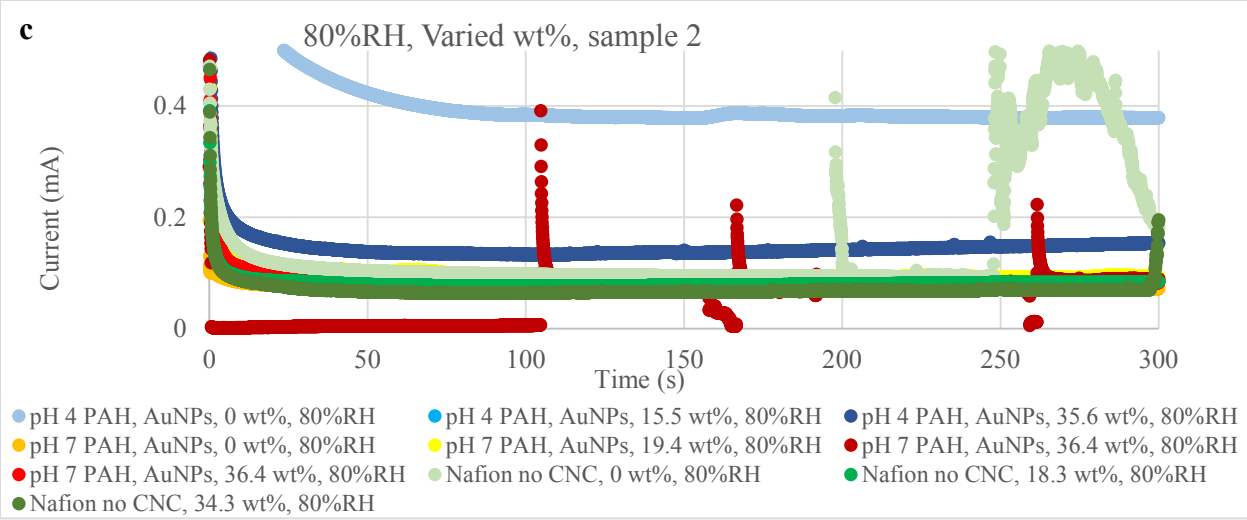

Figure D.4: Measurements grouped by %RH for sample 2-3 of each type of sample at varying %RH. Ionic liquid free samples have a slightly steadier current. Samples without ionic liquid have the largest average steady state current.